Ingenieurfakultät Bau Geo Umwelt

Lehrstuhl für Kartographie

Modeling of Public Transit Accessibility Driven by Spatial Movement Data

Diao Lin

Vollständiger Abdruck der von der Ingenieurfakultät Bau Geo Umwelt der Technischen Universität München zur Erlangung des akademischen Grades eines

Doktor-Ingenieurs (Dr.-Ing.)

genehmigten Dissertation.

Vorsitzender:

Prof. Dr.-Ing. Markus Disse

Prüfer der Dissertation:

1. Prof. Dr.-Ing. Liqiu Meng
2. Prof. Dr. Constantinos Antoniou

Die Dissertation wurde am 25.06.2020 bei der Technischen Universität München eingereicht und durch die Ingenieurfakultät Bau Geo Umwelt am 20.08.2020 angenommen.

Abstract

The recent development of dockless shared mobility, such as dockless shared bikes and shared e-scooters, provides new chances to improve the accessibility to public transport. Understanding such improvement is important for making policies related to public transit planning and shared mobility development. Traditionally, the accessibility analysis is conducted based on survey-format data, which is costly in data collection and usually limited to small data sizes. Dockless shared vehicles are typically equipped with GPS receivers, thus provide a convenient way of collecting large amounts of highly detailed trajectory data. With the focus on the integration of dockless shared vehicles and public transit, this thesis is dedicated to a systematic assessment of accessibility to public transit by using spatial movement data.

The thesis serves three objectives: 1) exploration of biking distances at individual transit stations from trajectory and smart card data, 2) investigation of transit catchment area to raise the public awareness of the transit accessibility at a general level, and 3) inspection of transit accessibility constrained by crowdedness at a fine-grained level.

With respect to the first objective, methods of how to identify bike-and-ride trips and process bike trajectory data are proposed. The effectiveness of these methods is demonstrated with a case study of measuring the bike distances to metro stations in Shanghai. Considering the second objective, a methodological framework of generating transit catchment areas by non-motorized transport is proposed. It consists of three components, namely subgraph construction, extended shortest path tree construction, and contour generation. The framework is provided as an open-source tool and applied to assess how bike-and-ride would change the accessibility to metro systems in Shanghai. The efficiency and effectiveness of the proposed framework are validated in a comparative study with four alternative methods. As for the third objective, an indicator called metro accessibility level is proposed. On the basis of the public transit accessibility level, the metro crowdedness is incorporated into the accessibility modeling, leading to the metro accessibility level as a new indicator. Its effectiveness is verified in a case study of measuring the accessibility to metro systems in Shanghai at the population grid level.

The proposed methods provide methodological support to the data-driven assessment of public transit accessibility. The developed framework and accessibility indicator are applicable to other scenarios of transit accessibility by non-motorized transport. The assessment of the transit accessibility at general and grid level can promote a comprehensive understanding of how dockless shared vehicles could change the accessibility to transit, and the analytical results may provide valuable insights into policymaking.

Zusammenfassung

Die jüngste Entwicklung der geteilten Mobilität ohne Andockstelle, wie z.B. stationsloser Fahrradverleih und E-Scooterverleih, bietet neue Möglichkeiten, den Zugang zu öffentliche Verkehrsmitteln zu verbessern. Solche Verbesserungsmöglichkeiten zu verstehen ist wichtig für die Gestaltung von Strategien im Zusammenhang mit der Planung der öffentlichen Verkehrsmittel und der Entwicklung der geteilten Mobilität. Traditionell wird die Zugänglichkeitsanalyse auf der Grundlage von Daten im Umfrageformat durchgeführt, was in der Datenerhebung kostspielig ist und sich in der Regel auf kleine Datengrößen beschränkt. Stationslose, gemeinsam genutzte Fahrzeuge sind in der Regel mit GPS-Empfängern ausgestattet und bieten somit eine komfortable Möglichkeit, große Mengen an sehr detaillierten Trajektoriedaten zu sammeln. Mit dem Schwerpunkt auf der Integration von stationslosen Verleihfahrzeugen und öffentlichen Verkehrsmitteln widmet sich diese Arbeit einer systematischen Bewertung der Zugänglichkeit von öffentlichen Verkehrsmitteln unter Verwendung von Raumbewegungsdaten.

Die Dissertation hat drei Ziele: 1) Untersuchung der Fahrraddistanzen an den einzelnen Transitstationen anhand von Trajektorien- und Smartcard-Daten, 2) Untersuchung des Transit-Einzugsgebietes zur Sensibilisierung der Öffentlichkeit für die Zugänglichkeit des Transits auf allgemeiner Ebene und 3) Untersuchung der durch Überfüllung eingeschränkten Zugänglichkeit auf Detailebene.

Im Hinblick auf das erste Ziel werden Methoden zur Identifizierung von Bike-and-Ride-Touren und zur Verarbeitung von Fahrradtrajektoriedaten vorgeschlagen. Die Effektivität dieser Methoden wird anhand einer Fallstudie zur Messung der Fahrraddistanzen zu U-Bahn-Stationen in Shanghai demonstriert. Im Hinblick auf das zweite Ziel wird ein methodischer Rahmen zur Generierung von Transiteinzugsgebieten durch nicht-motorisierten Verkehr vorgeschlagen. Der methodische Rahmen besteht aus drei Komponenten, nämlich der Teilgraphenkonstruktion, der erweiterten Baumkonstruktion des kürzesten Weges und

der Konturgenerierung. Das System wird als Open-Source-Werkzeug zur Verfügung gestellt und angewendet, um zu beurteilen, wie Bike-and-Ride die Zugänglichkeit zu dem U-Bahnsystem in Shanghai verändern würde. Die Effizienz und Effektivität des vorgeschlagenen methodischen Rahmens werden in einer vergleichenden Studie mit vier alternativen Methoden validiert. Als drittes Ziel wird ein Indikator namens *metro accessibility level für* den Grad der Metro-Zugänglichkeit vorgeschlagen. Auf der Grundlage des Zugänglichkeitsgrads des öffentlichen Nahverkehrs wird die Überfüllung der U-Bahn in die Zugänglichkeitsmodellierung einbezogen, was zu dem Zugänglichkeitsgrad der U-Bahn als neuem Indikator führt. Die Wirksamkeit des Indikators wird in einer Fallstudie zur Messung der Zugänglichkeit der U-Bahnsysteme in Shanghai auf der Ebene des Bevölkerungsrasters verifiziert.

Die vorgeschlagene Methodik unterstützt die datengestützte Bewertung der Zugänglichkeit der öffentlichen Verkehrsmittel. Der entwickelte methodische Rahmen und der Zugänglichkeitsindikator sind auf andere Szenarien der Transiterreichbarkeit durch nicht-motorisierten Verkehr anwendbar. Die Bewertung der Transitzugänglichkeit auf allgemeiner und Rasterebene kann ein umfassendes Verständnis dafür fördern, wie die Zugänglichkeit des Transits durch gemeinsam genutzte stationslose Fahrzeuge verändert werden kann und die Und die Ergebnisse der Analyse können wertvolle Erkenntnisse für die Konzeptentwicklung liefern.

Contents

List of Abbreviations

Full Name	Abbreviation
Global positioning system	GPS
Geographic information system	GIS
Transit catchment area	TCA
Public transport accessibility level	PTAL
Two-step floating catchment area	2SFCA
General transit feed specification	GTFS
Transit service indicator	TSI
Origin-destination	OD
Hidden Markov Model	HMM
Automated fare collection	AFC
Bike-ride-bike	BRB
Fast map-matching	FMM
Pedestrian catchment area	PCA
Bike catchment area	BCA
Forward–backward–forward	FBF
OpenStreetMap	OSM
Ordinary least-squares	OLS
Shortest path tree	SPT
Metro accessibility level	MAL
Scheduled waiting time	SWT
Average waiting time caused by crowdedness	AWTC
Total access time	TAT
Equivalent doorstep frequency	EDF

List of Tables

List of Figures

1 Introduction

1.1 Motivation

According to the report of World Urbanization Prospects, 55% of the world's population living in urban areas as of 2018, and the number is expected to increase to 68% by 2050 (United Nations, Department of Economic and Social Affairs, 2018). The growing urbanization poses many challenges for sustainable development and city management, including housing, transportation, energy systems, education, and health. The huge urban population creates high transportation demand, and at the same time, causing serious traffic-related problems, including Co_2 emissions, traffic congestion, and air pollution. Therefore, developing sustainable transportation systems is regarded as a major aim of transportation planning worldwide. As an important component of sustainable transportation, public transit plays a significant role in decreasing Co_2 emissions and relieving traffic congestion. In addition to these environmental benefits, public transit also provides valuable social benefits in terms of promoting social equality, and is particularly important for the mobility of disadvantaged groups, such as low-income households and the elderly people. Therefore, it is essential to optimize the use of public transit. Many efforts have been made to increase the quality of transit service, including constructing more transit systems, extending capability and service time, and increasing reliability, Taking the metro systems – a major public transport mode for large cities – as an example, the total serving length has been increased from 10,920 km to 13,903 km from 2013 to 2017 globally, with an increase of 27.3% (International Association of Public Transport, 2018). On the other hand, enhancing access to transit systems acts as an effective approach to improving the public transport chain, and thus is an alternative means to increase transit use. Major efforts in this aspect have been devoted to two directions: 1) decreasing the traveling cost of a certain access mode (e.g., improving the walking and biking environments), and 2) enhancing and developing alternative access services (e.g., improving feeder services).

Traditionally, the study of access to public transit mostly focuses on pedestrian perspective because walking is commonly regarded as the major access mode of public

transit. The recent years have witnessed increasing attention to other green and faster transit access modes (e.g., shared bikes) because of their potential to decrease the access time and increase the population coverage of transit. This trend is especially obvious during the last decade with the globally growing popularity of shared mobility provided by very light vehicles, such as shared pedal bikes, electric bikes, and electric scooters (e-scooters). With the development of smartphone technologies, the new generation of shared mobility typically adopts the dockless mode as compared with traditional station/dock-based bike/scooter-sharing systems. In this dockless mode, shared bikes/scooters are equipped with the global positioning system (GPS) receivers, making them easily positioned by users and operators. Users are no longer required to rent and return bikes/scooters at certain stations, they can find and rent nearby bikes/scooters using smartphone apps and leave them at users' convenience or any authorized areas (Zhang et al., 2018). As a result, this new shared mobility achieves huge success in terms of serving as a transportation mode for short journeys and acting as an important component of the sustainable transportation ecosystem. As an example, China – the origin of the new generation of dockless bikeshare – has approximately 221 million dockless bike-sharing users by the end of December 2017. Additionally, the dockless bikeshare has been extended to 21 countries outside China, including Singapore and the UK (China Internet Network Information Center, 2018), whereas some western countries prefer e-scooters, the e-scooter ridership of the United States, e.g., reached 38.5 million as compared with 9.5 million dockless bikeshare trips (including pedal and e-bikes) in 2018 (National Association of City Transportation Officials, 2018). As one of the major use scenarios, these shared vehicles are extensively used for connection with public transit because the last mile to/from public transit is regarded as a typical urban short journey. Additionally, from a planning perspective, promoting the integration of these vehicles with public transit is regarded as a means of improving the efficiency of the public transport chain and might promote the use of public transit. This motivates us to explore how the emerging shared mobility is used for connecting with public transit and how the accessibility to transit might be changed by integrating dockless shared mobility with public transit.

Traditionally, answering these questions largely depends on reliable travel survey data. However, the collection of survey data is usually time-consuming and costly; and hence, the datasets are usually limited to a small size and very difficult to update. Fortunately, the massive trajectory data automatically collected by the GPS devices now provide new data sources. GPS trajectory data usually provide more details about human travel characteristics in terms of spatiotemporal granularity, e.g., traveling speeds and route choices, as compared with survey-based data. Furthermore, the dynamic updating characteristics make the trajectory data especially suitable for the investigation of new transport modes because they are unlikely to be included in existing extensive travel surveys (e.g., national travel survey). However, how to model the accessibility to transit

at different scales with trajectory data remains a challenging task. Because trajectory data are commonly generated with noises and not specifically collected for the purpose of accessibility analysis.

In addition to the data perspective, a systematic assessment of accessibility to public transit also requires appropriate accessibility modeling and related technical support, especially geographic information system (GIS) technologies. As further steps toward these two aspects, this thesis strives to make contributions from a multidisciplinary perspective. From the technical perspective, it aims to develop an open-source methodological framework of generating catchment areas for evaluating the transit coverage. From the modeling perspective, it seeks answers to questions of why and how to integrate the information about crowdedness into accessibility measurements by comparing the accessibility modeling approaches from health geography and transit planning.

1.2 Research Tasks

The major objective of this thesis can be described as:

"*To investigate the bike-metro integration using spatial movement data and support a systematic assessment of accessibility to public transit*".

To achieve this objective, the thesis includes the following research tasks.

- To propose methods to identify trips connecting with transit systems and reconstruct the traveler's routes from the raw trajectories.
- To explore the factors associated with biking distances to individual transit stations.
- To propose a methodological framework for generating network-based catchment areas and evaluate its efficiency and effectiveness.
- To develop an open-source tool for generating network-based catchment areas.
- To introduce a new accessibility indicator by integrating the crowdedness information.

1.3 Thesis Structure

The thesis is structured in six chapters as shown in Figure 1.1 to address the aforementioned research tasks. Following this introductory chapter, the related theoretical and technical basics are presented in Chapter 2. In Chapter 3, we introduce the study area and propose methods to measure biking distances at individual metro stations, which are used as input for the two subsequent chapters. In Chapter 4 and

Chapter 5, we propose methods to assess the bike accessibility to metro systems at two different levels of detail, i.e., the general and the grid level. Chapter 6 concludes the thesis and discusses future work.

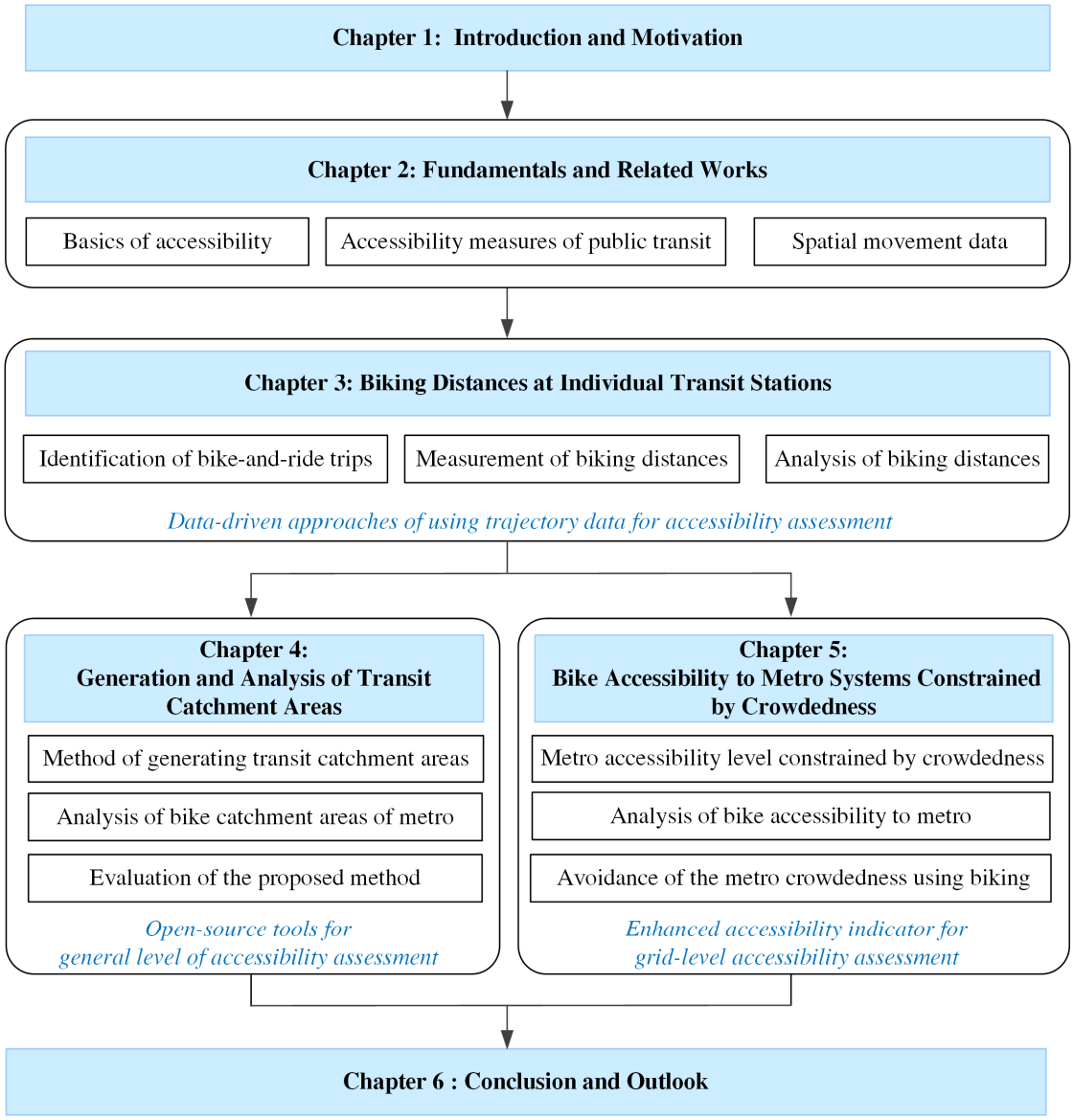

Figure 1.1. Thesis structure.

The main contents of these five chapters are described below.

Chapter 2 first describes several fundamental aspects of accessibility, including concepts, basic components, classification of existing measures and model calibration. The chapter centers on reviewing literature related to public transit accessibility from four aspects, i.e., the type of measure, influence factors, required data, and scale of analysis. Methodologies related to-transit and via-transit accessibility are discussed.

The data characteristics and basic processing techniques related to GPS trajectory and smart card data are explained in detail.

Chapter 3 deals with the measurement of biking distances at individual transit stations from trajectory data. We first introduce the study area and data preparation for the measurement of biking distances. Massive bike trajectory and smart card data collected in Shanghai are used for conducting extensive experiments. Then, we propose the methods of identifying bike-and-ride trips and reconstructing the travel routes using trajectory data. Based on the measured biking distances in Shanghai, the spatial distribution patterns of biking distances at individual stations are presented. Regression models are then used to explore factors that might be associated with them.

Chapter 4 proposes an open-source methodological framework for generating network-based transit catchment areas (TCAs). The components and implementation are illustrated in detail. Using the bike acceptable distances of individual stations derived from Chapter 3 as input, the proposed methods are applied to measure the bike catchment areas (BCAs) of metro stations in Shanghai. The efficiency and effectiveness of the proposed method are demonstrated by comparing with alternative methods.

Chapter 5 starts with a discussion of accessibility measurements in the fields of health geography and transport planning to explain the importance of crowdedness for the accessibility measurement. Then, an adapted accessibility indicator integrating crowdedness is proposed. Again, combining with the output of Chapter 3, the proposed indicator is applied to assess the bike accessibility to metro systems in Shanghai. At last, the chapter proposes a method to examine how bike-and-ride might help relieve the metro crowdedness.

Chapter 6 summarizes the major contributions of this thesis and discusses future work.

2 Fundamentals and Related Works

This chapter aims to provide theoretical and technical bases for this thesis. Section 2.1 explains the basic concepts, components, classification, and calibration of accessibility from a multi-disciplinary perspective (Section 2.1). Then, Section 2.2 identifies four fundamental aspects of public transit accessibility measures and gives a review of existing studies accordingly. Section 2.3 focuses on explaining the characteristics and basic processing techniques related to GPS trajectory and smart card data.

2.1 Basics of Accessibility

2.1.1 Concept of Accessibility

Accessibility, a concept frequently used in multiple fields such as transport planning, health geography, and urban planning, acts as an important indicator for policymaking. Although the term has been widely used, it is difficult to achieve a consensus on the precise definition of accessibility. The early definitions of accessibility can be dated back to the 1950s, Hansen (1959) defined accessibility as "the potential of opportunities for interaction". Ingram (1971) made the definition as "the inherent characteristic (or advantage) of a place with respect to overcoming some form of spatially operating source of friction (for example, time and/or distance)". Handy and Niemeier (1997) denoted that accessibility is mainly decided by the ease of reaching potential destinations and their characteristics (e.g., magnitude and quality). Geurs and van Wee (2004) defined accessibility as "the extent to which land-use and transport systems enable (groups of) individuals to reach activities or destinations by means of a (combination of) transport mode(s)." In general, researchers treat that accessibility as a measure of "the ease of potential opportunities can be reached".

2.1.2 Basic Components of Accessibility

Traditionally, land use and transport – two basic elements of urban form – are generally regarded as the core components of accessibility. Land use development decides the spatial distribution of potential opportunities (e.g., working places) and the origins of the corresponding potential trips (e.g., residential areas). On the other hand, the structure, capacity, and connectivity of transport systems jointly decide how potential opportunities can be reached by a transport mode and its impedances (e.g., travel time and cost). For both components, there is a confrontation between supply and demand. For instance, the restricted capacity of a working place may cause competition between different origins. Similarly, the capacity of a highway and its travel demand might jointly affect the travel speed on the highway.

Apart from these two components, Geurs and van Wee (2004) identified temporal and individual aspects as two additional components of accessibility. It is natural to understand the inclusion of the temporal component because the supply of activities (e.g., office opening hours) and transportation (e.g., bus serving time) can both vary across different times. The individual component emphasizes the importance of socio-demographic attributes in modeling accessibility. The impact of individual components, such as age, income, and car ownership, can be reflected from the perspectives of transport and/or land use as well. For instance, the selection of transport modes is affected by the car ownership of an individual, and the preference for a type of opportunity is affected by his/her age. Furthermore, from the perspective of time-geography, the available time for each individual can also be different (Kwan, 1998). As a result, two individuals may have very distinct accessibility to the same opportunities, even though they are located in the same location. Correspondingly, place-based accessibility aggregated by person-based accessibility (i.e., considering the individual differences) would be diverse from those measured without considering individual diversity.

From the perspective of defining a comprehensive accessibility measure, it might be better to incorporate all the above four components in an accessibility measure. In practice, some components might be omitted because of operational feasibility (e.g., technical/data limitation) and interpretability (i.e., easy to understand for policymaker) (Geurs and van Wee, 2004). As an alternative to incorporating every component, measuring the accessibility of different subgroups can also be a means to consider a component. For example, making a distinction between the accessibility of different periods (e.g., weekday and weekends) is an approach of considering the temporal component of accessibility. Similarly, the distinction can be made in terms of user groups with different socioeconomic statuses (e.g., different educational backgrounds), to stress the importance of individual components.

2.1.3 Classification of Accessibility Measures

Generally, accessibility measures can be classified into three categories, namely cumulative, gravity-based and utility-based measures (Geurs and van Wee, 2004; Handy and Niemeier, 1997; Páez et al., 2012). Cumulative measures, also known as contour-based and isochoric measures, measure the accessibility of a location/individual by counting the number of opportunities (e.g., shops) within a threshold time/distance. They emphasize the number of opportunities (i.e., the availability) and make no distinction between opportunities within the threshold time/distance. Typical examples of the application of cumulative measures include food accessibility (Apparicio et al., 2007; Sharkey et al., 2009) and transit accessibility (Lin et al., 2019; Zuo et al., 2018). The advantages of this type of measures include easy interpretation, simple implementation, and less demanding of data. The measure is frequently criticized for its oversimplification because all the opportunities within the threshold distance/time are equally treated, ignoring the effect of spatial decay.

Gravity-based measures, also known as potential accessibility measures, model accessibility by jointly considering the attractiveness of opportunities and transport impedance. The corresponding equation can be denoted as below.

$$A_i = \sum_j a_j f(C_{ij}) \tag{2.1}$$

where A_i represents the accessibility from location i to all potential opportunities. a_j represents the attractiveness of location j, for example, it can be represented by the number of jobs in location j (i.e., the supply). C_{ij} is the impedance (e.g., travel time or distance) between location i and j, and $f(C_{ij})$ is the corresponding impedance function. The impedance function reflects the decay impact of C_{ij} and can take several distinct forms such as inverse-power, Gaussian, exponential, and kernel density. Compared with cumulative measures, the decay impact is explicitly integrated into the gravity-based measure and thus can better reflect the impact of transportation impedance. Furthermore, the attractiveness of opportunities can be flexibly designated according to the application requirements.

The basic version of the gravity-based measure ignores the competition between demand locations, which may limit the usefulness of the measure. For instance, the attractiveness of an opportunity might decrease if too many demanding locations are competing for it. As an early effort towards this limitation, Weibull (1976) considered the competition from the demand side by calculating a potential demand for each supply location, and the ratio between the supply and potential demand is used as the indicator of attractiveness. The equations are denoted below.

$$A_i = \sum_j a_j f(C_{ij}) = \sum_j \frac{O_j}{D_j} * f(C_{ij}) \tag{2.2}$$

$$D_j = \sum_k P_k f(C_{jk}) \tag{2.3}$$

Where P_k represents the demand (e.g., population) at location k. C_{jk} denotes the impedance between location j and k. D_j represents the potential demand for opportunities in location j. O_j represents the supply of opportunities in location j. Joseph and Bantock (1982) adopted a similar measure to assess people's accessibility to general medical practitioners in rural areas. Shen (1998) applied equation (2.2) to calculate the job accessibility for low-wage workers. The author also gave additional proof to highlight an important property of equation (2.2), i.e., "the expected value, or weighted average, of accessibility scores equals to the ratio of the total number of opportunities to the total number of opportunity seekers". The popular two-step floating catchment area (2SFCA) method proposed by Luo and Wang (2003) and its enhanced versions (Luo and Qi, 2009; Luo and Whippo, 2012; Wan et al., 2012) also belongs to this category, where the potential demand is measured based on the catchment area of an opportunity (e.g., health center).

As indicated by its name, utility-based measures are defined following the utility theory, that tackles the problem of users' preferences among a set of choices. Applying this in transportation modeling, it can be understood that an (group of) individual(s) assigns a utility to each opportunity/destination among a choice set and select the alternative with the highest utility. Based on the random utility theory, Ben-Akiva (1979) first proposed the utility-based accessibility measure as the denominator of multinomial logit probabilities, i.e., the log-sum accessibility. The log-sum approach estimates the expected maximum utility that a user of a system would perceive among given choices (Nassir et al., 2016). The equation of this type of measure is denoted below.

$$A_i = \frac{1}{\mu} \ln\left(\sum_{k \in K} \exp(V_k)\right) \tag{2.4}$$

Where the accessibility A_i indicates the desirability of the full choice sets K for a (group of) individual(s) i. V_k is the observed temporal, spatial, and transportation components of the utility of the choice k. μ is the scale parameter. The utility measure is theoretically more attractive because of its strong link with microeconomic theory. Hence, utility-based accessibility can be easily transformed into important economic measures, such as total consumer surplus (Neuburger, 1971) and compensation variation (Small and Rosen, 1981). Apart from the random utility measures, the doubly constrained entropy model (Martínez, 1995) can also be applied for accessibility modeling, where further competition factors can be incorporated. More details of utility-based measures can be found in an insightful review by (Geurs and van Wee, 2004). Generally, the utility-based measure is theoretically sound but difficult to communicate and implement (e.g., very data demanding) and thus are less common in practice.

2.1.4 Calibration of Accessibility Measures

The calibration is a fundamental vehicle of handling the accessibility measures regardless of their types.

For cumulative measures, a threshold distance/time is needed and can be determined from two perspectives: 1) use a predefined threshold to reflect the expectation from analysts and planners, and 2) define the threshold as an acceptable distance based on revealed travel distance/time distributions. The former and latter correspond to the normative and positive implementation of accessibility, respectively (Páez et al., 2012). The normative perspective emphasizes how far people ought to travel, while the positive perspective emphasizes more on how far people actually travel. For instance, half a mile (as a measure of 10 minutes walking) is widely regarded as a reasonable threshold distance to measure accessibility to rail transit stations. However, the actual acceptable distances might be different from this value depending on the urban form and socioeconomic status. Therefore, it has been argued that the positive implementation of accessibility is better for assessing real transit gaps (El-Geneidy et al., 2014; Guerra et al., 2012). Accordingly, a combination of these perspectives would provide insightful knowledge on potential alterations of existing policies and the development of new policies (Páez et al., 2012).

For gravity-based measures, the calibration concerns two major aspects, namely the impedance function and the attractiveness of opportunities. With respect to the impedance function, the parameter (e.g., the standard deviation of Gaussian impedance function) reflects how the impedance affects the destination choice (Handy and Niemeier, 1997). The parameter can be either defined based on convention (e.g., based on published empirical studies) or estimated based on the trip distribution model (Iacono et al., 2008). The opportunity attractiveness is usually measured as its activity capacity, for example, the number of jobs is commonly used as the attractiveness of a workplace. If the individual component is considered during the calibration, the impedance and attractiveness parameters may differ from one user group to another because of socioeconomic differences.

For utility-based measures, the parameters are generally calibrated by means of destination choice models. This type of model relies on detailed travel data (e.g., travel survey data) as the evidence of how users value different choices (i.e., a trip represents a choice). The calibration includes three parts which are commonly included in utility-based measures, namely impedance, opportunity attributes, and individual attributes. As a result, the calibration is more complex and data demanding than gravity-based measures. On the other hand, the utility-based measure provides more flexibility for analysts to test alternative model configurations and compare the relative importance of different factors (Handy and Niemeier, 1997).

Since revealed travel data are commonly used for accessibility calibration, another concern arose because the revealed travel data reflect how residents react to the current circumstances instead of how they would behave under the desired circumstance (Handy and Niemeier, 1997; Morris et al., 1979). For instance, a person who walks longer to reach transit stations does not necessarily mean he/she has a greater willingness to walk. Instead, such behavior may be a result of the shortage of transit services and/or alternative transport modes (e.g., no vehicle). Therefore, it is important to analyze the relationship between the revealed behavior and factors related to transit supply and individual characteristics (e.g., user preferences). Such analysis, in turn, can provide a sound behavioral basis for interpreting the accessibility and policymaking.

2.2 Accessibility Measures of Public Transit

2.2.1 Multiple Aspects of Public Transit Accessibility

This section focuses on studies on public transit accessibility. It starts with a discussion of four aspects characterizing the existing transit accessibility measures: type of measure, influence factors, data required, and scale of analysis.

Type of measure: the transit accessibility measures can be divided into two categories: accessibility to transit services (termed as to-transit accessibility) and accessibility to opportunities via transit (termed as via-transit accessibility). To-transit accessibility measures typically take public transit (e.g., transit stations/lines) as the destination for accessibility measurement, measuring the ease of reaching public transit services. To-transit accessibility is also known as local accessibility (Bhat et al., 2006) or system accessibility (Lei and Church, 2010). Via-transit accessibility, also known as system-facilitated accessibility (Lei and Church, 2010), emphasizes the ease of reaching opportunities by using public transit as the major transport mode.

Influence factors: depending on the application, different influence factors can be combined to formulate an accessibility measure. Regarding to-transit measures, commonly considered factors from the supply perspective include transit service density, road network quality around transit station/stops, service quality of the transit services (e.g., frequency and operation hour). While factors from the demand side include socio-demographic attributes (e.g., population and employment distributions) and travel characteristics (e.g., travel demand rate). For via-transit accessibility, the factors include spatial distributions of facilities, facility characteristics, travel distances/times, travel costs, travel demand rates and socio-demographic attributes. Apart from these hard factors, soft factors, such as safety, lighting, comfort of riding and reliability of transit service, can also be integrated into both types of measures.

Required data: street network and transit network (i.e., transit spatial locations) are two basic datasets to measure the to-transit and via-transit accessibility. Corresponding to the aforementioned factors, further datasets, such as transit timetable/schedule, facility distribution, travel survey (e.g., travel demand and travel rate), and demographical data, can be integrated. The datasets and the modeling approach of accessibility mutually constrain each other.

Scale of analysis: the scale of analysis can be interpreted from two opposite views, either from the supply perspective or from the demand perspective. From the supply perspective, the transit accessibility can be measured by considering a specific transit station/stop, a transit line or a type of transit system. In most cases, transit accessibility is measured at the scale of a certain type of transit system (e.g., bus) or the entire transit system. From the demand perspective, the accessibility can be measured at different spatial resolutions, including point level, zonal level (i.e., subregional level) and regional level (a combination of several zones). At the point and zone levels, accessibility can be defined in two forms, namely accessibility of a pair of OD, and accessibility from one origin to all potential destinations (i.e., integral accessibility (Morris et al., 1979)). A higher level of accessibility can be calculated by aggregating the corresponding lower level of accessibility. For example, by summing the transit accessibility for all the subregions of a city, the transit accessibility for the entire city can be derived (Fu and Xin, 2007; Lei and Church, 2010).

Based on the above four aspects, existing studies related to transit accessibility are reviewed, and the results are listed in Table 2.1. In what follows, detailed analyses toward to-transit and via-transit accessibility are given.

2.2.2 Accessibility to Public Transit

The coverage-based measure is probably the most common and direct approach of combining supply and demand factors into an integrated to-transit indicator. The coverage-based measurement generally includes three steps: 1) defining and measuring the transit catchment areas (TCAs); 2) measuring the population covered by TCAs and 3) defining accessibility for a zone/region based on the population being covered.

1) Defining and measuring the TCAs

The catchment area of a transit represent geographical areas around the transit that the majority of users are typically be found (Lin et al., 2016). They can be defined at transit station level with examples in (El-Geneidy et al., 2010; Kittelson and Associates, 2003), and at transit route level with examples in (O'Neill et al., 1992; Polzin et al., 2002). As people access transit services via transit stops/stations, it has been proved that transit stops/stations provide a more accurate estimation of the coverage of catchment areas (Horner and Murray, 2004). The route/system level of catchment

areas can be calculated by aggregating the corresponding station catchment areas. Since catchment areas are commonly represented as a buffer area around the transit station, the key task of catchment area measurement is to decide the buffer distance/time (termed as cut-off distances/times). Traditionally, conventional cut-off distances used by analysts/planners for bus stops and rail stations are 400 m (0.25 mile) and 800 m (0.5 mile), corresponding to 5 minutes and 10 minutes of acceptable walking times (assuming an average walking speed of 5km/h) (Bhat et al., 2006). The buffer distance can be measured by using either the Euclidean distance or the network distance. According to previous studies (Foda and Osman, 2010; Gutiérrez and García-Palomares, 2008), the latter can generate a more accurate catchment area because people need to travel along roads in the real world. The Euclidean buffer-based method usually overestimates the sizes of catchment areas. As urban forms and demographic characteristics vary across space and time, conventional cut-off distances are adjusted according to the application scenario. The cut-off distance can be considered either as a reflection of planners' expectations or as a reflection of people's travel behavior (Páez et al., 2012). The latter is regarded as an effective means of identifying actual transit accessibility. A combination of these two perspectives can be used to identify the gaps between transit planning and real use (Páez et al., 2012). Hence, much effort has been made toward measuring more realistic cut-off distances/times based on travel survey data, examples include (El-Geneidy et al., 2010; Kittelson and Associates, 2003; Zhao et al., 2003). As the detailed trip routes are usually unavailable in survey-format travel data, a few studies tried to introduce GPS trajectory data to measure transit access distances to overcome this disadvantage (Lin et al., 2019; Zuo et al., 2018). More details regarding the definition of transit walkable distance can be found in a recent review (van Soest et al., 2019).

2) Measuring population covered by TCAs

Once the catchment areas are generated, the population being covered by them can be measured. The census data are commonly used as the input population data because of their easy availability. For a catchment area, the overlapped census units (e.g., census tracts) are identified at first. The total population covered by the catchment area can be measured by summing up the ratioed population in overlapping units. As the assumption of uniformed population distribution may be unrealistic, several studies have tried to model a more realistic population distribution by considering additional information. For example, O'Neill et al. (1992) relieved this issue by using the network ratio to substitute the area ratio to estimate the population covered by catchment areas. Biba et al. (2010) used the dwelling unit ratio between a parcel and a census block to estimate the population of a parcel. The population covered by a catchment area was then the sum of all the population of parcels within it. To consider the distance decay effect within the catchment area, Zhao et al. (2003) proposed to weigh the covered

population by using a spatial decay function, thus, to overcome the potential overestimation of the covered population.

3) Defining zonal/regional accessibility

Based on the population covered by transit systems in a region, the corresponding population coverage ratio can be derived and used as the indicator of transit accessibility for the region. Specifically, a higher proportion of the population being covered means better public transit accessibility. In addition to the accessibility assessment at the regional level, the population coverage ratio can be measured at the zonal level (e.g., transit analysis zones) for comparative accessibility assessment between different zones. In such a case, the population coverage ratio of a zone can be calculated directly based on its area covered by TCAs and the corresponding population density (for example, (Polzin et al., 2002)).

The above described is a basic version of the coverage-based measurement which mainly concerns with the spatial aspects of transit supply. The quality of transit services, such as the service frequency and hours (Currie, 2010; Polzin et al., 2002; Rood and Sprowls, 1998), can also be integrated into the accessibility measures (see Table 2.1 for details). Generally, higher transit frequencies and longer service hours represent better access to transit systems. For instance, the time-of-day-tool (Polzin et al., 2002) weighed the service frequency of each hour by the corresponding travel demand rate and tolerable wait time. The covered population by transit routes was weighed by the daily trip rate. Moreover, in addition to using the general population covered by catchment areas as the indicator, transport-disadvantaged user groups are particularly interesting for accessibility analysis because public transit is regarded as a type of social welfare and a tool for promoting social equality (Currie, 2010).

The coverage-based analysis is commonly measured at relatively coarse spatial resolutions (e.g., transit analysis zone). For measuring fine-grained accessibility, the London Borough of Hammersmith and Fulham developed the indicator: public transport accessibility level (PTAL). The PTAL jointly considered walking distances to transit services (i.e., the nearest station of a transit line/route), average waiting time (i.e., half of the headway) and multiple transport modes (Kerrigan and Bull, 1992). The PTAL is measured at Ordnance Survey grid base and thus can support comparisons of relative accessibility for grids within a Borough. Smaller grids can facilitate the accessibility comparison for grids within a catchment area. Wulfhorst et al. (2017) used 20 * 20 m grids to measure grid-level accessibility of public transit systems by considering closeness to reachable stops, stop types, service frequencies, average travel time to other stations and the number of transfers.

To incorporate competition factors into transit accessibility, Langford et al. (2012) adapted the 2SFCA method (Luo and Wang, 2003) to measure accessibility to transit

stations. The competition between potential demand locations for transit service is reflected by the supply-to-demand ratio, where the supply is represented as the service frequency, and the potential demand is modeled as the weighted population covered by the transit catchment area. Along the line of 2SFCA-based transit accessibility analysis, Xu et al. (2015) emphasized the significances of temporal dimension in modeling the transit demand and supply, where the supply is represented as a combination of transit frequencies and vehicle sizes, and the demand for a traffic zone is measured by summing up the travel demand to and from the traffic zone. Kyung et al. (2018) used mobile phone data to measure the transit demand by excluding population on the road area and measure the transit supply as a combination of the service frequencies, vehicle sizes, and occupy rates.

2.2.3 Accessibility to Opportunities via Transit

This type of accessibility emphasizes using public transport as the major transport mode (i.e., a public transport chain) to reach opportunities. As a special case of accessibility measurement, the via-transit accessibility can be measured by cumulative (Benenson et al., 2010; Lei and Church, 2010), gravity-based (Fayyaz et al., 2017; Fransen et al., 2015) or unity-based measures (Bhat et al., 2006).

Modeling the travel impedance of transit has been a core research question of via-transit accessibility related studies. A public transit journey consists of three sub trips: access transit trip, on transit trip and egress transit trip. Hence, the impedance for different trips can be measured in the same unit or multiple units. For instance, Pitot et al. (2006) developed a land use & public transport accessibility index to measure the to-transit and via-transit accessibility. The via-transit accessibility from a land parcel to reach a certain type of destination is decided based on the walking distance to transit and transit travel time.

More commonly, travel time is used as the unit to measure the total impedance of all three trips. The access and egress times usually are measured based on the access distance and assumed walking speed. The transit time can be either estimated based on travel surveys or transit schedules (Mavoa et al., 2012; Pitot et al., 2006). The latter is typically achieved by using GIS technologies. Furthermore, waiting time at access station, transit transfer time and decay time need to be considered when measuring the total transit time. In addition to these non-monetary impedances, monetary costs can also be integrated into the impedance because users need to pay for their transit trips. A common means to combine the monetary costs and non-monetary impedances is to use the generalized transport cost. For instance, Currie (2004) measured the generalized transport cost of public transit by considering the walking access/egress time, transit fare, waiting time, value of time, and transfer time.

The transit frequency and service hour may vary according to the day of the week and the time of the day. In light of this, much effort has been made toward modeling more realistic transit travel time by considering the detailed departure time and thus to integrate the temporal disparity of accessibility (Fayyaz et al., 2017; Fu and Xin, 2007). For instance, Fu and Xin (2007) measured the travel times of transit for both directions of a round trip based on the desired arrival time to a destination and the desired departure time from that destination. The accessibility from an origin to a specific destination is measured as the average travel time in both directions. As the specific travel time is given, waiting time can be estimated according to the time of arriving transit stops and the scheduled departure time. Such estimation is more realistic than using half of the headway as the estimation. More recently, the increasing availability of transit data in General Transit Feed Specification (GTFS)[1] format has further facilitated the time-dependent travel time and accessibility measurement. GTFS is a data specification developed by Google for transit agencies to publish transit schedules and associated geographic information. Recent examples that use GTFS data for time-dependent accessibility analysis can be found in (Fayyaz et al., 2017; Fransen et al., 2015; McGurrin and Greczner, 2011).

In addition to the gap analysis from the perspective of supply and demand (e.g., (Currie, 2004)), the gap analysis between public transit and car driving is of special interest for some researchers. Because a major aim of improving transit accessibility is to reduce the car travel. Fu and Xin (2007) measured the transit service indicator (TSI) between an origin-destination (OD) pair as the ratio between the total travel times by auto and transit. Based on the TSIs of individual OD pairs, the TSI between two activity zones, the TSI from one zone to all desired zones, and the TSI for the entire service area can be measured. Similarly, Lei and Church (2010) compared the accessibility between auto and transit of a pair of OD to explore the gaps between transit and car driving. Benenson et al. (2010) defined the access/service area around an origin/destination as a combination of areas that contain reachable destinations/origins via a transport mode. By comparing the access area ratio and service area ratio between bus and car, the gaps between these two modes can be identified. The access/service area ratio of an origin/destination can also be measured based on a specific type of desired destinations/origins.

[1] https://gtfs.org/

Table 2.1 Review of selected studies related to public transit accessibility.

Author	Measures	Factors	Major Data	Spatial scale of analysis	Highlight	Type of measure
(Kerrigan and Bull, 1992)	public transport accessibility level (PTAL)	-walking distances (in catchment area) -average waiting time -population distribution	-street network -transit network -transit timetable -census data	spatial grids	-easy to implement -finer scale of analysis -waiting time integrated	To transit
(Rood and Sprowls, 1998)	local index of transit availability (LITA)	-route coverage -route frequency -route capacity	-transit network -transit timetable -transit capacity	census tracts/transit analysis zones	-comfort and convenience are considered by using the capacity	To transit
(Polzin et al., 2002)	time-of-day-tool	-route frequency -tolerable waiting time -travel demand rate by hour -route coverage -population and employment -daily trip rate	-transit network -transit time table -demographic data -personal transportation survey	zones for regional planning	-the temporal travel demand is considered -gap identification for socially disadvantaged users	To transit
(Kittelson and Associates, 2003)	transit capacity and quality of service manual (TCQSM)	-stop coverage (weighted by terrain factors, street connectivity, population characteristics crossing difficulty) -household and job density	-street network -transit network -terrain's elevation data -demographic data	transport analysis zones	adapted sizes of stop service areas by using weighting factors	To transit
(Currie, 2004)	-network supply -need score	- trip purposes - walking time - transit time & fare - waiting time - value of time - demographic characteristics	-street network -facility distribution -transit network & schedules -travel survey -demographic data	census collector districts	-generalized travel cost - evaluating transit performance for transport-disadvantaged people	Via transit
(Pitot et al., 2006)	land use & public transport accessibility index (LUPTAI)	-walking distance to transit -different types of modes -transit frequency -transit travel time -different types of opportunities -population density	-street network -transit network and timetable -facility distribution -census data	land parcels	a combination of walking time and transit travel time/frequency	-To transit -Via transit
(Bhat et al., 2006)	transit accessibility measure and index (TCM and TCI)	-alternative destinations -trip purposes -walking distance -total transit travel time by different user groups	-street network -transit network -facility distribution -on-board transit survey data	-point level, i.e., origin-based -zone level	-utility-based accessibility measure for individual, -different levels of aggregations	Via transit

Author	Measures	Factors	Major Data	Spatial scale of analysis	Highlight	Type of measure
(Fu and Xin, 2007)	transit service indicator (TSI)	- door-to-door travel time by transit and walking - door-to-door travel time by auto -travel demand by time -population and employment	-street network -transit network data -demographic and employment -travel demand data	-point level a pair of OD -activity zones -entire transit service areas	-relative transit accessibility by comparing with auto -time-dependent travel demand as a weighting factor for zone-level accessibility	Via transit
(Currie, 2010)	-supply index -needs scores	-transit coverage by different modes -transit service level (number of vehicles per week) - socioeconomic characteristics	-transit network and timetable -socioeconomic importance -census data	census collector districts	gaps in public transport provision for socially disadvantaged people	To transit
(Lei and Church, 2010)	accessibility isochrones map	-specific departure times of a round trip - total travel time including walking, transfer, transit and waiting times	-street network -transit network and schedules -street network -destinations	-point level, i.e., origin-based -regional level	-GIS-based travel time modeling -specific departure times from double directions of a round trip	Via transit
(Sha Al Mamun and Lownes, 2011)	composite public accessibility index	-service coverage -service frequency -travel demand by hour -tolerable waiting time -demographic data -daily trip rate	-transit network and schedules -street network -destinations	census tracts	a weighting function for combining three different indicators	To transit
(Langford et al., 2012)	two-step floating catchment area (2SFCA)	-number of buses of a line -walking distance within service areas -population distribution	-transit network and timetable -street network -demographic data	population statistical areas	-competition for transit between demanding locations -adaption of the 2SFCA method by considering the transit characteristics	To transit
(Mavoa et al., 2012)	-public transport and walking accessibility index (PTWAI) -average transit frequency	- total transit travel time - different types of facilities	-street network -transit network and timetable - facility distribution	-land parcel level -mesh block	combination analysis of PTWAI and average transit frequency at the parcel level	To transit

Author	Measures	Factors	Major Data	Spatial scale of analysis	Highlight	Type of measure
(Xu et al., 2015)	temporal 2STFCA	-trip production rate -trip attraction rate - travel time to transit stop - passenger carrying capacity	-transit network and timetables -census data -travel survey data	transit analysis zones	time-dependent transit demand and supply	To transit
(Fransen et al., 2015)	gravity-based accessibility index	-total travel time -trip purposes (different facilities) -population density	-facility distribution -census data -GTFS data	transit analysis zones	GTFS-based total travel time measurement	Via transit
(Saghapour et al., 2016)	public transit accessibility index (PTAI)	-walking catchment area -walking distance -transit frequency	-transit network and timetable -demographic data	census collector districts	integrating transit population coverage with public transit accessibility level	To transit
(Wulfhorst et al., 2017)	adapted LUPTAI	-walking distance to transit stations -transit station types -transit service quality -population density	-transit network -street network -census data	spatial grids	integrating service frequency, average travel time to other stations, and the number of transfers as a service quality indicator	To transit
(Kyung et al., 2018)	adapted 2STFCA	-walking distances -vehicle occupancy rate -transit frequency -number of bus lines -dynamic population density	-transit network and timetable -transit boarding and alighting data -mobile phone data	spatial grids	using mobile phone data to estimate the dynamic demand	To transit

2.3 Spatial Movement Data

The rapid development of information communications technology provides unprecedented chances for collecting massive geospatial data, such as GPS trajectory data (e.g., taxi trajectories), geotagged social media data (e.g., tweets with location information), mobile phone data, and smart card data. These geospatial data have been widely used to explore various aspects of our society, such as human activity patterns, transportation use, land use characteristics, and social relationships. The following sections focus on the analysis of GPS trajectory data and smart card data because they are two major types of mobility data used in this thesis.

2.3.1 GPS Trajectory Data

A GPS trajectory represents a trace of a moving object that recorded by GPS or GPS-enabled devices, which is usually represented as chronologically ordered points as $\{p_1, p_2, \dots, p_n\}$. A point p_i consists of a coordinate and a timestamp which can be represented as $\{x_i, y_i, z_i, t_i\}$, where (x_i, y_i, z_i) typically correspond to $(latitude, longitude, altitude)$. Depending on the application, additional information such as direction can be included in a point, and the altitude may be ignored. A GPS trajectory can be generated by a pedestrian, a vehicle (e.g., bike or taxi), or an animal.

Trajectory mining is a hot research topic in several disciplines, such as computer science, GIS science, and transportation, because of its broad applications. From the application domain of GIS science and transportation, trajectory data are applied to a series of applications, such as travel time estimation (Jenelius and Koutsopoulos, 2013; Wang et al., 2014), road map construction (Ahmed et al., 2015; Biagioni and Eriksson, 2012), and movement pattern mining (Antoniou et al., 2018; Ding et al., 2016; Zhang et al., 2019). As compared with traditional survey-based data such as the self-reported travel surveys, GPS trajectory data usually provide a finer spatiotemporal scale of human movement. For instance, self-reported travel surveys tend to suffer from the problem of imprecise trip details, such as imprecise departure/arrival times and missing traveling routes. Furthermore, as trajectory data can be automatically collected by GPS/GPS-enabled devices, it is much easier to acquire big data in terms of sampling size and duration of data collection. On the other hand, travel data in trajectory format alone also suffer from certain limitations related to uncompleted semantic information (e.g., unknown travel purposes) and information redundancy (e.g., the owner forgets to shut down the device when there is no movement). Due to the unique characteristics of GPS trajectory data (e.g., GPS errors) and application-specific requirements, many techniques are developed to support trajectory data processing, managing, and mining. The following two sub sections are dedicated to explaining the basic trajectory

processing techniques relevant to this thesis. More techniques regarding trajectory data managing and mining can be found in a review by (Zheng, 2015).

2.3.1.1 Basic Processing Techniques of GPS trajectories

Noise filtering: due to sensor noise and other factors (e.g., signal occlusion by high-rise building), raw trajectories may contain some unusually deviating GPS points, or outliers. Noise detection can thus be regarded as a special issue of outlier detection. A natural method to detect such noises is to compare the speeds of a point with its predecessor and successor, if speeds from both sides are larger than a specific threshold, the point can be regarded as noise point. Similarly, a density can be defined for each point by counting points within a certain distance and points with density smaller than a threshold can be regarded as noise. Apart from outlier detection-based methods, noise filtering can also be achieved by using Kalman and Particle filters. For instance, the Kalman filter can generate an estimation of trajectory with fewer noises based on the measurement and motion models. Detailed procedures regarding the application of Kalman and Particle filters for noise reduction can be found in (Lee and Krumm, 2011).

Stop/stay point detection: during the moving, an object may stay at one or more locations for a certain period of time. For instance, taxi drivers need to wait when the traffic light is red, and a commuter may stay at a restaurant for breakfast on the way to work. Such stay points may be of special interest for some applications, such as identifying popular points of interest and detecting traffic congestion locations. On the other hand, for applications, such as travel time/distance estimation, it is necessary to exclude stop points to derive a more precise estimation. An intuitive approach for detecting stop points is to find consecutive trajectory points with a speed below a threshold. The speed-based method is effective if a user stays at a location without movement, and the GPS gives an accurate localization. In the case of a user wander around a location, the speed-based method is likely to lose its effectiveness. Under such a condition, additional factors, such as the moving (Euclidean) distance and moving direction, can be considered to improve the stay point detection. For instance, Li et al. (2008) designed an algorithm to detect stay points by finding a set of consecutive points within a certain distance to an anchor point for a certain period of time. Sultan et al. (2017) measured the directions between an anchor point and points around it and assign these directions into different slices. If the slice number of the anchor point is larger than a predefined threshold, then the anchor point is regarded as a stop point.

Trajectory compression: a higher sampling rate (i.e., a short sampling interval) means a fine-grained trajectory and requires larger storage and computational power. Therefore, a desired trajectory compression always seeks to make a compromise between data size and accuracy. The compression can be conducted either offline or online. For the offline practice, a given trajectory is compressed by discarding less

important points. The Douglas-Peucker algorithm (Douglas and Peucker, 1973) is one of the most popular algorithms to serve this purpose. For the online practice, the compression takes place in a real-time by retaining certain newly generated GPS points. The retaining criteria can be based on the distance metric (Meratnia and Rolf, 2004) or speed and direction (Potamias et al., 2006). For instance, Meratnia and Rolf (2004) applied a heuristic of the Douglas-Peucker algorithm to an open window to keep points above a certain distance to the segment of the first and last points in the window.

2.3.1.2 Map Matching Basics

Map matching is the process to align raw GPS trajectory points with the road network and reconstruct the corresponding travel route as a sequence of road network edges. Early map-matching algorithms can be categorized into geometric, topologic, and probabilistic algorithms (Zheng, 2015). As an advanced combination of these aspects, the Hidden Markov Model (HMM) based method proposed by Newson and Krumm (2009) and Lou et al. (2009) has been widely adopted since 2009, because of its elegant integration of geometric, topologic, GPS errors and other factors (e.g., speed limitation). Since then, various studies are devoted to improving the HMM-based algorithms, either from the perspective of accuracy (Li et al., 2013; Yuan et al., 2010) or from the perspective of efficiency (Huang et al., 2013; Yang and Gidófalvi, 2018).

Given a trajectory $\{p_1, p_2, \dots, p_n\}$, the HMM-based algorithm firstly iterate each point p_i to find its candidate edges $\left(e_i^1, e_i^2, \dots, e_i^{N_i}\right)$ within a certain distance r and the candidate points $\left(c_i^1, c_i^2, \dots, c_i^{N_i}\right)$ can be identified by projecting point p_i to the corresponding candidate edges. For a point p_i, the number of candidate edges is N_i; thus, the total number of candidate path $N_{\text{cp}} = \prod_{i=1}^{n} N_i$. As illustrated in Figure 2.1, the processing of HMM-based map matching can be modeled by a transition graph, and the goal is to find the most probable path.

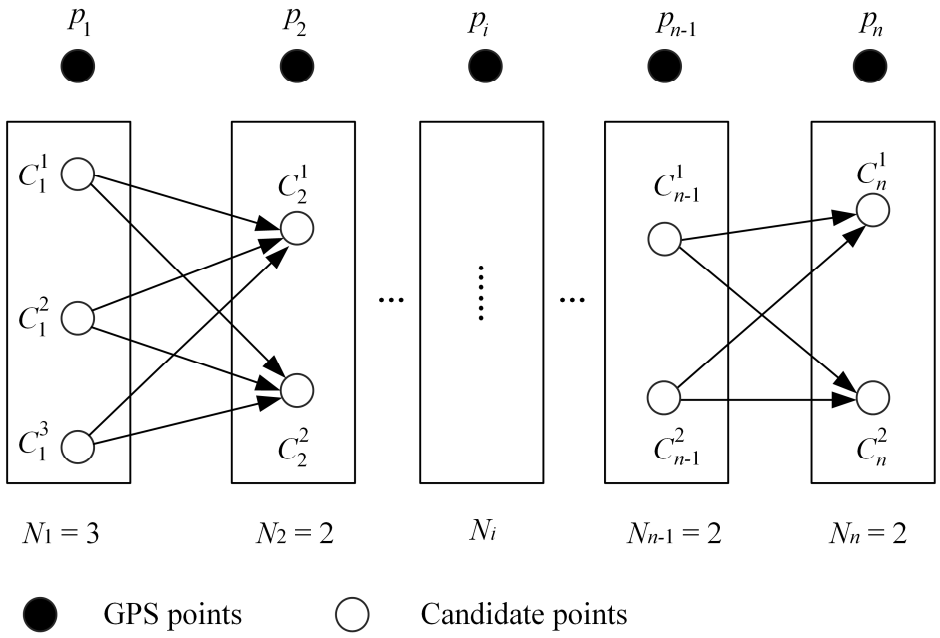

Figure 2.1. Illustration of the transition graph corresponds to a trajectory map matching.

Given a candidate edge e_i^j of p_i, there is an emission possibility reflecting the likelihood that p_i is actually a sampling point on it. The possibility is measured by assuming a Gaussian distribution of GPS errors, which is denoted below.

$$ep_i^j = \frac{1}{\sqrt{2\pi}} e^{-\frac{\left(d\left(p_i,\ c_i^j\right)-\mu\right)^2}{2\sigma^2}} \tag{2.5}$$

Where $d\left(p_i,\ c_i^j\right)$ is the Euclidean distance between the two points p_i and c_i^j. μ and σ are corresponding mean and standard deviation of the Gaussian distribution of GPS errors, respectively. By defining the emission probability, candidate edges near to a GPS point are potentially the real traversed edges.

To integrate the topologic information, a transmission probability is defined for a pair of neighboring candidate points c_{i-1}^s and c_i^e.

$$tp(c_{i-1}^s \rightarrow c_i^e) = \frac{d(c_{i-1}^s,\ c_i^e)}{ns(c_{i-1}^s,\ c_i^e)} \tag{2.6}$$

Where $d(c_{i-1}^s,\ c_i^e)$ and $ns(c_{i-1}^s,\ c_i^e)$ represent the Euclidean distance and the shortest distance along the road network between two neighboring candidate points, respectively (see an example in Figure 2.2). The rationale behind this definition is based on the observation that people tend to choose the shortest path (Lou et al., 2009).

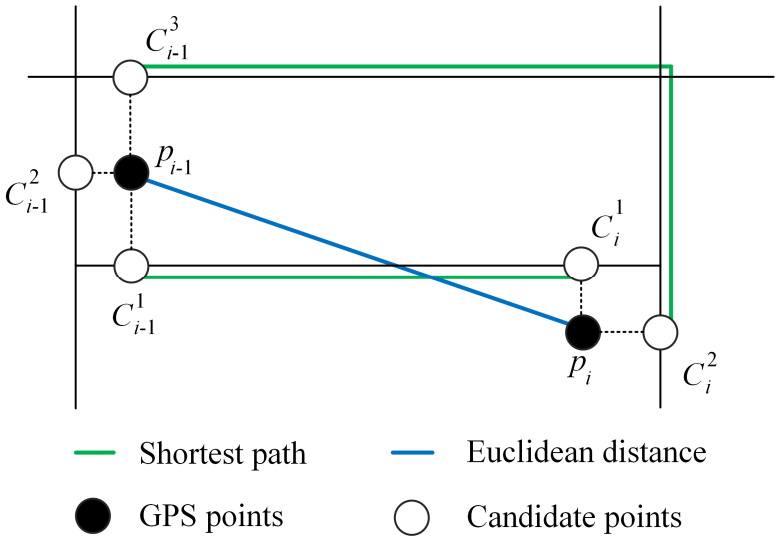

Figure 2.2. Example of the transition between two neighboring points.

By combing the emission probability and transmission probability, an integral probability for the transition from c_{i-1}^s to c_i^e can be measured as their product.

$$itp(\mathrm{c}_{\mathrm{i}-1}^{\mathrm{s}} \rightarrow \mathrm{c}_{\mathrm{i}}^{\mathrm{e}}) = ep_i^e * tp(c_{i-1}^s \rightarrow c_i^e) \tag{2.7}$$

Given a candidate path CP with a sequence of candidate points as $\left(\mathrm{c}_1^{s_1}, c_2^{s_2}, \ldots, c_n^{s_n}\right)$, the overall probability is calculated as:

$$P(\mathrm{CP}) = \sum_{i=2}^{n} itp(\mathrm{c}_{\mathrm{i}-1}^{\mathrm{s}_{i-1}} \rightarrow \mathrm{c}_{\mathrm{i}}^{\mathrm{s}_i}) \tag{2.8}$$

In this way, the candidate path with the largest overall probability is treated as the optimal map-matching result. In practice, there is no need to iterate all the N_{cp} candidate paths. The Viterbi algorithm (Forney, 1973) can be used to find the optimal path efficiently.

2.3.2 Smart Card Data

The wide deployment of automated fare collection (AFC) systems offers an easy approach to continuously collecting massive smart card records regarding public transit use. In addition to the aim of revenue collection, smart card data have been used for a series of applications related to transit performance evaluation and network planning (Jang, 2010; Trépanier et al., 2009), travel pattern analysis (Ma et al., 2013; Seaborn et al., 2009), transit time and reliability analysis (Jang, 2010; Sun et al., 2016; Zhao et al., 2013) and transit demand modeling (Sun et al., 2017; Tu et al., 2018).

The procedures of using a smart card within a public transport chain are illustrated in Figure 2.3. As showed in Figure 2.3 (a), a user may be required to swipe in before

his/her boarding and swipe out after his/her alighting. For instance, metro systems usually take this form and smart card readers are equipped at specific entry/exit points. Otherwise, smart card readers are equipped inside vehicles, and users are thus required to swipe in after their boarding and swipe out before their alighting. The latter form is more common in bus and tram systems. Such a distinction is important for applications, such as smart card-based travel time estimation and transit reliability modeling, because travel times measured by smart card records are based on the time difference of swiping in and out. The AFC systems can be categorized into entry-only systems and entry-exit systems. The entry-only system only requires users to swipe the card at the beginning of the travel (e.g., New York Subway), while the entry-exit system requires to swipe at both ends of the transit (e.g., London Underground and Shanghai Metro). The entry-only system is more suitable for flat rate fare systems and the entry-exit system is usually required by distance-based fare systems.

The processing of smart card data usually starts with a data cleaning procedure to remove error transaction records, including duplicate transaction records (e.g., swipe in and out at the same station and time) and uncompleted transaction records (e.g., missing transaction time). After the data cleaning, a common processing procedure is to reconstruct transit trips as they are the basis for analyzing travel patterns either at the individual or at transport system levels (e.g., OD matrix between transit stations). For entry-exit systems, as the boarding and alighting information are recorded in transaction records, it is easy to construct a transit trip by chronologically ordering transaction records of a smart card user. Then, every two consecutive transaction records can be organized as a trip (Lin and Zhu, 2019). By combining multiple consecutive trips, a journey consisting of several individual trips can be constructed. For example, a bus-metro journey can be recovered by combining the corresponding bus and metro trips. Such construction is usually based on the assumption that walking distance and time between the preceding alighting location and current boarding location should be limited within a certain threshold. For most of the metro systems, no swiping is required for transferring between different lines; hence, trips constructed by two consecutive records may contain additional transfer trips in between.

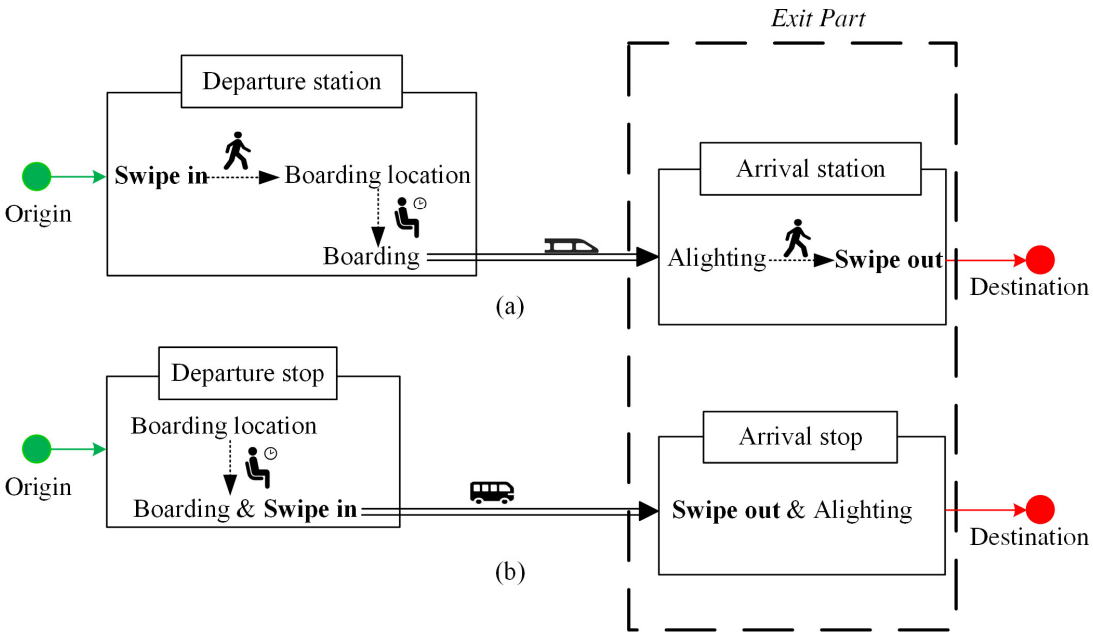

Figure 2.3. Procedures for using a smart card to ride public transit. (a) example for a metro system, and (b) example for a bus system.

For entry-only systems, the trip construction is more difficult because no information regarding the exit/alighting is recorded by the smart card records. Additionally, the entry/boarding information may also be incomplete, for instance, the boarding stops of bus trips are not included in smart card records in a number of Chinese cities such as Beijing, Chongqing, and Nanjing (Ma et al., 2012). Therefore, many studies have been devoted to developing methods to infer the missing OD information. For the estimation of boarding location, the boarding time and additional information, such as transit schedules and vehicle trajectories, can be integrated to infer the boarding locations (Gordon et al., 2013; Ma et al., 2012; Tu et al., 2018). For the estimation of alighting information, most studies have adopted trip-chaining methods proposed by (Barry et al., 2002) under two key assumptions:

1) A high percentage of users start their trips at the alighting stations of their preceding trips.

2) Most users usually go back to the first departure station at the last trip of the day.

These two assumptions are widely accepted as the basis of destination inference. To be more realistic, some studies tried to relax these two assumptions based on applications under consideration. Specifically, the boarding station/stop of the current trip may be a new one that is near to the alighting station/stop of the preceding trip. Similarly, the second assumption can be relaxed as a user may return to a station/stop near to the

first departure station of the day (Trépanier et al., 2007). An insightful evaluation of commonly used OD estimation algorithms is given by (Alsger et al., 2016).

3 Biking Distances at Individual Transit Stations

The acceptable distance (or cut-off distance) of transit stations is a fundamental element for the assessment of accessibility to transit, either using coverage-based (see Chapter 4) or grid-based measures (see Chapter 5). This chapter aims to propose methods to measure the acceptable distances of individual transit stations by using trajectory and smart card data. Furthermore, to interpret the disparity of acceptable distances, regression models are used to explore the associations between the biking distances of individual metro stations and potential factors.

Section 3.1 describes the necessity of measuring biking distances at individual stations for accessibility assessment and related technical challenges. The study area and data preparation are described in Section 3.2. Section 3.3 explains how to identify bike-and-ride trips based on bike trajectory and smart card data. Section 3.4 illustrates the methods of bike trajectory processing, especially focusing on the trajectory map matching. Analytical results regarding the identified bike-and-metro trips in Shanghai are shown in Section 3.5. Section 3.6 summarizes this chapter. Part of the materials in this chapter have been published in (Lin et al., 2019).

3.1 Challenges of Measuring Biking Distances

As an important approach of promoting access to public transit, the integration of bike and public transit (i.e., bike-and-ride) has been advocated by many governments. Depending on the stage of bike use, bike-and-ride can take three forms: bike-ride, ride-bike, and bike-ride-bike (BRB). The recent popularization of dockless bike-sharing service has further promoted the integration of bike and public transit because the dockless shared bikes are widely used for connecting with public transit (Shen et al., 2018; Zhou et al., 2018). To date, most bike-and-ride related studies (Lee et al., 2016; Martens, 2004; Pan et al., 2010; Wang and Liu, 2013), have been focused on private bikes and dock-based shared bikes. Inadequate efforts were reported for the

integration between dockless shared bikes and public transit. Additionally, most of the existing studies are based on survey data, in which the detailed traveling routes are usually missing. As a result, bike trip lengths are usually estimated by using the shortest path algorithm.

Fortunately, the biking trajectories of dockless shared bikes can be easily recorded by the embedded GPS devices. Thus, trajectory data can be used to investigate the integration of dockless shared bikes and public transit, providing a new chance to derive more accurate acceptable biking distances. The variable "acceptable biking distances" of individual stations obtained from trajectory data offer a fine-grained basis to model the actual accessibility (Páez et al., 2012), as compared with a predefined acceptable distance or a unified value for the entire region. Furthermore, understanding the disparity of acceptable distances at different stations is important for the interpretation of the measured accessibility relying on actual travel data and policymaking (see Section 2.1.4).

The major challenge in using trajectory data to measure the bike distances is twofold: 1) bike trajectories are not specifically collected for transit accessibility analysis; hence, it is necessary to develop a method to extract bike-and-ride trips, and 2) for estimating accurate distances of bike-and-ride trips, we need to construct the real biking paths using the raw trajectories. To tackle the first issue, bike trips used for BRB trips are extracted firstly. Then, the threshold for identifying bike-and-ride trips are decided based on the distribution of the BRB bike trips. To tackle the second issue, the raw bike trajectories are preprocessed by resampling and stop point filtering, and an adapted map-matching algorithm is proposed to align them with road networks. The proposed methods are applied, taking Shanghai as a case study to extract the bike trips intended for connecting with metro systems (i.e., bike-and-metro trips) and to measure biking distances at individual metro stations.

3.2 Study Area and Data Preparation

With a population of 24.2 million as of 2018, Shanghai is the most populous urban area in China, also a global center for finance, innovation, and transportation (Shanghai Municipal Bureau of Statistics, 2019). The central city of Shanghai corresponds to the areas within the outer ring road and has a compact area of 660 km^2 (Figure 3.1 (a)). According to the Shanghai Master Plan 1999–2020, the central city is the urban core of Shanghai, where its six major business districts are located (Shanghai Municipal Government, 1998). Shanghai Metro is a major public transport mode in the city, ranking as the world's longest rapid transit system by route length totaling 676

kilometers as of December 2018[2]. The average daily volume of Shanghai Metro is 10.16 million ridership in 2018 (Shanghai Municipal Bureau of Statistics, 2019). Shanghai is one of the biggest dockless bike-sharing markets in the world. By the end of August 2017, there are more than 1.5 million dockless shared bikes in Shanghai (Xinmin Evening News, 2017) and the shared bikes are widely used to connect with public transit. According to a recent study (Zhou et al., 2018), more than one-third of the respondents shifted from other modes to use shared bikes as the metro access/egress mode after the dockless bike-sharing was launched in Shanghai. These characteristics make Shanghai a representative area for investigating the integration of dockless shared bikes and public transit.

Major data used for measuring the biking distances include bike road network, metro-related data, smart card data, and bike trajectories.

Bike road network: the road network is download from OpenStreetMap (OSM) via the Python package OSMnx (Boeing, 2017) by specifying the network type as "bikeable". To increase data reliability, the downloaded bike networks are assessed by comparing them with randomly selected 50,000 raw trajectories. For each trajectory, the distances from its GPS points to the nearest roads are measured, if the distance for a point is larger than 50, it might indicate missing roads around the point. Google Satellite images and Baidu street views are then jointly used to verify the potential missing roads. Eventually, 10,700 extra road network edges are added to the original network. The final road network contains 74,800 nodes and 106,300 edges.

Metro-related data: metro timetables and basic attributes, including the number of entrance and terminal station information, are collected from the official website of Shanghai Metro. The geographic information of metro stations (e.g., entrance locations) and bus stops around metro stations are collected via Gaode map API (a leading map service provider in China). In total, 1,223 metro station exits/entrances of 301 different stations of 14 metro lines are obtained[3].

Smart card data: the smart card data are used for estimating the average traveling time between metro stations. The dataset covers the transaction records generated in a normal week in 2015 of Shanghai, with a total number of 98.2 million transaction records. Each record includes user ID, date, time, bus line ID or metro station name, transport mode, fee, and discount. The transport mode specifies which transport mode a smart card is used because the smart card in Shanghai can be used for taking various transport modes, such as metro, bus, ferry and taxi. Thus, the records correspond to

[2] Data comes from Shanghai Metro:
http://www.shmetro.com/node49/201812/con115165.htm
[3] To keep consistency with the dockless shared bike data, the metro stations that opened later than 1 October 2017 are ignored, and 3 metro stations located in KunShan (a city near Shanghai) are ignored as well.

metro trips are identified by extracting records with the transport mode as “metro”. The automated fare collection (AFC) system of Shanghai Metro belongs to the entry-exit system, i.e., passengers are required to swipe in before boarding and swipe out after alighting. Hence, both the boarding and alighting stations and times are recorded in the transaction records. A data cleaning procedure is applied to remove error records such as duplicated records and uncompleted records. The transaction records belong to each smart card user are ordered in a chronological sequence. Then, every two consecutive transaction records can be organized as a metro trip. A total of 28.5 million metro trips are identified and the average traveling time between two metro stations is measured accordingly.

Bike trajectories: the trajectory dataset is provided and authorized by one of the leading bike-sharing company, Mobike. As of March 2017, there are over 3.65 million shared bikes owned by Mobike, generating about twenty million trips per day[4]. The dataset used in this thesis is generated by randomly selecting a certain number of users, who specified their registration locations as Shanghai in their personal accounts. After excluding the trips made outside Shanghai, 777,896 trips by 135,239 users are kept, covering 15 days of transactions from September 16th to 30th, 2017. Each trip record includes trip ID, user ID, bike ID, longitudes and latitudes of the origin and destination, timestamps of the origin and destination, and a trajectory consists of sampling points recorded during the trip. Each sample point is represented as a tuple of (longitude, latitude, timestamp).

[4] http://www.sootoo.com/content/670814.shtml

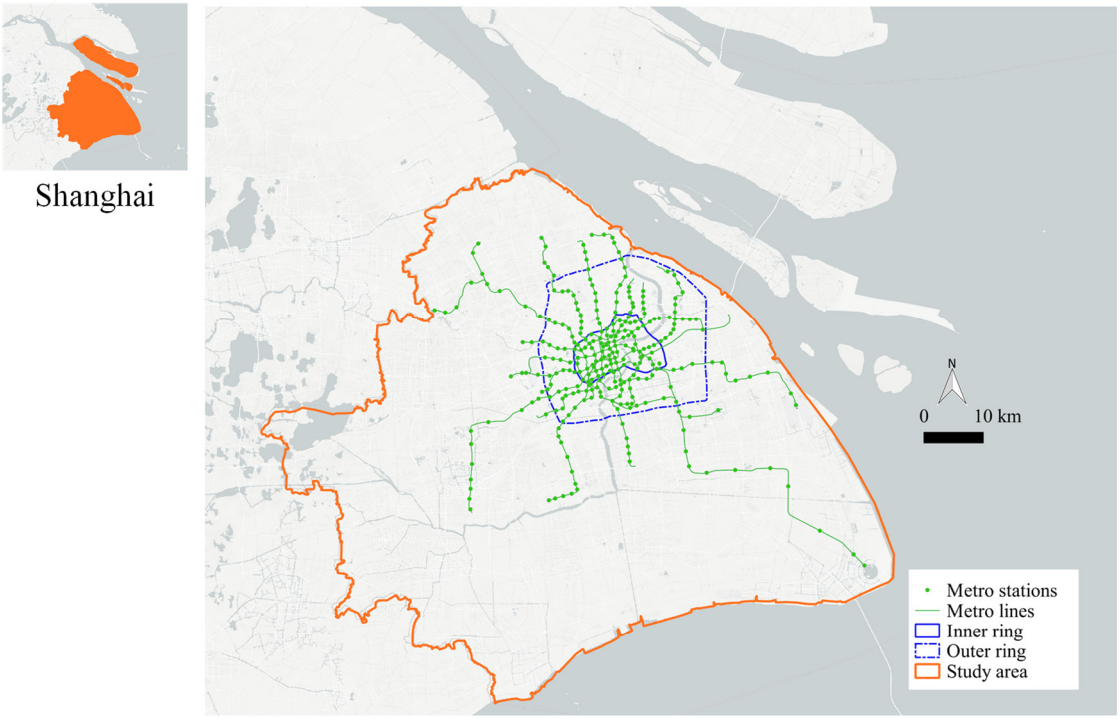

(a)

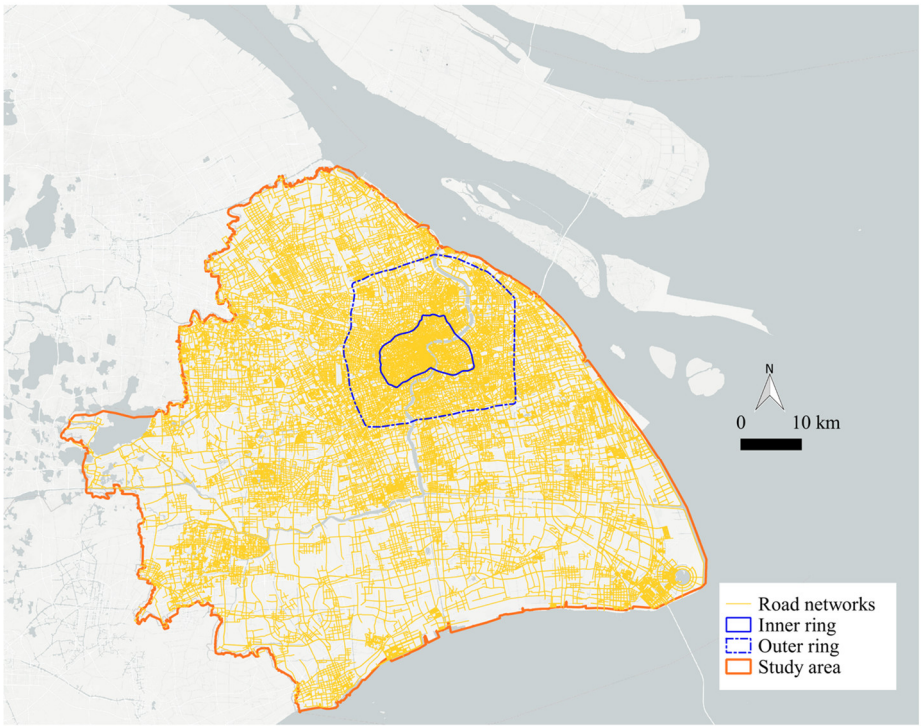

(b)

Figure 3.1. The study area. (a) the metro stations and lines, and (b) the road networks of Shanghai.

3.3 Identification of Bike-and-Ride Trips

Extracting bike trips intended to connect with transit systems is difficult because no clear information is available regarding the purposes of bike trips. A straightforward approach of extracting the bike-and-ride trips of a station is to determine the trips with an origin/destination within a certain distance to the stations. Since transit stations in metropolitan areas (e.g., Shanghai) usually have complex structures with more than one exit/entrance. The entrances of a station, rather than the station center, are thus used to build circular buffers. By dissolving the entrance buffers of a station, the station buffer area can be constructed (Figure 3.2). The key issue here is to determine a suitable threshold for the circular buffer, to reflect how far users usually park/pick their bikes around the station entrance. For an individual bike trip, there is no evidence if it belongs to a bike-and-ride trip or not. However, it is possible to identify BRB trips, i.e., transit trips that use bikes as the access and egress modes. Figure 3.3 illustrated an example of a BRB trip.

To extract BRB trips, potential bike-and-ride trips at the access and egress sides are extracted by setting a relatively large buffer threshold D_{max}. Correspondingly, the sets of the potential access and egress bike trips are represented as A and E, respectively. Supposing we have one potential access trip $a_i \in A$ and one potential egress trip $e_j \in E$, corresponding to transit stations m_i and m_j, respectively. The timestamps of the destination of trip a_i and the origin of trip e_j are denoted as $t_{a_i(d)}$ and $t_{e_j(o)}$, respectively. The time duration between $t_{a_i(d)}$ and $t_{e_j(o)}$ can thus be measured and denoted as $T_{a_i e_j}$. The average traveling time between station m_i and m_j is denoted as $T_{m_i m_j}$, which can be measured using smart card data. Then, the following three criteria can be used to decide if trip a_i and trip e_j belong to the same BRB trip.

- Trip a_i and trip e_j belong to the same user.
- Station m_i is different from m_j, i.e., $m_i != m_j$.
- The difference between $T_{a_i e_j}$ and $T_{m_i m_j}$ should be limited to a certain time duration. Theoretically, $T_{a_i e_j}$ should be larger than $T_{m_i m_j}$ because users need additional time to walk from bike parking locations to swipe in locations and walk from swipe out locations to bike fetching locations. Thereby, the following criterion should satisfy.

$$0 < T_{dif} < \varepsilon, \text{ where } T_{dif} = T_{a_i e_j} - T_{m_i m_j}$$

By iterating all the potential combination of a_i and e_j, the bike trips that belong to the BRB trips can then be identified. The corresponding access and egress trips of the BRB bike trips are denoted as A_{brb} and E_{brb}, where $A_{brb} \subseteq A$ and $E_{brb} \subseteq E$. For a trip from

A_{brb} (E_{brb}), the Euclidian distance between its destination (origin) to the nearest entrance of its corresponding transit station can be measured, assuming users parking (fetching) a bike at the nearest transit entrance. Then, the distances between the bike parking locations and the nearest transit entrances, and the distances between the bike fetching locations and the nearest entrances can be obtained, respectively. Their distributions are used as references to define the circular buffer for extracting bike-and-ride trips (see Section 3.5.1).

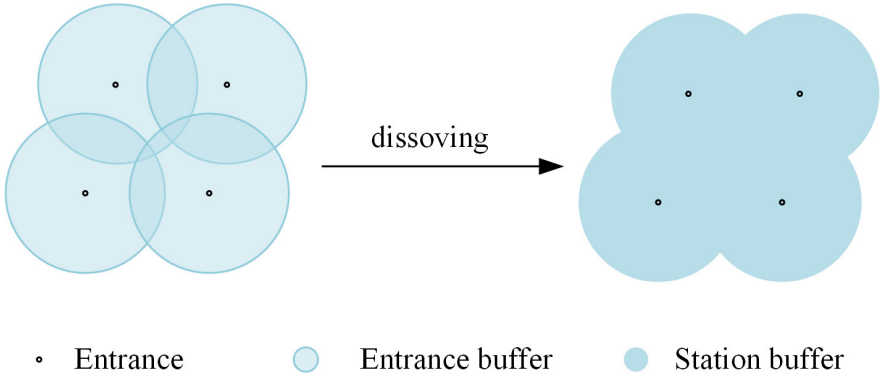

Figure 3.2. Example of constructing the buffer area of a station.

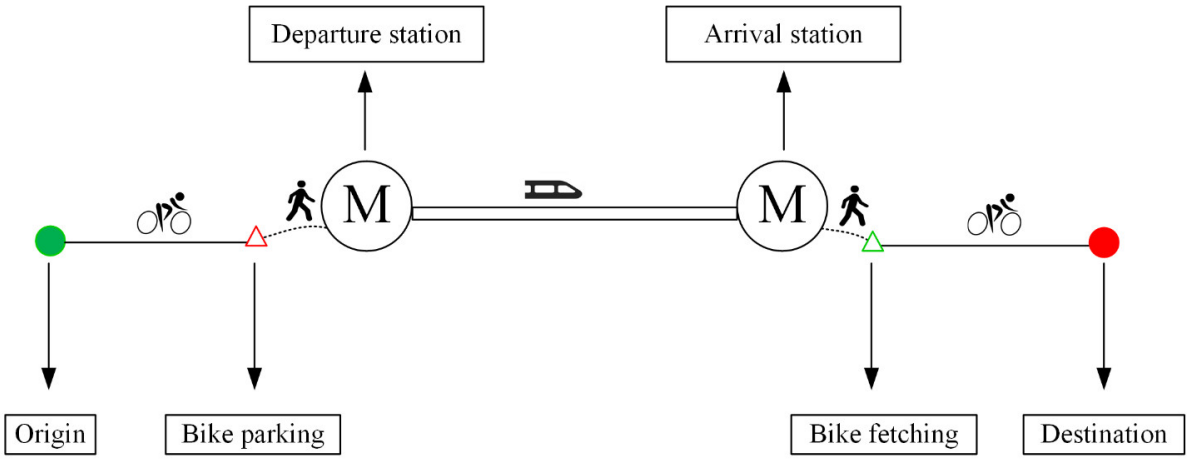

Figure 3.3. Illustration of the bike-ride-bike (BRB) trip.

3.4 Trajectory Processing

3.4.1 Pre-Processing

Resampling: trips with an abnormal length or duration are excluded, i.e., only trips within the length interval of (50 m, 30 km) and with a time duration of larger than 60 s are kept. Since the original bike-and-ride trips are recorded at a high sampling rate (66% trips with a sampling interval under 5 s), resulting in GPS point redundancy and may introduce additional errors in map matching. The raw trajectories are thus resampled to a larger sampling interval. The new interval of the resampling is jointly decided by the original sampling intervals and biking speeds, to achieve a balance between computational efficiency and critical information for map matching.

Stop point removal: as stop points may introduce errors to trajectory map matching and trip distance estimation, they need to be cleaned. The orientation-based stop point detection method proposed by (Sultan et al., 2017) is applied to identify stop points among the trajectories. Specifically, given a trajectory $\{p_1, p_2, \dots, p_n\}$, the distances between every two consecutive points are calculated and represented as $D = \{d_1, d_2, \dots, d_{n-1}\}$, where d_i is the distance between p_i and p_{i+1}. Then, a search radius $r_s = \text{mean}(D) + 2 * \text{std}(D)$ can be defined for the trajectory, where $\text{mean}(D)$ and $\text{std}(D)$ represent the mean and the standard deviation of D, respectively. A circular area centered at a point p_i with a radius of r_s can be constructed, and points within the circular area can be found (denoted as P_i). The circular area is equally divided into eight sectors and each point in P_i is assigned to one of the eight sectors. If P_i are distributed at more than four sectors, the examining point p_i is considered as a stop point because of the discontinuity of moving direction (Sultan et al., 2017). Figure 3.4 illustrates an example of orientation-based stop detection. The middle points (the yellow point on the left and green point on the right) in the center represent the point under examination, and red points represent the corresponding nearby points. Since there are 5 different slices on the left side and 3 different slices on the right side, the examined yellow point is considered as a stop point and the green point is regarded as a normal one.

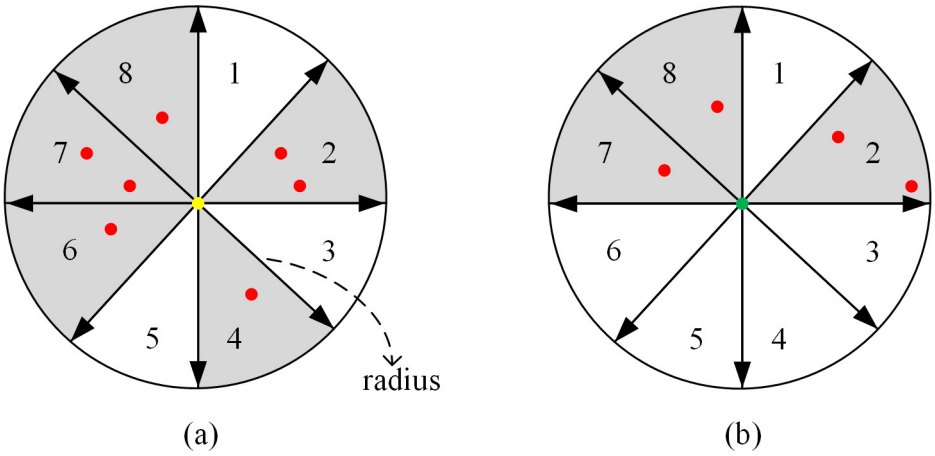

Figure 3.4. Illustration of the orientation-based stop point detection. (a) the examined point (yellow) is identified as a stop point, and (b) the examined point (green) is regarded as a normal sampling point.

3.4.2 Trajectory Map Matching

After the preprocessing, the Fast Map-Matching (FMM) algorithm (Yang and Gidófalvi, 2018) is applied to reconstruct the actual routes of the bike-and-ride trips from the trajectories. The FMM algorithm is selected because it offers an efficient approach to align a large number of trajectory points and provides an open-source implementation. The FMM is an adapted version of map matching based on the Hidden Markov Model (HMM) (see Section 2.3.1.2), which improves the original algorithm by precomputing the shortest paths between each network node and its nearby nodes within a *delta* distance. The precomputed shortest paths are then used to accelerate the HMM-based map matching from two aspects: 1) the measurement of the shortest paths between neighboring candidate points, and 2) the construction of the optimal path. Furthermore, the FMM can also handle the problem of reverse movement (back and forth movement on a bidirectional road segment) that frequently observed in the results of HMM-based map matching.

When using FMM directly for the map matching of bike trajectories, the map-matching results tend to be very sensitive to GPS errors along the opposite movement direction. This is illustrated in Figure 3.5 by two examples observed in the trajectory dataset. $\{p_1, p_2, p_3, p_4, p_5, p_6, p_7\}$ are the seven GPS points of an input trajectory. The real traveling path is $\{e_{12}, e_{23}, e_{34}\}$. The raw trajectory shows a fake backward movement from p_3 to p_4 because of a large GPS error along the opposite moving direction at p_4. As a result, the FMM algorithm tends to give a matching result as the edge sequence of $\{ p_{12}, p_{23}, p_{32}, p_{23}, p_{34} \}$, with a sequence of "forward–backward–forward" (FBF)

segments $\{e_{23}, e_{32}, e_{23}\}$ included in the matching results. For trajectories recorded at a low sampling rate (i.e., sparsely sampled trajectories) or generated by vehicles with faster speed (e.g., taxi trajectory), the moving distance between two neighboring points is usually larger than GPS errors along the opposite moving direction. Hence, the phenomenon of fake backward movement and FBF segments are less likely to occur. However, the FBF artifacts may likely to occur when dealing with trajectories at a low speed (e.g., biking) and with a high sampling rate (e.g., a sampling interval of 5 s). Since such an FBF movement is unlikely to happen to normal biking trips, it is reasonable to assume that the matching results are affected by the GPS errors along the opposite direction of moving if FBF segments are detected. An iterative assessment is used to check if any FBF segments are presented among every output edge sequence (i.e., the optimal path) obtained by the FMM algorithm and only the first forward edge of the FBF segments is kept.

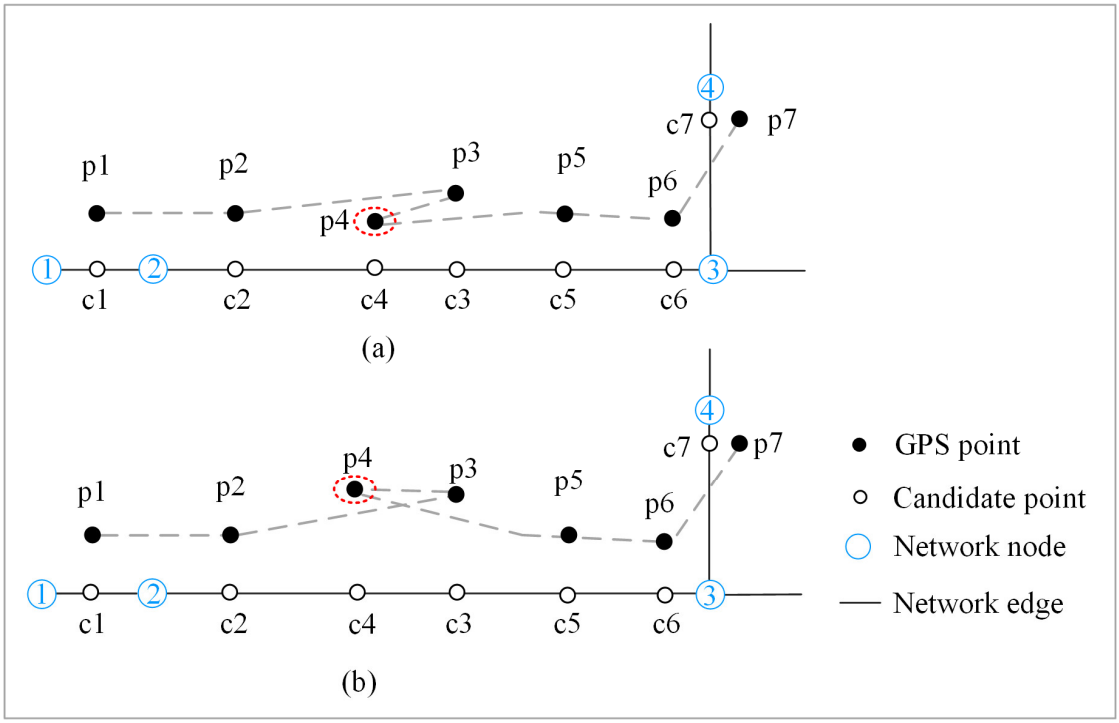

Figure 3.5. Two typical examples of GPS points with positioning errors along the opposite moving direction (a) and (b). For both examples, the trajectory is represented by chronologically ordered GPS point $\{p_1, p_2, p_3, p_4, p_5, p_6, p_7\}$. The actual traversed routes are $\{e_{23}, e_{32}, e_{23}\}$. The GPS positioning errors along the opposite moving direction occur at point p_4.

3.5 Analytical Results

3.5.1 Identified Bike-and-Metro Trips

The D_{max} is set as 100 m by assuming bike-and-metro users park/fetch bikes at a maximum distance of 100 m. We argue such an assumption is reasonable for dockless shared bikes because users are not required to park/fetch their bikes at designated bike stations. In terms of parameter ε, a series of values, ranging from 4 to 15 minutes, are used to extract the corresponding bike-metro-bike trips. Their corresponding statistics of the distances between parking/fetching locations and the nearest metro entrances are shown in Table 3.1. The percentile values at the access side are quite close to the corresponding values at the egress side. The increase of ε only shows a slight impact on the percentile values at both the access and egress sides. For example, the 75th percentile distance between the bike parking locations and the nearest entrances only increases by 2.5 m as the ε increase from 4 to 15 minutes. Therefore, the major question here is to decide which percentile value should be selected as the reference for setting the circular buffer. In general, the smaller the buffer distance, the stricter the validation condition. With the increase of the buffer distance, some non-connecting trips may be identified as bike-and-metro trips (Ji et al., 2018). For example, the 50th percentile distance could be a relatively conservative value for the circular buffer, and the 90th percentile distance could be a relatively risky choice. As a compromise, the 75th percentile distances are thus used as the reference to estimate how far most people park (fetch) bikes before (after) they enter (exit) the metro stations. The circular buffer is thus set to be 50 m, leading to the identification of 163,048 bike trips as bike-and-metro trips.

Table 3.1. Statistics of the distances between parking/fetching locations to the nearest entrances. The parking and fetching correspond to the access and egress sides of the bike-metro-bike trips, respectively.

ε	**Access**: distances between parking locations and entrances (m)			**Egress**: distances between fetching locations and entrances (m)		
	50^{th}	75^{th}	90^{th}	50^{th}	75^{th}	90^{th}
4	30.3	47.2	66.2	29.9	46.4	65
5	30.5	47.7	67.3	30.1	46.5	65.7
6	30.8	47.7	68.2	30.4	46.8	66.6
7	30.9	48.4	68.7	30.5	47.2	67.1
8	31.0	48.7	69.8	30.7	47.6	67.7
9	31.1	49.1	69.2	30.9	48.2	68.2
10	32.2	49.2	69.3	31.0	48.4	68.7
11	31.2	49.4	69.6	31.2	48.5	68.9
12	31.3	49.5	69.6	31.3	48.7	69.2
13	31.4	49.6	69.9	31.3	48.8	69.3
14	31.5	49.7	70.2	31.3	48.8	69.2
15	31.5	49.7	70.2	31.6	48.9	69.6

Among the identified bike-and-metro trips, there are 21,874 trips without sampling points, whose routes are estimated by using the shortest path algorithm. Knowing that the majority of remaining trips have a small sampling interval (66% under 5s) and the average biking speed is 10.3 km/h, 15 s is selected as the resampling interval, resulting in a considerable reduction of GPS points, from 15.2 to 3.3 million. During the stop point removal, 31,824 trips are found to have stop points, and 127,990 stop points are removed. Figure 3.6 gives an example of a trajectory before and after the stop point removal. As shown in Figure 3.6 (a), the original trajectory has two clusters of stop points (marked by the red circle). One is near the road cross, which is likely caused by the waiting for the traffic light. Whereas the other is not near any road cross and unlikely related to traffic congestion. Such an observation indicates that bikers have more freedom and convenience to stop their biking, which in turn implies the necessity of removing stop points. After the preprocessing, 141,174 trips with 3,193,268 trajectory points remain to be aligned with the road network via map matching.

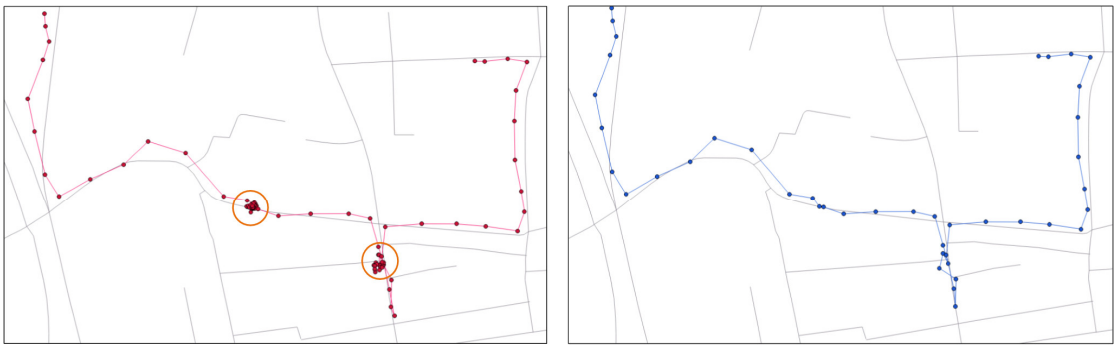

Figure 3.6. Example of removing stop points. (a) trajectory with stop points, and (b) trajectory after removing the stop points.

The FMM parameters are set as follows through a number of experiments: for the pre-computation of the shortest paths, the *delta* is set as 2.5 km; the searching radius $r = 50$ m; the maximum number of edge candidates $k = 6$; and the standard deviation σ is configured to 30 m. Table 3.2 shows the results of map matching, indicating a success rate of 90.1%, approximately 9.9% of the trajectories failed for reasons, such as large GPS errors (i.e., larger than the searching radius of 50 m) and biking along prohibited roads, among others. The distances of the failed trips are thus measured as their trajectory lengths. A total of 42,384 edges generated by 17,249 trips are deleted during the FBF handling of the successfully matched trips. The large proportion (12.2%) of the FBF trips demonstrates the necessity of handling the FBF case to improve the map-matching results.

Table 3.2. Map-matching results of the bike-and-metro trajectories.

	Number	Percent
Successfully matched trips	12,7187	90.1%
Failed matched trips	13,987	9.9%
FBF trips	17,249	12.2%

3.5.2 General Trip Characteristics

Figure 3.7 shows the spatiotemporal distributions of the bike-and-metro trips. The trip frequencies over 7 days * 24 hours are depicted in Figure 3.7 (a), three patterns can be observed: 1) more trips are observed during the commuting periods (7–9 am and 5–7 pm); 2) more trips are generated during the morning peak than the afternoon peak (i.e., 23,399 vs. 17,925 trips, respectively); and 3) no obvious peak pattern is observed during the weekend. The first and third pattern are in line with the metro ridership pattern in

Shanghai (Lin and Zhu, 2019). The second pattern indicates that more people use the metro during the morning peak than during the afternoon peak (Lin and Zhu, 2019). It may be interpreted as a fact that fewer people use bike to access/egress metro stations at the afternoon peak because they have less time pressure after work. Figure 3.7 (b) shows the spatial distribution of trip ODs by using a 500 * 500 m grid. Obviously, more trips are observed in the city center because more metro users are living in the densely populated urban area of Shanghai.

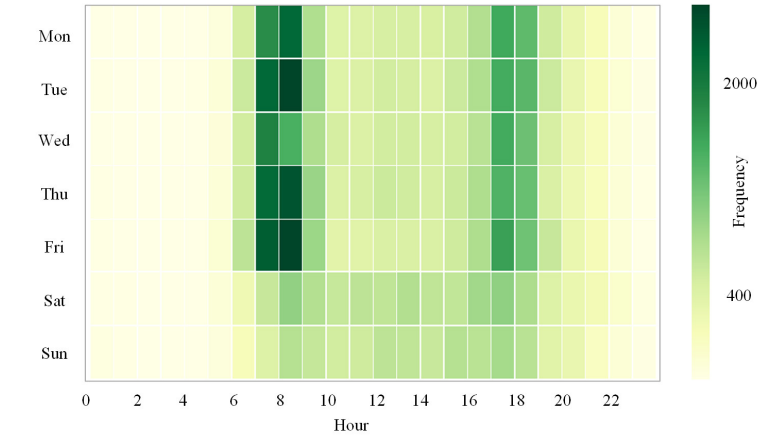

(a)

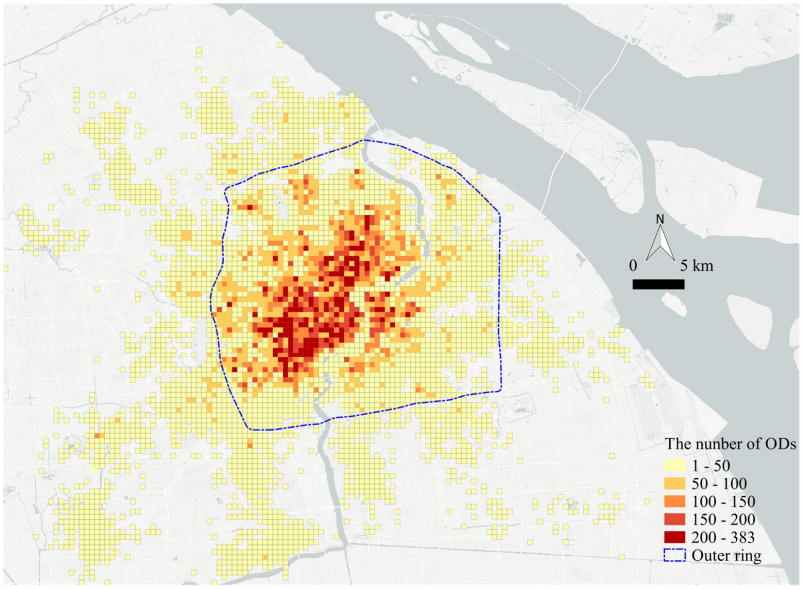

(b)

Figure 3.7. Spatiotemporal distribution of bike-and-ride trips. (a) temporal distribution of one-week bike-and-metro trips, and (b) the spatial distribution of the origins and destinations for all the bike-and-metro trips.

The distributions of the trip lengths, durations, and speeds for the bike-and-metro trips are shown in Figure 3.8. For the sake of clarity, the 1% largest values for the trip lengths, durations and speeds are not considered in the corresponding distributions.

Trip length: the average trip length is 1319 m. The length is shorter than the average trip length (1598 m) of the entire bike trajectories, indicating a greater willingness among people to bike farther when using shared bikes for non-connecting purposes. 49% and 84% of the trips are restricted to 1 km and 2 km, respectively. The distribution shows an increasing trend at the beginning and followed by a decreasing trend from the bin of 500 to 750 m. The decreasing trend can be explained by the spatial decay effect of people's travel behavior, although the holistic pattern does not match with the spatial decay effect very well.

Trip duration: the average duration for the bike-and-metro trips is 8.2 minutes. The overall pattern for the trip duration is very similar to that of the trip lengths. The proportions of trips with a duration of fewer than 5 minutes and 10 minutes are 34% and 77%, respectively. The majority of bike-and-metro trips are constrained within 10 minutes and the most frequent biking duration located in the bin of 4 to 5 minutes.

Trip speed: the average trip speed for bike-and-metro trips is 10.3 km/h. Assuming an average walking speed of 5 km/h, biking could save half of the time to access/egress the metro station. Compared with the distributions of the trip length and duration, the speed distribution shows a more centralized pattern, with approximately 46% trips within the bins of 9 to 12 km/h.

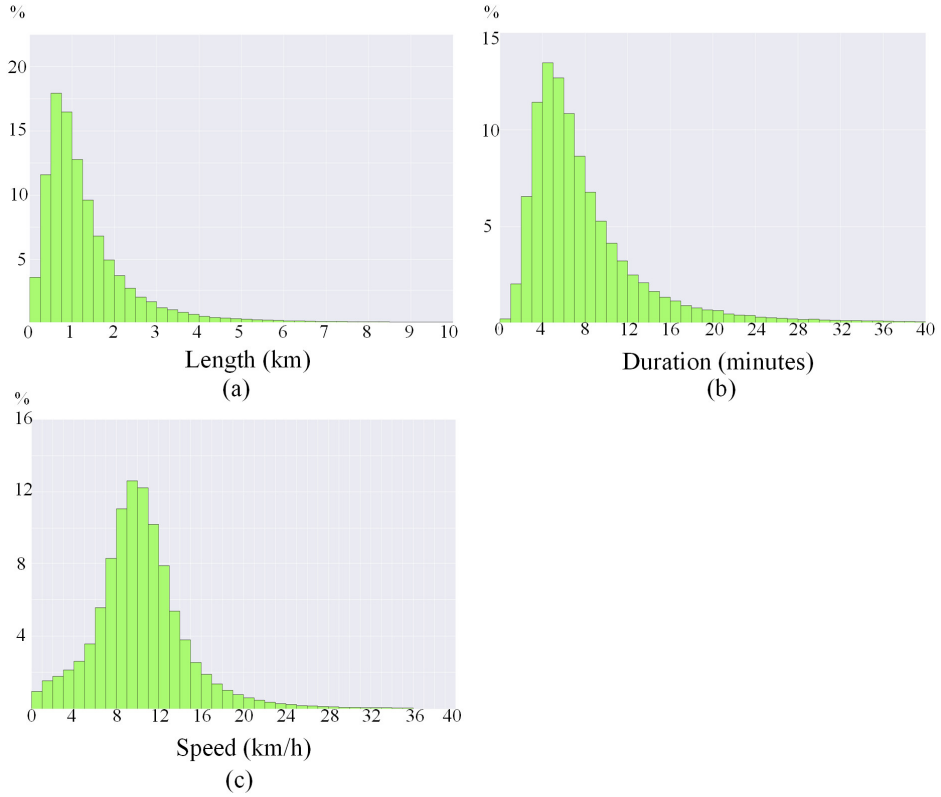

Figure 3.8. Distributions of the bike-and-metro trips. (a) length distribution, (b) duration distribution, and (c) speed distribution.

As compared with the bike access/egress distances derived in other study areas (see (Lee et al., 2016) for an overview), the overall biking distances in Shanghai appeared to be shorter than the biking distances reported in several European countries, such as the Netherlands, Germany and the UK (Givoni and Rietveld, 2007; Martens, 2004). For instance, 54% of the access trips to train stations have a distance larger than 3 km (Givoni and Rietveld, 2007) in the Netherlands, reflecting more longer bike trips are generated. Similarly, the mean bike access distances to train stations in Atlanta and Los Angeles are reported to be 1.7 km and 4.5 km (Hochmair, 2015), which are larger than the mean trip length in Shanghai (1.32 km). The disparity of biking distances is likely to be attributed to the disparity of biking willingness and transit station density. Compared with train stations, metro stations in urban areas are usually more densely distributed. For example, the mean biking access distances to the metro stations reported in Seoul, South Korea (Lee et al., 2016) and Beijing, China (Wang et al., 2016) are 1.47 km and 1.45 km, respectively, which are quite close to the counterpart in Shanghai.

3.5.3 Statistics of Biking Distances at Individual Stations

To eliminate potential biases caused by insufficient sample size, metro stations with fewer than 40 trips are omitted, and the remaining 280 stations are used for analysis[5]. For each station, its mean, 75th and 85th percentile trip distances are calculated accordingly. Based on the ring roads in Shanghai (i.e., inner, middle and outer rings, see Figure 3.9), the entire study area is divided into four non-overlapping zones: inner zone (areas within the inner ring), middle zone (areas between the inner and middle rings), outer zone (areas between the middle and outer rings), and suburban zone (areas outside the outer ring). Table 3.3 lists the average values of mean, 75th and 85th percentile trip distances for different zones. The average values show a noticeable increase from the inner zone to the suburban zone. For instance, the average mean biking distance increases from 1076 m (inner zone) to 1576 m (suburban zone). Correspondingly, the average 75th percentile distances for these two zones are 1376 m and 2073 m, respectively. Figure 3.9 shows the spatial distributions of the 75th percentile biking distances at individual metro stations. The visualization also confirms the increase of biking distances from the city center to the suburban.**Table 3.3. Average values of the mean, 75th, and 85th percentile biking distances in different zones.**

	Mean (m)	75th percentile (m)	85th percentile (m)
Inner zone	1,076	1,370	1,744
Middle zone	1,203	1,544	1,946
Outer zone	1,314	1,682	2,125
Suburban zone	1,576	2,073	2,584
Entire area	1,268	1,634	2,059

[5] All the stations within the outer ring are kept, i.e., with a trip number over 40.

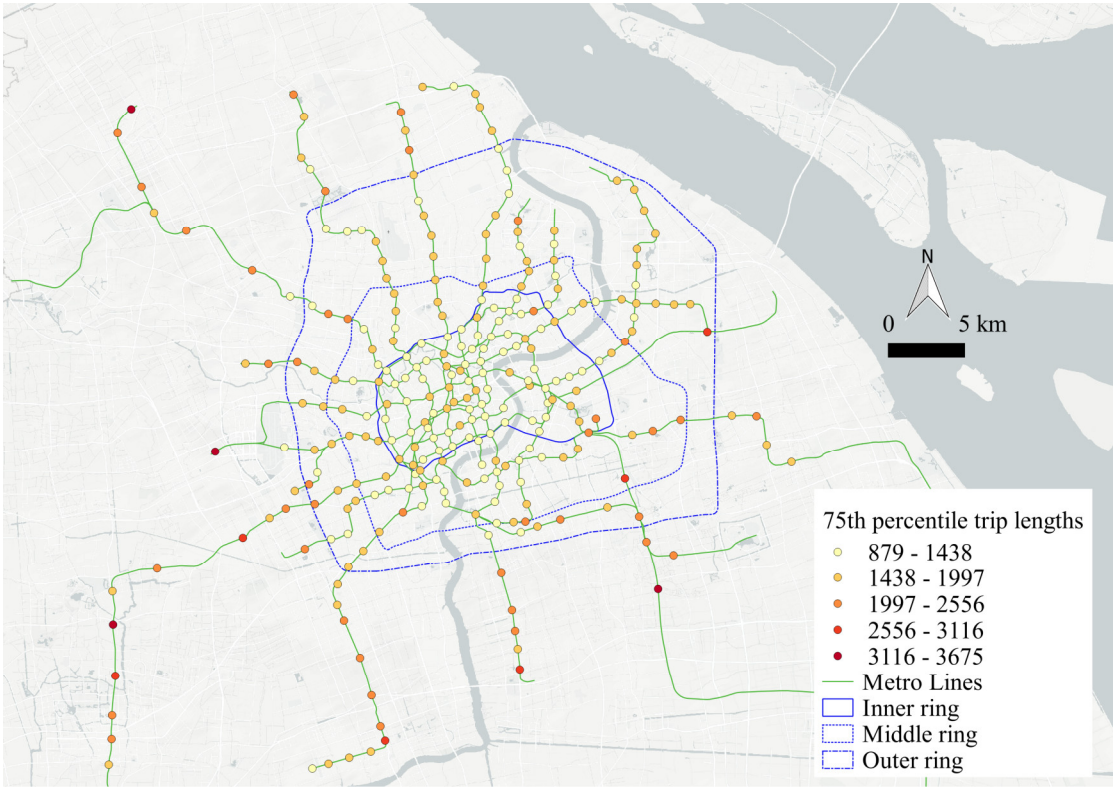

Figure 3.9. Spatial distributions of the 75th percentile biking distances at individual stations.

3.5.4 Regression Modeling of Biking Distances

To understand the disparity of biking distances at individual metro stations, we apply ordinary least-squares (OLS) regression to explore the associations between biking distances and potential factors. According to (Cheng and Lin, 2018; Hochmair, 2015; La Paix Puello and Geurs, 2016), potential factors that may contribute to the biking distances at individual stations can belong to four categories: socioeconomic attributes, station attributes, built environment, and trip attributes. The socioeconomic attributes are not available for this thesis due to the privacy issue; thus, the remaining three groups are considered. Additionally, locational attributes are added as a new group of explanatory variables because of the spatial disparity of biking distances reflected in Section 3.5.3. Table 3.4 lists the statistics of the explanatory variables. The average train interval is measured as the train frequency of a station. The road straightness reflects the detour degree of roads around a station. For a station, 100 road network nodes are randomly sampled from all the nodes within 2 km distance, their network and Euclidean distances to the station are measured accordingly. Then, the average ratio between the network distances and the Euclidean distances is deemed to be the road straightness. The number of bus stations within 300 m reflects the potential

competition from buses. The average distance of four nearest metro stations represents the density of the metro station. The unique user ratio represents the degree of user diversity, which is measured as the proportion of distinct users among the entire trips. The morning and evening trip ratios correspond to the proportions of the trips generated during the morning and evening peak hours, respectively. The locational attributes are represented as dummy variables by using stations in the inner zone as the reference. Similarly, non-terminal stations are used as the reference to specify the dummy variable "terminal". The road density and the number of bus stations around 2 km of the metro station are ignored because of their high correlation with the metro density. Additionally, some potential factors, such as trip purposes and bike availability, are not included because of their limited availability.

Table 3.4. Statistics of the explanatory variables (N = 280).

Variable	Min	Max	Mean	Std
Station attributes				
Average train interval (minutes)	3.75	14	6.2	2.1
Number of entrances	1	20	4.08	2.44
Terminal (0–1)	0	1	0.057	0.232
Built environment				
Average distance of the four nearest stations (m)	860	6520	2090	1060
Road straightness within 2 km	1.03	2.875	1.33	0.156
Bus station number within 300 m	0	12	3.14	1.91
Trip attributes				
Unique user ratio	0.349	0.932	0.568	0.088
Morning trip ratio (7:00–9:00)	0.134	0.576	0.345	0.072
Evening trip ratio (17:00–19:00)	0.061	0.396	0.205	0.051
Locational attributes				
Middle zone (0–1)	0	1	0.23	0.43
Outer zone (0–1)	0	1	0.24	0.42
Suburban zone (0–1)	0	1	0.21	0.41

The mean (termed as model 1) and 75th percentile trip distances (termed as model 2) of the metro stations are used as the dependent variables, respectively. The 75th percentile

is selected because it is usually regarded as the "acceptable" distance of a station (Lin et al., 2019; Wang et al., 2016). On the other hand, the mean value reflects the average biking willingness (Hochmair, 2015). Table 3.5 summarizes the results. The largest variance inflation factor for both models is 3.65, indicating low multicollinearity. As reflected by the adjusted R^2 values, model 1 (adjusted R^2 = 0.562) achieves a better fit than model 2 (adjusted R^2 = 0.533). This indicates that the mean trip distance is a better statistical variable for modeling the biking distances at the station level. The two models show a consistent association for every individual independent variable with slight differences in statistical significance. The entrance number is positively associated with the corresponding dependent variables in both models, which might be explained by the observation that stations with more entrances usually attract users from more diverse directions. The average distance of the four nearest stations shows a positive association with the dependent variables, indicating that users living in areas of fewer metro stations tend to bike farther to access metro stations. According to the exploratory regression analysis, the metro station density acts as the most significant variable, implying that the supply of metro stations plays a critical role in shaping the "acceptable" biking distance of users.

On the contrary, the train interval is negatively associated with the dependent variables. A larger train interval means more waiting time, which makes a metro station less attractive for users living farther. Terminal stations tend to have larger mean and 75th percentile distances in comparison to non-terminal stations. All three trip-related variables are statistically significant for both models. Specifically, stations associated with diverse users tend to have larger biking distances. More morning and evening trips lead to larger biking distances, which might be explained by the observation that more trips originating from residential areas are generated during these periods, especially in the morning (Hochmair, 2015). In line with the spatial distribution of biking distances revealed in Section 3.5.3, the three locational variables reflect statistical significance in both models, which also demonstrate the rationality of integrating locational variables into the OLS regression model. The Moran's I test is employed to the spatial autocorrelation of the standardized residuals of the two models. No statistical significance has been detected for both models, i.e., the values of (z-score, p-value) for model 1 and model 2 are (1.42, 0.16) and (0.88, 0.38), respectively. This also indicates the effectiveness of incorporating location attributes into OLS models to solve the issue of spatial autocorrelation, which is a major concern of applying OLS models to spatial problems.

With regard to the statistically significant variables, the associations reflected by station type (i.e., terminal or not), train interval, station density, morning trip ratio and distance to the city center (indicated by the locational variables) are in line with previous findings (Daniels and Mulley, 2013; Hochmair, 2015; Sanko and Shoji, 2009). Additionally, three factors (i.e., evening trip ratio, unique user ratio, and entrance

number) that have been hardly examined in the literature show statistical significance in the regression modeling. Hence, integrating these variables to estimate the biking distances at individual stations is recommended. As model 1 achieves a better R^2, the obtained mean values are used to estimate the 75th percentile distance by following a similar procedure described in (Hochmair, 2015). Specifically, a new estimation of the 75th percentile distances can be generated by multiplying the obtained mean distances by the ratio of the 75th percentile distance over the mean distance. The adjusted R^2 for the newly estimated 75th percentile distances is 0.527, which is slightly smaller than the adjusted R^2 of model 2 (i.e., 0.533). Thus, using the regression model directly to estimate the 75th percentile distance is recommended because the procedure is even simpler than that described in (Hochmair, 2015).

Table 3.5. Results of the two regression models. The model 1 and model 2 use the mean and 75th percentile trip distances as the dependent variables, respectively.

	Model 1			**Model 2**		
Variable	Coefficient	t-stat	P	Coefficient	t-stat	P
Constant	-233	-1.1	0.274	−383.8	−1.23	0.219
Average train interval	−20. 3**	−2.97	0.003	−30.0**	−2.98	0.003
Terminal	114.5*	2.04	0.04	197.4*	−2.40	0.017
Number of entrances	19.9***	3.65	0.000	31.8***	3.98	0.000
Average distance of the four nearest stations	0.12***	6.40	0.000	0.15***	5.52	0.000
Road straightness	184.4*	2.20	0.029	217.7	1.77	0.078
Bus station number	7.6	1.11	0.269	13.0	1.3	0.195
Unique user ratio	828***	4.91	0.000	1125.3***	4.55	0.000
Morning trip ratio	675.5**	2.81	0.005	1046.3**	2.97	0.003
Evening trip ratio	939.9**	3.10	0.002	1123.2*	2.53	0.012
Middle zone	78.4*	2.17	0.031	119.3*	2.26	0.025
Outer zone	176.7***	4.49	0.000	250.0***	4.33	0.000
Suburban zone	277.4***	4.90	0.000	429.2***	5.12	0.000
R^2		0.581			0.553	
Adjusted R^2		0.562			0.533	

***p < 0.001; **p < 0.01; and *p < 0.05

3.6 Summary

This chapter introduces methods to identify bike-and-ride trips and to construct the biking routes of them using bike trajectory data. For the former task, a method to identify BRB trips is proposed and their distributions are used to decide the circular

buffer of extracting bike-and-ride trips. For constructing biking routes, an adapted version of the FMM map-matching algorithm is proposed to handle the issue of FBF segments. The methods are applied to Shanghai as a case study to measure the biking distances at individual metro stations. The experiments show the effectiveness of the proposed methods. Moreover, the general characteristics of bike-and-metro trips are presented in terms of trip length, duration and speed. The spatial distribution patterns of biking distances at individual stations are revealed. The associations between the selected factors and biking distances are then analyzed in detail.

The obtained results of the Shanghai case will be used as input for the two subsequent chapters. For chapter 4, the 75^{th} percentile distances of individual metro stations will be used as the cut-off distances for generating the bike catchment areas (BCAs) of metro stations. For Chapter 5, the 75^{th} percentile distances and bike speeds at individual metro stations will be used for identifying population grids inside the BCAs and their biking access times to metro stations.

4 Generation and Analysis of Transit Catchment Areas

Generating the transit catchment area (TCA) is a prerequisite for coverage-based accessibility analysis. The objective of this chapter is to propose an open-source framework of generating TCAs by non-motorized transport. Using the proposed framework and the acceptable biking distances derived in Chapter 3, the bike catchment areas (BCAs) of metro stations in Shanghai are then generated and assessed by comparing with pedestrian catchment areas (PCAs).

Section 4.1 investigates the existing methods of modeling and generating transit catchment areas. Section 4.2 presents the methodological framework of generating TCAs by non-motorized transport. In Section 4.3, the proposed framework is implemented and applied to Shanghai, to answer how bike-and-ride would change the population coverage and overlap degree of metro systems. Comparative experiments are conducted to evaluate the accuracy and time efficiency of the proposed framework in Section 4.4 and followed by a discussion of the potential extension of the proposed methods in Section 4.5. Finally, we conclude the chapter in Section 4.6. Part of the materials in this chapter have been published in (Lin et al., 2020).

4.1 Introduction to the Generation of Transit Catchment Areas

There are different types of transit catchment areas, depending on the feeder model of transit stations, which can be walking, biking, bus riding and car driving. The modeling methods, i.e., how to represent a TCA, can be based on buffer or probability. The buffer-based method represents the catchment area of a transit station as a buffer area around the station, referring to an area within which the majority of users can be located. The buffer distance can be either measured by the Euclidean distance or the network distance. According to previous studies (Foda and Osman, 2010; Gutiérrez and García-Palomares, 2008), the latter can generate a more accurate catchment area because

people need to travel along roads in the real world. This buffer-based method is widely accepted and commonly used for modeling TCAs by non-motorized transport. The probability-based method represents a catchment area as a set of sub-areas with corresponding probabilities. This type of modeling is tightly correlated with station choice modeling and usually used for modeling TCAs by motorized transport modes (Lin et al., 2016) or multiple transport modes (Lieshout, 2012; Young, 2016). Lin et al. (2016) proposed an enhanced huff model to measure the probabilities of train station choice for park-and-ride users living in different suburbs. The derived probabilities of station choice are used to redefine the origins of each train station and thus the catchment area is constructed based on the redefined origins. Lieshout (2012) applied multinomial logistic regression to model the passengers' airport choices. The catchment area of an airport is then represented as a combination of hinterland regions in which the airport has a market share of over 1%. We herein focus on the generation of buffer-based TCA.

Several studies have discussed how to generate buffer-based TCAs. The Euclidean-based TCAs can be easily generated by drawing a circular area centered at the transit stations. By combining the Thiessen polygons and the Euclidean-based buffer areas of transit stations, mutually exclusive polygons can be generated to represent non-overlapped catchment areas (Haggett et al., 1977). With respect to generating buffer-based TCAs based on the network distance, there are two types of input data models to represent streets, namely raster data models and network data models. In the raster data model, a study region is represented by a tessellation of cells (e.g., square cells). In order to measure the network distance, additional strategies are needed to integrate the road network information into the raster data model. For example, Upchurch et al. (2004) proposed a strategy that assigns different weights to network cells (i.e., cells representing roads) and off-network cells (i.e., cells representing areas without roads). By setting a "large" weight to the off-network cells, the pathfinding algorithm can guarantee the obtained shortest paths are constrained to the road network. Additionally, areas without road network can be explicitly represented as off-network cells and thus provide an easy way to measure off-network distances. The accuracy of the obtained TCAs by the raster data model largely depends on the cell size. Smaller size can generate more accurate catchment areas because more details, such as the turns of roads and the differences of neighboring lanes, can be included in the model. However, a smaller size also means a larger number of cells, which would exponentially increase the time required for computation (Upchurch et al., 2004). In contrast, a large size of the cell can help speed the computation process at the cost of accuracy.

On the other hand, generating TCAs based on the network data model (termed as network-based TCAs) is a more straightforward approach because the roads generally stored as network data (i.e., nodes and edges, see section 4.2.1). No additional data transform between the network data model and the raster data model is needed. The

distance along the road network can be accurately measured based on the network data model. As a result, this solution is frequently applied to build TCAs in practice. Most of the existing studies (Delamater et al., 2012; Lin et al., 2019) mentioned that the network-based TCAs are generated based on the service area tool of ArcGIS [6]. However, few studies have discussed the detailed algorithms for generating network-based TCAs. Additionally, few studies have discussed how to evaluate the accuracy of network-based catchment areas. Although a study by (Delamater et al., 2012) showed that the catchment areas based on the raster data model tend to identify more underserved area and population as compared with those identified by the network data model, a quantitative evaluation of the accuracy of the network-based catchment area is still missing.

This chapter focuses on methods of generating the network-based TCAs by non-motorized transport. More specifically, an open-source framework of generating network-based TCAs by non-motorized transport (i.e., walking and biking) is proposed. Furthermore, combining with the obtained acceptable distances derived in Chapter 3, the proposed framework is applied to generate the BCAs in Shanghai and a coverage-based accessibility assessment is presented accordingly.

4.2 Methodological Framework

4.2.1 Problem Definition

Given a road network graph $G = (N, E)$ (where the node set N represents road intersections and the edge set E represent the corresponding roads) and a transit facility p with a cut-off distance $delta$, the network-based TCA of p is defined as:

> *An area that exactly encompass all the points with a distance to p less than or equal to delta.*

We refer the points within the *delta* distance of p as the accessible points; and points beyond this distance are termed as inaccessible points. By using "exactly", we mean all the inaccessible points should be excluded in the catchment area. The distance between a point (e.g., a in Figure 4.1) and a facility (e.g., p in Figure 4.1) consists of two parts: network and off-network distances. Two assumptions are made for the distance measurement. First, users are assumed to choose the nearest road of the origin (e.g., p to p') to start their traveling along the road network and leave the road at the nearest road of the destination (e.g., a' to a). Second, users are assumed to choose the shortest

[6] ArcGIS is a leading commercial GIS software. The description of its service area tool can be found in: http://desktop.arcgis.com/en/arcmap/latest/extensions/network-analyst/service-area.htm

path to travel along the road network (e.g., p' to a'). Based on these two assumptions, the network and off-network distances can be easily calculated and the distance between facility p and any point can be obtained accordingly.

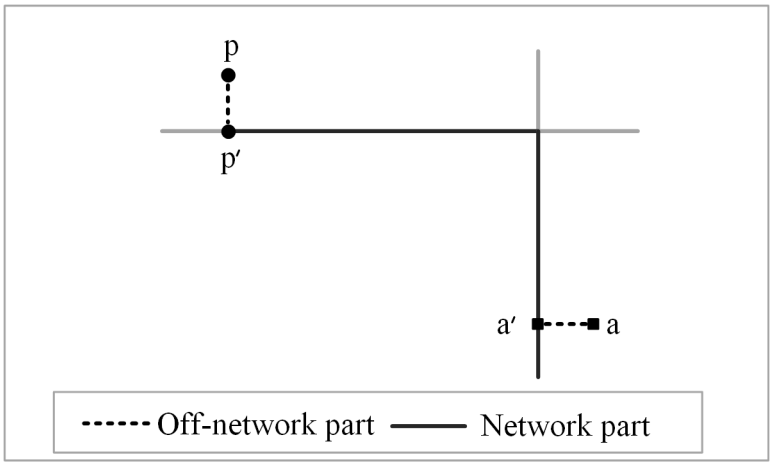

Figure 4.1. Illustration of network and off-network distances. p and a represent the locations of a facility and a point, respectively.

Based on the definition of the network-based TCA, the problem under consideration is described as:

> *Given a road network graph* $G = (N, E)$ *and a set of facilities* $\{p_1, p_2, \dots, p_n\}$, *Each facility* p_i *has an associated cut-off distance* $delta_i$. *The aim is to design a method to generate n TCAs for these facilities in an efficient and accurate way*.

The "efficient" here means the method should be fast in terms of generating a large number of catchment areas. The "accurate" means the generated catchment area should match with the TCA definition as much as possible, i.e., the generated catchment area should include more accessible points and fewer inaccessible points (see the detailed evaluation metrics in Section 4.3.2.3).

4.2.2 The Basic Framework

The TCAs can be measured in two directions, namely to-facility and from-facility directions, corresponding to using the facility as the destination and origin, respectively. For an undirected road network, the distance measured in to-facility direction equals that measured in from-facility direction; thus, the to and from catchment areas are the same. In contrast, it is necessary to differentiate between to and from facility catchment areas in a directed road network. In addition to representing a facility as a point, the facility can also be geometrically represented as a set of points (i.e., multiple points), a

polyline, or a polygon. In this section, we focus on illustrating the framework of generating the TCAs by non-motorized transport using the case of the undirected road network and point-based facility. The methods on how to generalize the framework to directed graph and non-point-based facility are described in Section 4.2.3.

Figure 4.2 illustrates the structure of the proposed framework. The general idea is to build a triangulation to interpolate the contour at the cut-off distance, and the areas enclosed by the contour is used as the catchment area. Specifically, given the input road network and facilities, the process of TCA generation includes three components: subgraph construction, extended shortest path tree (SPT) construction, and contour generation. These three components are elaborated in the following subsections.

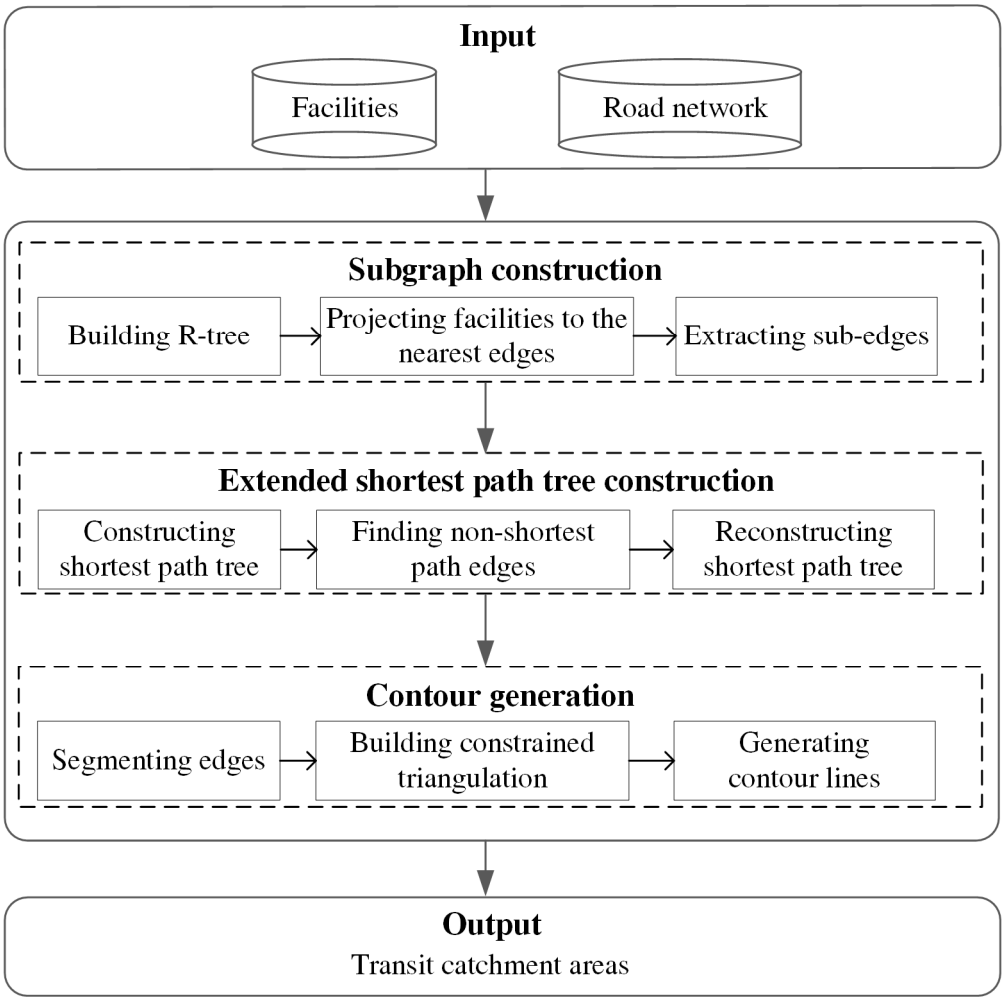

Figure 4.2. Framework of generating the network-based transit catchment areas (TCAs) by non-motorized transport.

4.2.2.1 Subgraph Construction

Since the cut-off distances for TCAs by non-motorized transport are relatively small, a subgraph is constructed for each facility to speed up the construction of extended shortest path tree (see Section 4.2.2.2) by limiting the searching of shortest path to a small size of subgraph (i.e., graph with fewer nodes).

- **Building R-tree**

Based on the input road network edges, an R-tree (Guttman et al., 1984) is built to accelerate the nearest road searching and sub-edge extraction.

- **Projecting facilities to the nearest edges**

In order to measure the distance from/to a facility, each facility point needs to be projected to its nearest edge. Specifically, the nearest edge of a facility can be retrieved using the nearest neighbor query of R-tree (Roussopoulos et al., 1995). Then, each facility can be projected to its nearest edge by using a linear reference algorithm, which iterates through every segment (a segment is a line connecting two neighboring points of an edge) of the edge to determine the nearest segment (Yang and Gidófalvi, 2018). As shown in Figure 4.3, p' is the corresponding projected point of the facility p.

- **Extracting sub-edges**

We extract the sub-edges of each facility based on its projected point. Given a facility p with its projected point p' and the cut-off distance $delta$. A square searching box with a side length of l and centered at p' is created (Figure 4.3). The sub-edges of each facility are then extracted by finding the edges that intersect with its searching box with the assistance of the intersection query of R-Tree.

The corresponding subgraph G_p of the facility p can be easily constructed based on the extracted sub-edges of each facility. Additionally, the projected point p' is inserted into G_p as a new node. The parameter setting of l needs to satisfy two requirements: 1) all the accessible edges (i.e., edges whose distance to/from p are less than or equal to $delta$ should be included in G_p; and 2) some edges beyond the distance of $delta$ need to be included in G_p, which will be used to interpolate additional boundary points of TCAs during the triangulation procedure (see Section 4.2.2.3). Therefore, l should satisfy the following criterion

$$l \geq 2 * (delta - d(p, p')) \tag{4.1}$$

Where:

$d(p, p')$ is the distance between p and p'

$delta$ is the cut-off distance of p

Under the condition that these two requirements are satisfied, l should be as small as possible to improve the computation efficiency. As the detour ratios of roads are usually bigger than 1 and $d(p, p')$ is usually bigger than 0, l can thus be set to $2 * delta$.

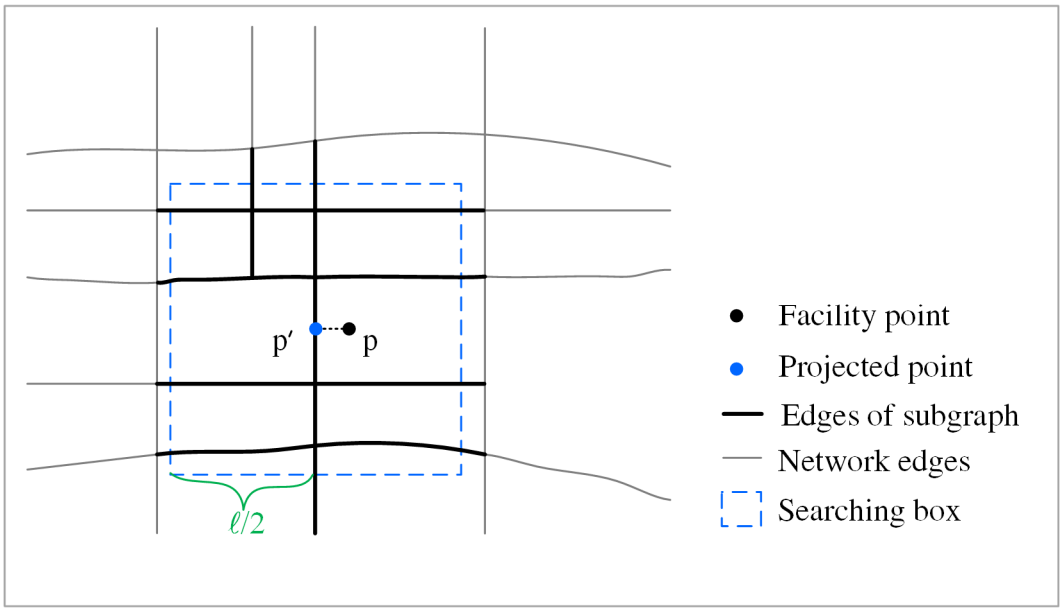

Figure 4.3. Example of subgraph construction of a facility.

4.2.2.2 Extended Shortest Path Tree Construction

An extended SPT is constructed for each subgraph, based on which the distance from a node to any point along the road network can be easily calculated (Okabe et al., 2006).

- **Constructing shortest path tree**

Given a node as the root node, the SPT starting from a root node can be constructed by employing the Dijkstra's algorithm.

- **Identifying the non-SPT edges**

As illustrated using an example in Figure 4.4, some edges (the red edges in Figure 4.4 (b)) are not included in the SPT, which are referred to as non-SPT edges. In order to construct an extended SPT that includes these non-SPT edges, additional points need to be inserted into them. According to (Okabe and Sugihara, 2012), if a given $edge\ (u, v)$ is a non-SPT edge, there must be a point q (termed as break point) on this edge that satisfies the following

$$D[u] + d(u,\ q) = D[v]\ +\ d(v,\ q) \tag{4.2}$$

Where:

$D[u]$ and $D[v]$ are the distances from the root node to nodes u and v

$d(u, q)$ and $d(v,\ q)$ are the distances between point q and nodes u and v

How to efficiently find the non-SPT edges and the corresponding break points is a key issue for the construction of the extended SPT. We represent a non-SPT edge as a tuple $(u, v,\ l_b)$, where $l_b = d(u,\ q)$. The Algorithm 4.1 describes the means of identifying the non-SPT edges of a facility (denoted as $NSPEs$). The input of this algorithm is the output of the Dijkstra's algorithm (i.e., the output of the previous step), including the sequence of the examined nodes of the Dijkstra's algorithm (denoted as EN), the predecessors of the examined node (denoted as P), and the shortest distances from the examined nodes to the root node (denoted as D). By iterating the examined nodes in a backward direction, the non-SPT edges can be efficiently identified (Line 4-12 in Algorithm 4.1).

Algorithm 4.1: Identifying the non-SP tree edges of a facility

Input:

The examined nodes (*EN*), and their corresponding predecessors (*P*) and shortest path distances (*D*)

Output:

A set of non-SP tree edges *NSPEs*

```
1.  for each node u in EN
2.      color[u] := White
3.  end for
4.  for each node u in EN (fetching in backward direction )
5.      color[u] := Gray
6.      pre_u := P[u]
7.      for each node v in the Adj[u]
8.          if v != pre_u and color[pre_u] != Gray
9.              l_b := (D[v] – D[u] + d(u, v)) * 0.5
10.             add tuple (u, v, l_b) to NSPEs
11.     end for
12. end for
13. Return NSPEs
```

- **Reconstructing shortest path tree**

In this step, each non-SPT $edge\ (u, v,\ l_b)$ is split into two edges at its break point q. Two new edges, namely (u, q') and (q'', v) are generated, where q' and q'' have the same location at q. Although the q' and q'' occupy the same location, they are regarded as two distinct nodes to make sure that no circular roads exist in the graph after inserting the

break points (Okabe and Sugihara, 2012). After the insertion of every single non-SPT edge, an updated graph can be obtained. Then, by re-running the Dijkstra's algorithm on this updated graph, the extended SPT can be generated (Figure 4.4 (c)).

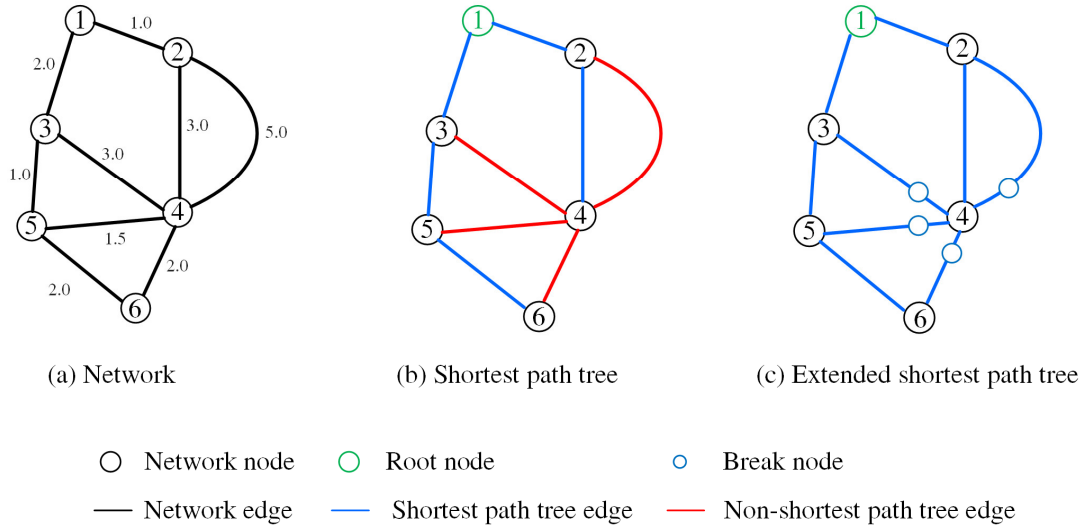

Figure 4.4. Demonstration of an extended shortest path tree.

Compared with the SPT, the extended SPT can include all the non-SPT edges. The inclusion of these edges is crucial for the interpolation of distance to the root node during the contour generation (see Section 4.2.2.3). Figure 4.5 illustrates the interpolations based on the SPT and extended SPT by using two non-SPT edges shown in Figure 4.4 (b). As demonstrated, if no break point is inserted for a non-SPT edge, the interpolation along the edge could be incorrect. For instance, the distance from the root node to point m_1 is 2.5. Under the condition of the extended SPT, the distance to m_1 can be correctly determined through the interpolation along the $edge\ (3, m_5)$ (see Figure 4.5 (b)). Under the condition of the SPT, the distance is wrongly determined as 2.33 if the interpolation is conducted along the $edge\ (3, 4)$ (see Figure 4.5 (a)). Similarly, under the condition of the SPT, the interpolated distances to points, n1, n2, n3, and n4, are incorrect if the interpolation is conducted along the $edge\ (2, 4)$ (Figure 4.5 (c)). Since a non-SPT edge (e.g., $edge\ (2, 4)$) might be used as an edge of the triangulation, it is essential to build the extended SPT to guarantee a correct interpolation during the triangulation.

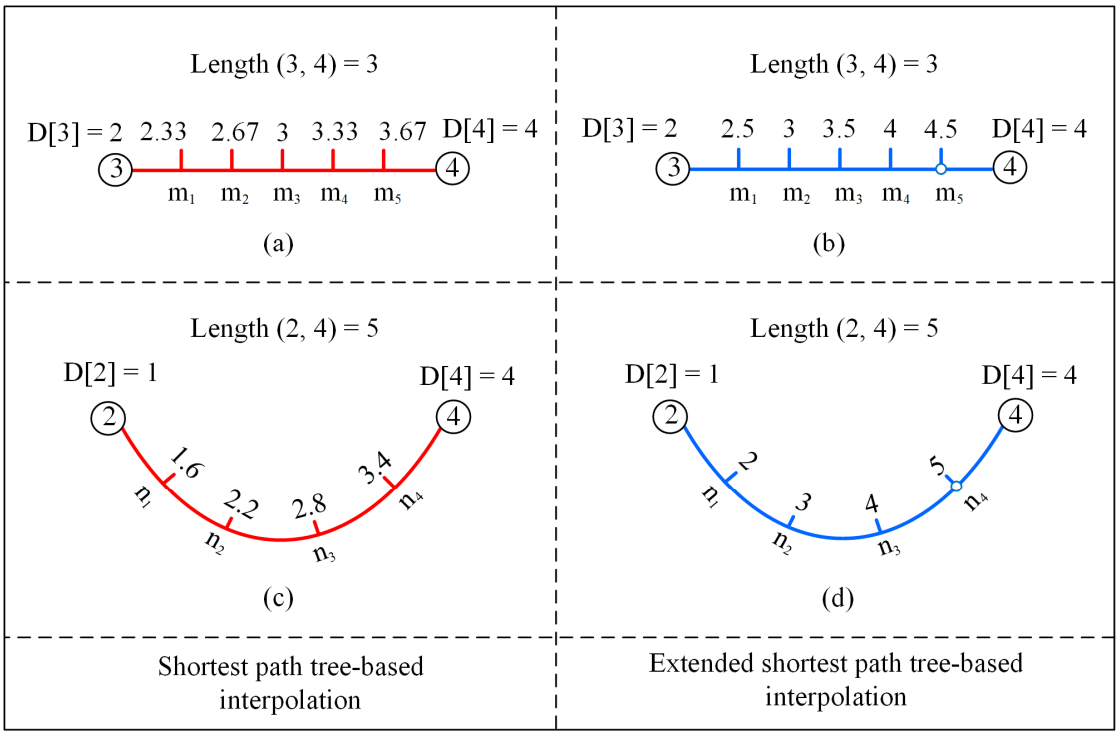

Figure 4.5. Illustration of the interpolations based on the shortest and extended shortest path trees.

In the context of the TCA generation, the root node of the extended SPT is set to be the projected point p' of facility p. The network corresponds to the subgraph G_p of the facility p. By following the above three steps, an extended SPT can be generated for each subgraph.

4.2.2.3 Contour Generation

Based on the extended SPT constructed in Section 4.2.2.2, the contour lines at the distance of $(delta - d(p,p'))$ is generated for a facility p as the boundaries of its catchment area in the following three steps.

- **Segmenting edges**

Given an edge $e = (u, v)$ represented by a polyline $(u, m_1, m_2, \dots m_n, v)$, where m_1 to m_n are n intermediate points of the edge. We divide the polyline-based edge into $n + 1$ segments because the constraints used for constrained Delaunay triangulation are represented as segments instead of the polyline. The obtained segments are added as the constraints during the triangulation and their endpoints thus act as the vertices of the triangulation. Since every single edge is included in the extended SPT, the distance from a root node to an intermediate point m_i can be calculated by the following formula.

$$D(m_i) = D[u] + d(u, m_i) \quad (4.3)$$

Where:

$D(m_i)$ is the distance from the root node to the intermediate point m_i

$D[u]$ is the distance from the root node to node u

$d(u, m_i)$ is the distance from node u to the intermediate point m_i

- **Building constrained triangulation**

Based on the constrained segments obtained in the previous step, a constrained Delaunay triangulation is built for each extended SPT by using the Computational Geometry Algorithms Library (Boissonnat et al., 2007).

- **Generating contour lines**

Using the constrained Delaunay triangulation as input, the contour lines specified at the cut-off distance (i.e., $(delta - d(p, p'))$) are generated by employing a tracing-based contour generation algorithm (Watson, 1992).

The reason for constructing the constrained Delaunay triangulation instead of Delaunay triangulation is because the edges of Delaunay triangulation may intersect with network edges and lead to incorrect distance interpolation during the contour generation. Figure 4.6 illustrates the interpolations based on Delaunay and constrained Delaunay triangulations for a road network. Figure 4.6 (b) shows a triangulation $edge\ (2, 4)$ intersects with a network $edge\ (3, 5)$ at point m. In such case, the distance from the root node to point m is interpolated based on the triangulation $edge\ (2, 4)$ because the network $edge\ (3, 5)$ is not included in the Delaunay triangulation. As a result, the interpolated distance is different from the real distance from node 1 to point m (following a path $1 - 2 - 3 - m$). In contrast, since every network edge is included in the constrained Delaunay triangulation (Figure 4.6 (c)), the distance from the root node to any point along the network edge can be correctly determined.

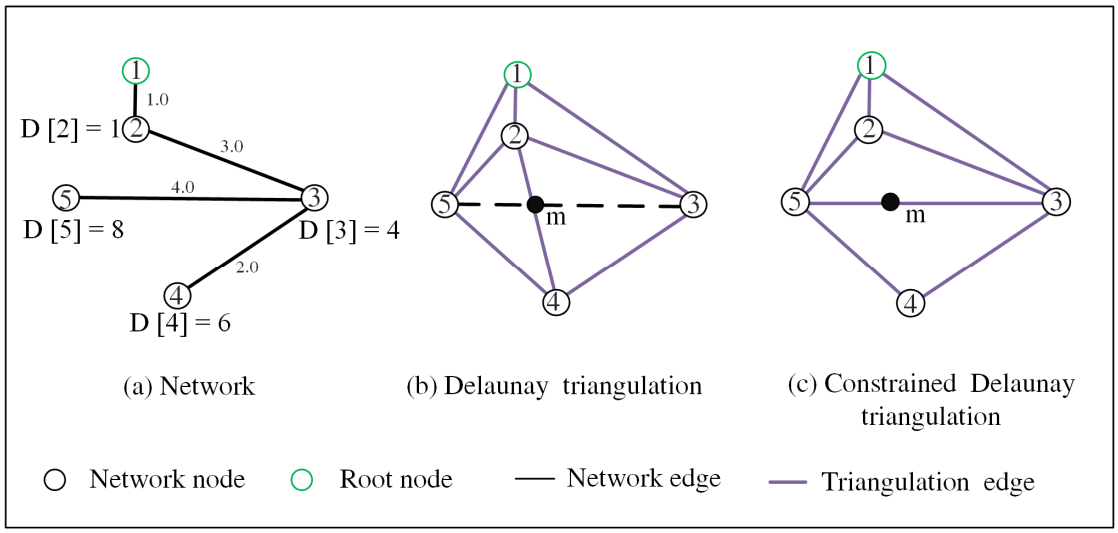

Figure 4.6. Illustration of the interpolations based on the Delaunay and constrained Delaunay triangulations.

Based on the generated contour lines of a facility, the corresponding TCA can be easily constructed and represented by the areas enclosed by the contour lines. Using the Da Muqiao metro station in Shanghai as an example, the process of catchment generation is shown in Figure 4.7. In this example, the road network is represented as an undirected graph, and the station is represented as a point. The cut-off distance $delta = 1$ km, the side length of the searching box $l = 2$ km. Figure 4.7 (a) shows the sub-edges extracted by using the searching box. Figure 4.7 (b) shows the SPT edges and non-SPT edges among the sub-edges. Figure 4.7 (c) shows the constrained Delaunay triangulation. The intermediate points and segments are included in the triangulation as its vertices and edges, respectively. Figure 4.7 (d) shows all the accessible edges and the corresponding catchment area. The catchment area is represented by a polygon consisting of an exterior ring and three interior rings (i.e. the "holes" in Figure 4.7 (d)), corresponding to four contours lines obtained during the process of contour generation. Obviously, all the accessible edges can be successfully covered by the generated catchment area. Moreover, the inaccessible areas within the exterior ring can be identified and excluded in the generated catchment area.

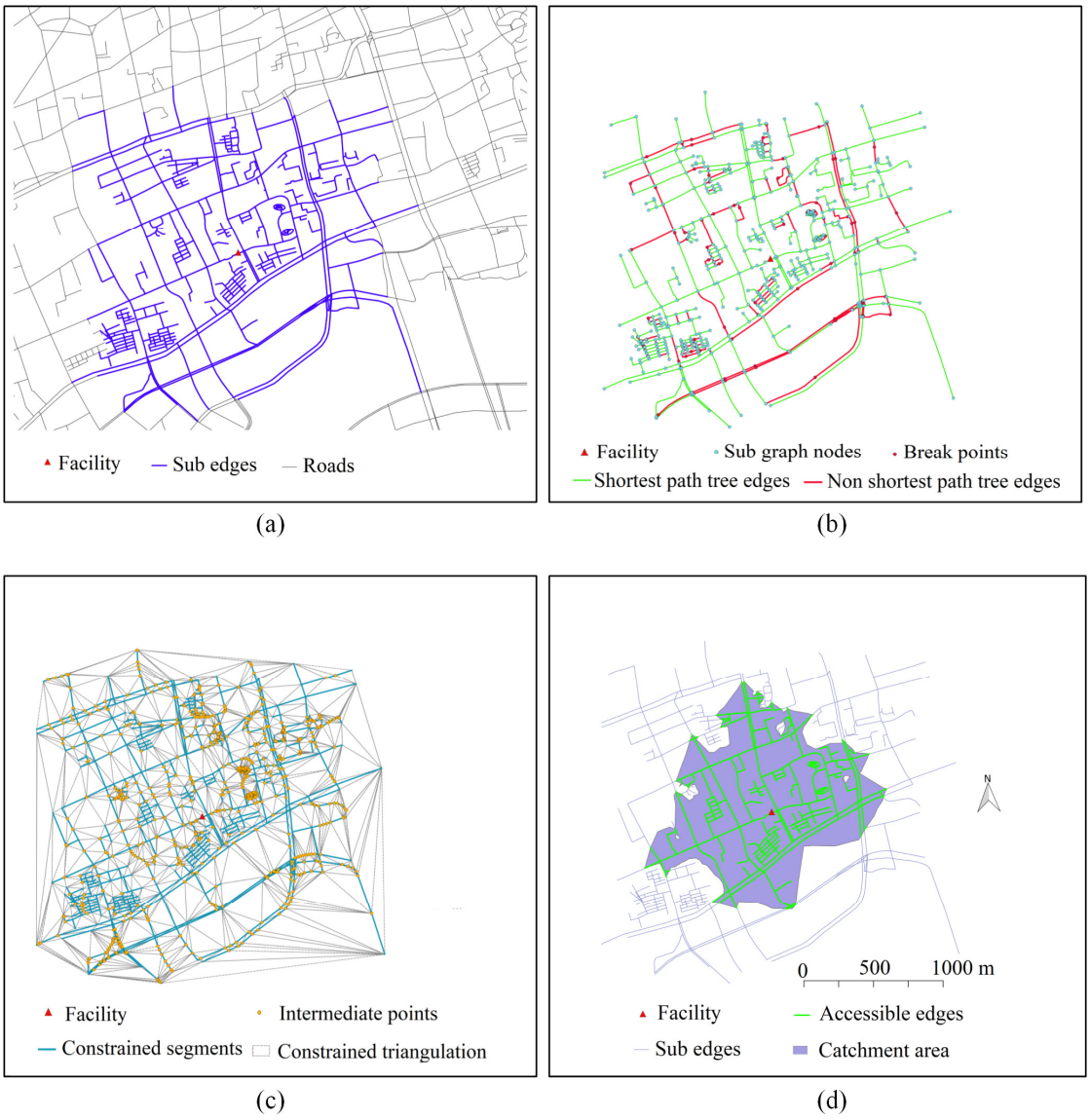

Figure 4.7. The process of catchment area generation of a point facility based on an undirected road network. (a) sub edges, (b) SPT and non-SPT edges, (c) constrained Delaunay triangulation, and (d) accessible edges and catchment area.

4.2.3 Generalization of the Framework

In Section 4.2.2, the basic framework is illustrated based on two assumptions: 1) the road network is represented as an undirected graph, and 2) the facility is geometrically represented as a point. Generally, these two assumptions match well with numerous real-world applications. Since the road network for non-motorized transport usually can be considered as an undirected road network and transit facilities (e.g., bus stations) are commonly geometrically represented as a point. However, some cases might be

more complicated. For instance, the road network for bikers may be modeled as a directed road network because some cities have roads that only allowing biking in a single direction. To get a more accurate TCA, it is better to represent a large transit hub as a set of entrance points instead of one single point of its station center. The methods on how to generalize the framework to the cases of the directed road network and non-point facilities are presented in this section.

4.2.3.1 Generalization to a Directed Road Network

The major differences between the directed and undirected road networks occur at the process of constructing the "Extended shortest path tree" with the following modifications.

- First, for the directed graph, the adjacent nodes in Line 7 of Algorithm 4.1 specify the start nodes of the in-edges of node u (i.e., edges with the target node at node u). Whereas for the undirected graph, there is no need to distinguish the in-edges and the outer-edges of a node.
- Second, if an edge (u, v) that corresponds to a single-direction road edge is a non-SPT edge, which means $D[u] + d(u, v) \geq D[v]$. Then, it is only possible to find a point q at the location of v that satisfies Equation (4.2). Therefore, there is no need to insert any break point under such conditions. One the contrary, if a non-SPT edge (u, v) corresponds to a bi-direction road edge, a break point can thus be inserted as the case of the undirected graph. Although no break point is added into a non-SPT edge when it corresponds to a single-direction road edge, during the segmentation of road edges (see Section 4.2.2.3), the distance between an intermediate point m_i and the root node can be correctly calculated using Equation (4.3) as well.
- Third, during the reconstruction of the shortest path tree, both edges (i.e., edge (u, v) and edge (v, u)) of a bi-direction edge need to be split at the break point q. Additionally, instead of inserting two points (i.e., q' and q'') with the same location, only one break point q is needed.

With respect to the directed graph, the catchment area of a facility can be further classified into to-facility and from-facility catchment area as noted in Section 4.2.1. By default, the root node of the Dijkstra's algorithm is set to be the projected facility point, which corresponds to the from-facility catchment area. With respect to the generation of the to-facility catchment area, the only modification is to reverse the direction of each edge during the construction of subgraph (Section 4.2.2.1). Then, by using the projected facility point as the root node, we can obtain the to-facility catchment areas.

Figure 4.8 illustrates an example of generating a TCA based on the directed road network. The directed road network is constructed by manually modifying some bi-

directional edges (Figure 4.7) to single-direction edges (the red edges in Figure 4.8), other parameters are the same as that of Figure 4.7.

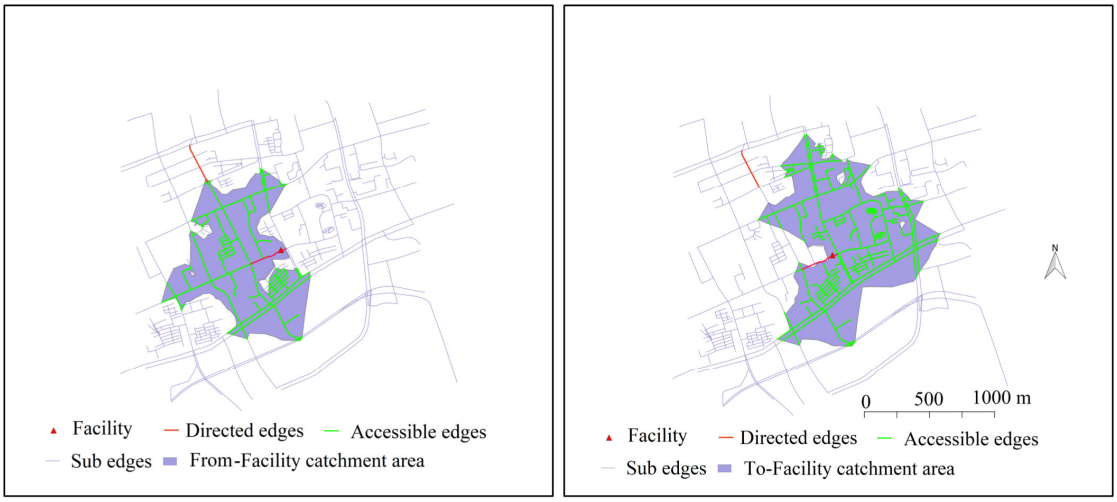

Figure 4.8. Two catchment areas of a point facility based on a directed road network. (a) from-facility catchment area, and (b) to-facility catchment area.

4.2.3.2 Generalization to Non-point Facilities

In addition to modeling a facility as a point, a facility can also be geometrically represented by a set of multiple points, a polyline, or a polygon. Generally, polylines and polygons can be transferred into multiple points by using a discretization strategy. Therefore, we use the case that a facility is represented as multiple points to illustrate how its catchment area is generated. Assuming a facility p is represented by k sub points $(p_{(1)}, p_{(2)}, \dots, p_{(k)})$ and their corresponding projected points are $(p'_{(1)}, p'_{(2)}, \dots, p'_{(k)})$. An intuitive method of generating the catchment area of p is to dissolve all the individual catchment areas of its k sub points (termed as dissolving-based method). However, we propose another method, termed as virtual node-based method, to generate the catchment area of p in a more efficient way. Specifically, the virtual node-based method requires two modifications.

- First, during the processing of subgraph construction, the searching box should be set as the bounding box of all the searching boxes of $(p'_{(1)}, p'_{(2)}, \dots, p'_{(k)})$.
- Second, a virtual node needs to be added to each subgraph during the subgraph construction. The weights between the virtual node and any of point in $(p'_{(1)}, p'_{(2)}, \dots, p'_{(k)})$ are set to be zero. Then, this virtual node is used as the root node to construct the extended SPT and generate the corresponding contour lines.

Figure 4.9 shows an example of the catchment area of a multiple-point facility generated by the virtual node-based method. In this example, Da Muqiao metro station is represented by its six entrances (i.e., six points of the multiple points). The cut-off distance is set to be 1 km. The catchment area boundaries of each individual entrance by using 1 km as the cut-off distance are generated as well (in yellow dotted lines). As shown in Figure 4.9, the generated catchment area is almost the same as that obtained by dissolving the individual catchment areas of each entrance (i.e., the dissolving-based method). This demonstrates that the virtual node-based method can be effectively applied to generate catchment areas for non-point facilities.

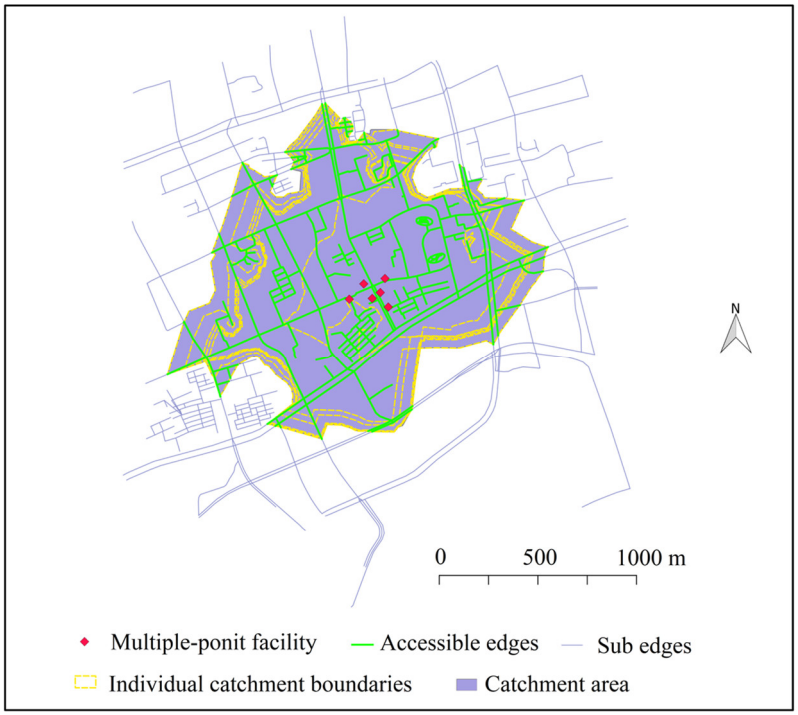

Figure 4.9. Catchment area of a multiple-point facility based on an undirected road network.

4.3 Implementation and Application to Shanghai

4.3.1 Implementation

The proposed framework is implemented as an open-source C++ program[7] and its user interface is shown (Figure 4.10). The program provides functions for generating TCAs with different configurations. Specifically, the input road network can be undirected

[7] https://gitlab.com/Drsulmp/tcageneration

roads or directed roads; the input facilities can be geographically represented as a single point or multiple points. Additionally, the corresponding accessible edges within the TCAs can be generated as well.

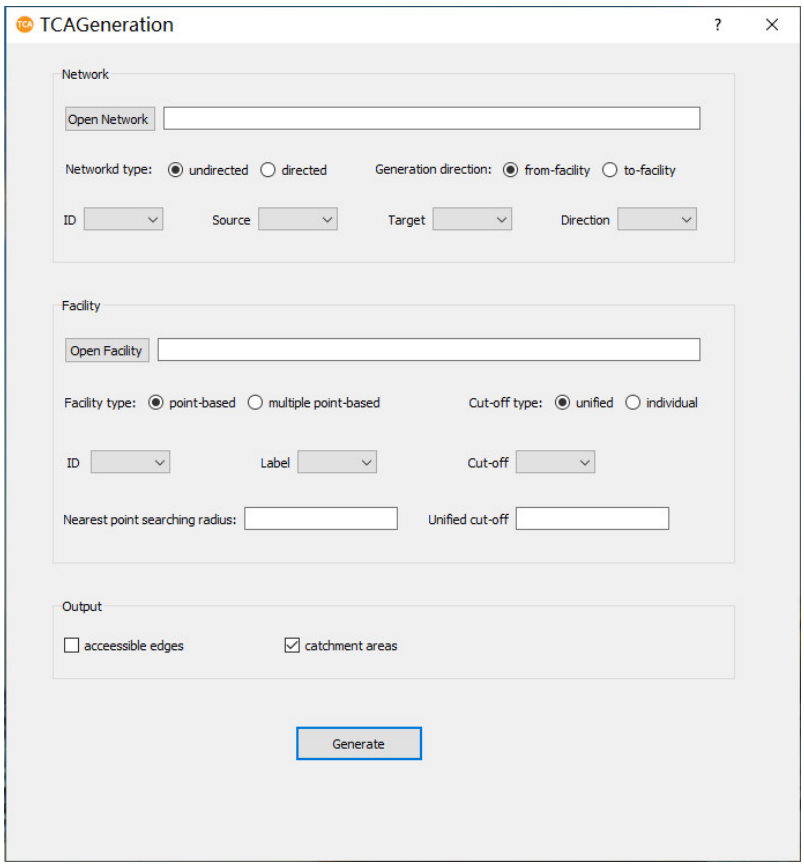

Figure 4.10. User interface of the TCA tool.

4.3.2 Analysis of the Catchment Areas of Shanghai Metro System

In this section, we apply the proposed methods to generate the BCAs of metro stations in Shanghai by representing each station as its entrances (i.e., multiple point facility). The 75th percentile distances of individual stations obtained in Chapter 3 are used as the cut-off distances. The road network and metro stations related data are the same as that used in Chapter 3. Additionally, a population dataset originated from the 250 * 250 m Global Human Settlement (GHS) is used for population coverage analysis (Schiavina et al., 2019).

To understand how dockless shared bikes could change the accessibility to transit, the BCAs are compared with 800 m PCAs. The obtained catchment areas corresponoding to the PCAs and BCAs are showed in Figure 4.11. Two indicators, namely population

coverage ratio and overlap degree, are used for quantitative comparison. The population coverage ratio is the proportion of the population being covered in a zone (see Section 2.2.2). A large population coverage ratio means a good accessibility to metro systems. For a location inside a zone, the overlap degree is reflected by the number of overlapped catchment areas, i.e., covered by how many catchment areas of metro stations. Thus, a location with a large overlap degree means many stations are available within acceptable distances. Table 4.1 lists the population coverage ratios corresponding to different zones in Shanghai. All the zones show an increase in population coverage, and the increase of the coverage ratio for the middle and outer zones is especially noticeable (increased by 103% and 162%, respectively). The increase demonstrates the benefits of the integration of dockless shared bikes and the metro system. Given the fact that areas outside the inner zone have a higher increase of population coverage but a relatively low trip density; bike-sharing sectors should be aware of the potential scarcity of shared bikes in these areas. Furthermore, a small proportion of the population within the central city is still beyond the coverage of the BCAs. The uncovered population should be given special attention in case of potential scarcity of metro feeder services. If necessary, measures, such as enhancing bus services and adding roads, may help improve the accessibility to metro stations.

Table 4.1. The population coverage ratios in different zones corresponding to 800 m pedestrian catchment areas (PCAs) and bike catchment areas (BCAs).

	Inner zone	Middle zone	Outer zone	Central city
PCA	0.751	0.432	0.265	0.471
BCA	0.952	0.876	0.693	0.839
Increase	26.8%	103%	162%	78.1%

As illustrated in Figure 4.11, the catchment areas are classified into five categories based on the overlap degrees: areas covered by 1, 2–3, 4–5, 6–7, and 8–9 stations. The maximum overlap degrees for the PCAs and the BCAs are 5 and 9, respectively. Similar to the population coverage, the overall overlap degree can also be largely increased by bike-and-metro, particularly in the inner zone. From the perspective of demand, the increased overlap degree indicates bike-and-ride offers users more choices of metro stations. In other words, metro stations that are not accessible within the walking distance can be accessed by biking. Such an overlapping phenomenon might also indicate that bike-and-ride could be used to relieve the issue of overcrowded metro in Shanghai by guiding users to less crowdy metro stations. Further examination is needed to check in which locations such possibility may exist (see Chapter 5). From the perspective of supply, a high overlap degree might indicate an excessive system

redundancy (El-Geneidy et al., 2014). The overlap degrees of the PCAs are mostly smaller than 4, indicating a reasonable level of system redundancy. In contrast, the overlap degrees of the BCAs are very high in the inner zone, indicating a high system redundancy. However, since walking still acts as the primary metro access mode, the conclusion of a system redundancy can only be drawn with some special caution. Further examination regarding the traffic flow, bike availability, and people's biking willingness is necessary.

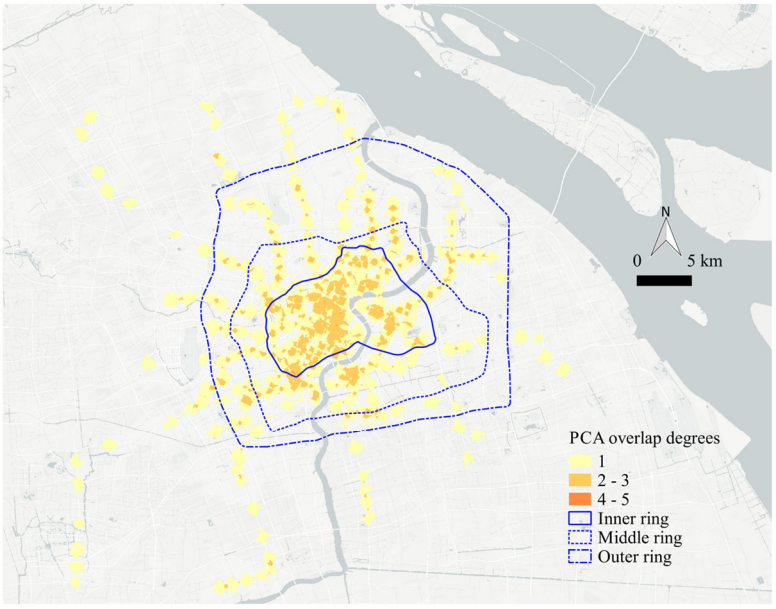

(a)

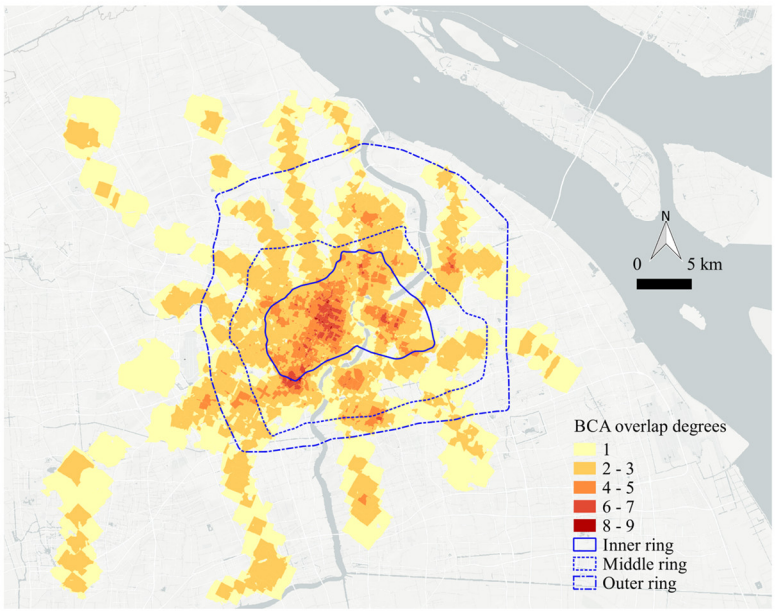

(b)

Figure 4.11. Pedestrian and bike catchment areas of metro stations in Shanghai. (a) 800 m pedestrian catchment areas, and (b) bike catchment areas.

4.4 Comparative Experiments and Evaluation

4.4.1 Data and Experimental Set-up

Two major datasets, namely the metro station dataset and road network dataset, are used for experiments. In total, 280 metro stations and the associated 1143 metro entrances in Shanghai are included. The data collection methods are illustrated in Section 3.2. All the experiments are conducted on a desktop computer with Intel Quad Core CPU 3.40 GHz and 32 GB RAM.

4.4.2 Comparison with Alternative methods

To illustrate the effectiveness of the method developed in this thesis, the author investigated four alternative methods.

Method 1: Convex hull-based method. This method first finds the cut-off points along with the network, whose distance to/from the facility is equal to the cut-off distance. Then, the convex hull of the cut-off points is used to represent the catchment area.

Method 2: A SPT-based triangulation method. This method is a simplified version of the proposed framework. Specifically, after the construction of subgraph, a normal SPT is built to obtain the distances between network nodes and the facility. Then, using the network nodes as the input, a Delaunay triangulation is built to generate the contour lines at the specific cut-off distance.

Method 3: An extended SPT-based triangulation method. As indicated by the name of this method, the difference between this method and the proposed method only occurs at the part of triangulation construction. Instead of a constrained Delaunay triangulation, a Delaunay triangulation is constructed based on the nodes of the extended SPT. The contour lines are then generated based on the constructed Delaunay triangulation.

Method 4: The ArcGIS method. In this method, the service area tool provided by ArcGIS is used to generate the network-based catchment areas. The ArcGIS method is conducted via the ArcGIS Desktop 10.6, where the polygon type of the service area is set to be “detailed” and the other parameters are set as default.

Using the same input and setting as that of Figure 4.7 (Section 4.2.2.3), the catchment areas generated by the four above methods and our proposed method are visualized in Figure 4.12. It is noticeable that some inaccessible edges are wrongly included in the catchment area generated by method 1. Very few inaccessible edges are wrongly included in the catchment areas generated by method 2 and 3. As shown by the dotted

black circle 4 in Figure 4.12 (c), the method 3 has improvements on excluding inaccessible edges than method 2 because the non-SPT edges are included in the extended SPT. Some accessible edges are not correctly included in the catchment areas generated by method 2 and 3. Specifically, these accessible edges are marked by the dotted back circles 1, 2 and 3 in Figure 4.12 (b) and Figure 4.12 (c). In contrast, all accessible edges are correctly included, and inaccessible edges are correctly excluded in the catchment areas generated by method 4 (Figure 4.12 (d)) and our method (Figure 4.12 (e)). Slight differences can be found in terms of the shapes of these two catchment areas (e.g. marked by the dotted black circle 6 in Figure 4.12 (d) and Figure 4.12 (e)). The comparison between the proposed method and method 3 illustrates the necessity of building the constrained Delaunay triangulation. The comparison between method 3 and method 2 shows the advantages of the extended SPT over the normal SPT.

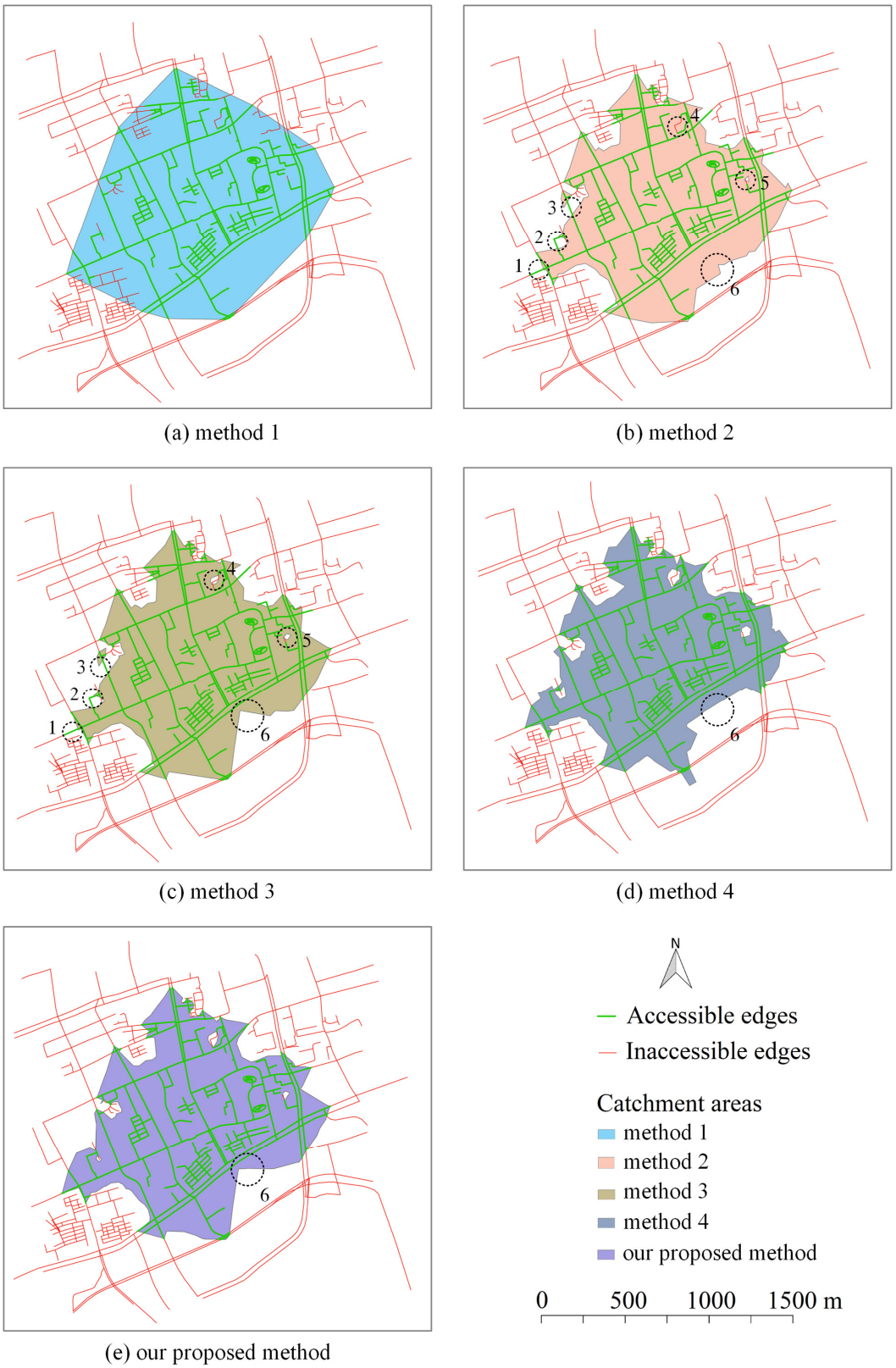

Figure 4.12. The catchment areas generated using five different methods.

4.4.3 Accuracy Evaluation

In this section, the accuracy of TCAs generated by the proposed method is evaluated. Based on the visual analysis of Figure 4.12, we select the ArcGIS method as a comparison because it has the closest result as ours. For the accuracy evaluation, a benchmark is needed to represent the "correct/actual" catchment area of a facility with a given cut-off distance. Corresponding to the TCA definition given in Section 4.2.1, a set of regular grid points within the searching box of each facility are generated (see Figure 4.13). The distance between any grid point and the facility can be easily calculated based on the extended-SPT. The grid points can then be classified into accessible points and inaccessible points, depending on whether they are within or beyond the cut-off distance as shown in Figure 4.13.

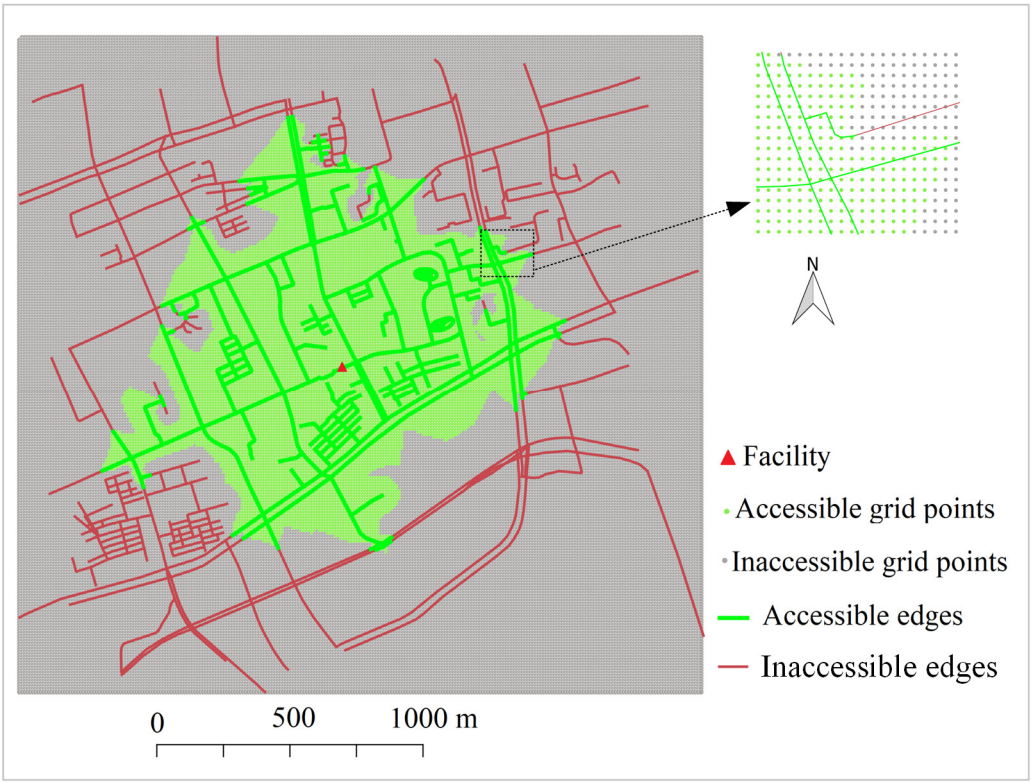

Figure 4.13. Illustration of accessible and inaccessible points within the searching box.

Theoretically, a good catchment area should satisfy two criteria:

- a high ratio of the correctly included accessible points to all the included points
- a high ratio of the correctly included accessible points to all the accessible points

In this way, the accuracy evaluation of catchment areas is reduced to a binary classification issue. Specifically, the first criterion means a high precision; and the second criterion means a high recall. Furthermore, another commonly used integrated metric, i.e., F1 score, is used as an integrated metric of accuracy evaluation. F1 score is

the harmonic average of the precision and recall, and a higher F1 score represents a better accuracy of the generated catchment area. Mathematically, the precision, recall and F1 score are measured as follows.

$$Precision = \frac{N_{acc\_cat}}{N_{cat}} \tag{4.4}$$

$$Recall = \frac{N_{acc\_cat}}{N_{acc}} \tag{4.5}$$

$$F_1\_score = 2 * \frac{Precision * Recall}{Precision + Recall} \tag{4.6}$$

Where:

N_{acc_cat} denotes the number of accessible grid points within the catchment area
N_{cat} denotes the number of grid points within the catchment area
N_{acc} denotes the number of accessible grid points
$P, R,$ and F_1_score denote the precision, recall, and F1 score, respectively

For evaluation, the 32 station centers of the metro line 12 are used as the input facilities. Corresponding to non-motorized transport mode, the cut-off distances are set to be 0.8 km, 1 km, and 1.2 km, respectively. The size of the grid is set to be 10*10 m for the generation of grid points. Given a cut-off distance, the corresponding precision, recall and F1 score for each station are measured. The average values of the precision, recall and F1 score for the 32 stations are listed in Table 4.2. As indicated by the average number of grid points in the TCAs, the TCAs generated by the proposed method are larger than those generated by the ArcGIS method. The two methods both obtain a mean F1 score larger than 90% for all the three cut-off distances, indicating that both methods can be suitably used for the generation of network-based TCAs. As reflected by the mean values of F1 score, the proposed method generally achieves better performance than the ArcGIS method. The ArcGIS method generally gets a higher precision than the proposed method, indicating that less inaccessible grid points are wrongly included in the TCAs generated by the ArcGIS method. On the contrary, the proposed method achieves higher recall than the ArcGIS method, indicating more accessible grid points are correctly included in the catchment areas.

Table 4.2. Statistics for 32 stations under different cut-off distances.

Cut-off distance (km)	Average number of grid points in the TCAs		Average Precision		Average Recall		Average F1 score	
	ArcGIS	Ours	ArcGIS	Ours	ArcGIS	Ours	ArcGIS	Ours
0.8	9271	10217	0.932	0.908	0.885	0.954	0.904	0.928
1.0	15120	16798	0.948	0.916	0.891	0.962	0.914	0.937
1.2	22480	25049	0.955	0.921	0.899	0.973	0.924	0.946

4.4.4 Time Efficiency

The time efficiency is evaluated by using two experiments. In the first experiment, we compare the efficiency of generating TCAs of point-based facilities by using our method and ArcGIS method. In the second experiment, we compare the efficiency of generating TCAs of multiple-point facilities by using the dissolving-based and virtual node-based methods (see Section 4.2.3.2).

Experiment 1: Point-based facility

The running times of the ArcGIS and our method are used as the metric for efficiency evaluation. For the ArcGIS method, the running time includes two parts: the time used for searching the projected points of facilities and the time used for generating the catchment areas. For the proposed method, the running time is the entire process time from input to output. The experiment requires to set two parameters, namely the number of point-based facilities and the cut-off distance. Similar to Section 4.4.3, the cut-off distances are set to be three different values: 0.8 km, 1 km, and 1.2 km. With respect to the number of facilities, three different levels (i.e., 32, 64, and 128 facilities) are selected. The facilities are randomly selected from the 165 metro entrances of line 12. By combining these two parameters, we get nine different experimental settings. For each experimental setting, the same experiment is conducted for three times, and the average running time is taken as the final running time.

The running times listed in Table 4.3 reveal that our method is at least two times faster than the ArcGIS method. Under the same cut-off distance, more facilities lead to an increase in the running time for both methods. And the increase for the ArcGIS method is more obvious than that of ours, as indicated by the increase of running time ratios between the ArcGIS method and ours. It is also noticeable that our method is more sensitive to the change of cut-off distance. An increase in the cut-off distance causes a larger increase in running time in our method than the ArcGIS method. A larger

distance of the cut-off distance leads to a larger size of subgraph; hence, the overall running time of our method has been increased.

Table 4.3. Running times of generating the catchment areas of point-based facilities using the ArcGIS and the proposed methods.

Experimental setting		Running time (seconds)		ArcGIS running time /Our running time
Number of facilities	Cut-off distance (km)	ArcGIS	Ours	
32	0.8	177	54.1	3.3
64	0.8	376	65.3	5.8
128	0.8	714	84.8	8.4
32	1.0	177	58.8	3.0
64	1.0	377	76	5.0
128	1.0	717	105.5	6.8
32	1.2	178	65.4	2.7
64	1.2	380	92.1	4.1
128	1.2	728	135	5.4

Experiment 2: Non-point facility

In this experiment, we randomly select 5 different numbers of metro stations (Table 4.4) from the 280 metro stations to test the running time based on the dissolving-based and virtual node-based methods. The two methods are conducted using the proposed method and the cut-off distance is set to be 1.2 km. For the dissolving-based method, the running time represents the time used for generating individual catchment areas of all the entrances, i.e., the time for dissolving the catchment areas is not included. Similar to experiment 1, the same experiment is conducted three times for each experimental setting, and the average running time is deemed to be the final running time. As shown by the results listed in Table 4.4, we observe a sharp drop in the running time when the virtual node-based method is used for generating the metro catchment areas. Such a drop indicates that the virtual node-based method can largely improve the time efficiency, and the improvement is more obvious with the increase of the number of input facilities. Furthermore, no additional dissolving procedure is required by the virtual node-based method. Combined with the results obtained in Table 4.3, we can infer that the virtual node-based method can achieve an even larger improvement in efficiency if compared with conducting the dissolving-based method via ArcGIS. For instance, the running time for generating the catchment areas of 1143 entrances by using ArcGIS is 5326 s, which is 22 times as much as the running time required by the virtual node-based method (i.e., 236.4 s).

Table 4.4. Running times of generating the catchment areas of non-point facilities using the virtual node-based and dissolving-based methods. Both methods are conducted via the proposed method and the cut-off distance is 1.2 km for all the experimental settings.

Experimental setting		Running time (seconds)		VNB running time /DB running time
Number of stations	Number of entrances	Virtual node-based (VNB)	Dissolving-based (DB)	
50	193	75.6	152.5	2.0
100	393	119	321.8	2.7
150	633	152	480.2	3.2
200	830	189.6	631	3.3
250	1022	219.6	747.4	3.4
280	1143	236.4	814.4	3.5

4.5 Discussions

The impedance of a network edge is measured by its length in this study. In practice, we may use travel time rather than length as the impedance. The proposed framework can be easily applied to generate the TCA within a given cut-off time through minor modifications. Specifically, the modification occurs at the step of subgraph construction, i.e., the cut-off time needs to be transferred to a cut-off distance to define the size of the searching box. Such transfer can be achieved by multiplying the cut-off time by the maximum speed of road edges.

Furthermore, other potential environmental factors, such as road quality (e.g., road material) and connectivity, can be incorporated into the travel impedance modeling. For instance, the sidewalk is an important element that may need consideration for defining the travel impedance of walking. Correspondingly, cyclists may pay more attention to the number and quality of bike lanes. In general, the impact of these elements can be modeled by incorporating additional weighing factors to the length of road edges. The updated travel impedance of an edge e denoted as follows.

$$Tp(e) = f(d(e)) \tag{4.7}$$

where $Tp(e)$ is the new impedance of e, $d(e)$ is the length of e, and $f(*)$ is the weighting function determined by considered influence factors. Hence, a new weighted road network can be constructed and used to support the new approach for the generation of TCAs.

The interpolation based on the constrained Delaunay triangulation is one of the key components of the proposed framework. Since all road segments are included as the constraints during the triangulation, the interpolated distances along the network are thus guaranteed to be accurate. On the other hand, the interpolation by triangulation cannot guarantee an accurate result for the off-network area. This is reflected by the accuracy evaluation of generated TCAs (i.e., the precision and recall are both below 100%). Generally, the high F1 score indicates that such a triangulation-based method offers a reasonable accuracy of TCAs in the urban context. This can be partly explained by the high density of roads in urban areas because a high road density means more network nodes are involved during the interpolation. Figure 4.14 shows an example of the scatter plot between the road density and the F1 scores. The road density is measured as the ratio of the total length of subgraph edges to the area of the corresponding searching box. The F1 scores correspond to the evaluation of the 32 catchment areas generated by our framework under the cut-off distance of 1.2 km (see Section 4.4.3). As shown, although it is not a linear relationship, the distribution generally indicates that a higher density of road is likely to have a better F1 score.

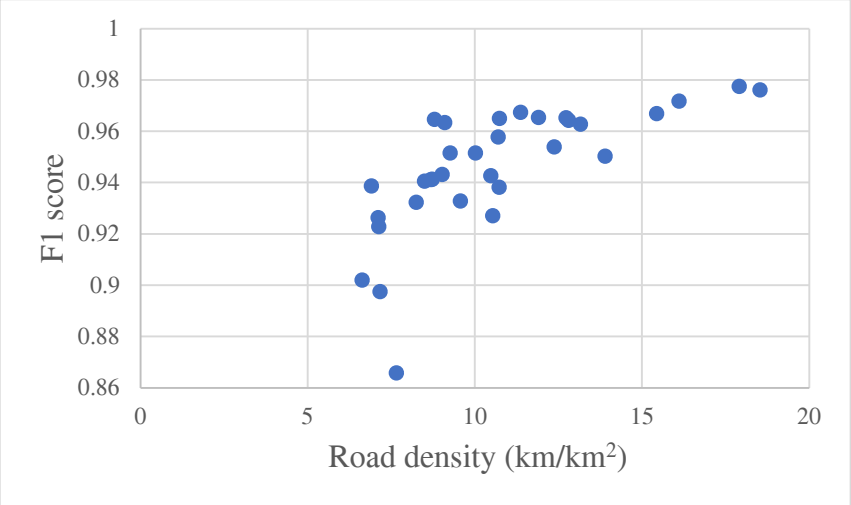

Figure 4.14. Relationship between road densities and F1 scores. The F1 scores correspond to the evaluation of the 32 catchment areas generated by our framework under the cut-off distance of 1.2 km.

It is important to note the F1 score is an integrated accuracy evaluation from the geometrical perspective. A high F1 score means a high similarity of the generated catchment area and the real catchment area. In this way, such a metric is especially useful when the generated catchment area is employed to differentiate the transit-covered areas from underserved areas. If the generated catchment area is specifically used for estimating the population being covered by a station (e.g., for transit ridership modeling), we may need additional metrics to evaluate the performance of a TCA

generation method, i.e., metrics to test how the covered population estimated by the generated TCAs is different from the real covered population. For instance, a comparison of the total population of the accessible points and the covered population by the catchment area could be a possible approach.

As demonstrated by the time efficiency evaluation, the proposed framework is especially useful for a fast TCA generation of non-point transit facilities (e.g., rail transit stations). For instance, identifying a suitable cut-off distance for transit ridership modeling from a series of candidates (e.g., 600 – 1200) is a typical time-consuming scenario. The running time of our method is largely affected by the cut-off distance. A larger cut-off distance means a larger size of subgraph and more computing time for the construction of the extended SPT and constrained Delaunay triangulation. For transit catchment areas by non-motorized transport, the cut-off distances usually are small (e.g., less than 3km), which makes the running time can be limited at a reasonable level. In our test, we find that the most time-consuming part of the processing is the construction of constrained Delaunay triangulation. Therefore, reducing the number of constraint edges is a possible way to improve time efficiency. Correspondingly, a preprocess of road simplification (e.g., remove the intermediate points within a straight road edge) could help speed up the generation of catchment areas.

4.6 Summary

Generating the network-based TCA is one of the prerequisites for coverage-based accessibility analysis. It is therefore highly desirable to make this service sharable and transparent to the public. Our open-source framework of generating TCAs by non-motorized transport is developed for this purpose. The methodological framework includes three components of the process: subgraph constructions, extended SPT construction, and contour generation. The methods on how to extend the framework to the directed graph and non-point facilities are developed. The implementation of the framework is provided as an open-source prototype. Using the proposed framework and the derived acceptable distances in Chapter 3, the BCAs of metro stations in Shanghai are generated. Comparing with 800 m PCAs, the population coverage ratio of the central city has been increased from 47.1% to 83.9% by using dockless shared bikes as the feeder mode. The overall overlap degrees for catchment areas have also been increased noticeably by bike-and-ride. The maximum overlap degrees for PCAs and BCAs have been increased from 5 to 9. These results provide us a general picture of how bike-and-ride could change the accessibility to Shanghai Metro.

The feasibility and effectiveness of the proposed framework are evaluated. The results show that the precisions and the recalls of the generated TCAs are above 90% and the F1 scores are comparable with the ArcGIS method. The running time of the proposed

method is much faster than the ArcGIS method under the nine different experimental settings. The proposed framework is especially efficient in generating a larger number of catchment areas of non-point facilities.

5 Bike Accessibility to Metro Systems Constrained by Crowdedness

The coverage-based analysis offers a general picture of how bike-and-ride could change the accessibility to the metro system (Section 4.3). However, it failed to provide a finer-scale assessment of the accessibility inside the catchment areas of metro stations. The first objective of this chapter is to assess the bike accessibility at the population grid level. To achieve this objective, an indicator called metro accessibility level (MAL) is introduced to measure accessibility to metro systems. As mentioned in Section 4.3, bike-and-ride could offer a possibility to avoid crowdy stations by shifting to less crowdy stations; thus, the second objective is to examine in which population grid(s) such possibilities exist.

Section 5.1 analyzes the importance of grid-level accessibility and reasons for the necessity of incorporating crowdedness. Section 5.2 elaborates the modeling of the MAL indicator. In Section 5.3, the proposed indicator is applied, taking the same test site Shanghai. The decision procedure of whether a population grid can be shifted from crowded to non-crowded stations is presented in Section 5.4, and the case of morning peak is analyzed accordingly. Section 5.5 discusses the analytical results and potential improvements on the MAL indicator. Section 5.6 summaries this chapter.

5.1 The Role of Crowdedness in Accessibility Modeling

Among the numerous assessment approaches of public transit accessibility assessment, the coverage analysis of transit catchment areas (TCAs) is easy to implement and interpret. Generally, a large area/population coverage of a transit system is regarded as an indicator of good accessibility of the transit system (Currie, 2010). The coverage-based analysis is useful for capturing a general picture of the accessibility to public

transit. However, the area/population coverage of a transit system is a simplified indicator because all the traveler inside the catchment is deemed to have the same degree of accessibility (García-Palomares et al., 2013).

The public transport accessibility level (PTAL) introduced in Chapter 2 can be adopted to model the accessibility at a finer spatial scale. It involves differentiation factors, such as average waiting time and access time, to assess the accessibility of individual spatial grids. The finer-scale measurement can offer subtle insights into micro-level transport planning. For instance, specific areas that need accessibility improvement can be determined by a joint analysis of accessibility and the corresponding population distributions. Therefore, the PTAL has shown its wide applicability outside London (i.e., the origin of the PTAL), including cities such as Manchester (the UK) (Transport for Greater Manchester, 2016), Melbourne (Australia) (Saghapour et al., 2016), and Surat (India) (Adhvaryu et al., 2019). As one of the limitations of the PTAL, the impact of transit crowdedness is not considered in the accessibility modeling. This is partly because of the difficulty in modeling and incorporating the impact into the PTAL. However, for metropolitans (e.g., Shanghai and London) that suffer from high-level transit crowdedness during peak hours, it is crucial to consider the impact of crowdedness on transit accessibility. Existing studies have shown that transit crowdedness affects traveling from several aspects. First, the crowdedness could increase the train dwelling time and cause train delay depending on the number of boarding, alighting, and onboard passengers (Kim et al., 2015; Lin and Wilson, 1992). Second, the crowdedness can lead to additional waiting time if passengers cannot board an overcrowded train (Raveau et al., 2014). Third, the crowdedness also affects the comfort of riding and leads to problems such as anxiety and stress. As a result, the transit crowdedness is an important component of transit reliability and can affect users' modal choices (Tirachini et al., 2013) and route choices (Kim et al., 2015; Raveau et al., 2014).

The crowdedness can be understood as a result of the imbalance between the supply and demand of transit services, i.e., a result of the excessive competition from passengers. To incorporate the competition into transit accessibility measurement, several studies (Kyung et al., 2018; Langford et al., 2012; Xu et al., 2015) adopted the two-step floating catchment area (2SFCA) method to measure the transit accessibility. The original 2SFCA method (Luo and Wang, 2003) is developed for measuring accessibility to health services and consists of two steps. Step 1 measures the supply-to-demand ratio of a facility as the ratio between its supply and potential demand (e.g., population in the catchment area of the facility). Step 2 measures the accessibility of a location as the cumulative supply-to-demand ratios of all the facilities within its catchment area. In addition to some adaptions (e.g., the model of transit supply and inclusion of distance decay effect) need to suit the transit accessibility characteristics, the core value the 2SFCA-based methods added to the transit accessibility

measurement is the inclusion of the supply-to-demand ratio. As argued by (Langford et al., 2012), the supply-to-demand ratio (in step 1) can reflect the impact of excessive demand on transit accessibility. Hence, the transit "crowdedness" is implicitly integrated into the accessibility measurement. Generally, a larger supply-to-demand ratio acts as an indicator of a lower "crowdedness". However, the supply-to-demand ratio is still "biased" to some extent. Given a bus with 60 seats as its supply and two different scenarios with different levels of demands, i.e., scenario 1 with 10 passengers and scenario 2 with 20 passengers. In this case, the supply-to-demand ratio of scenario 1 is two times as that of scenario 2, although there is no crowdedness for both scenarios. In addition, the 2SFCA methods usually model potential transit demand based on the population inside the pedestrian catchment areas (PCAs) without considering the demand beyond the PCAs.

To integrate the crowdedness into the accessibility measurement, we propose an indicator called metro accessibility level (MAL) on the basis of the PTAL. We explicitly incorporate the transit crowdedness into MAL by transferring the crowdedness into additional waiting time. We then apply the MAL indicator to measure bike accessibility to the metro system in Shanghai. To provide a better spatiotemporal granularity of accessibility analysis, the accessibility during morning and evening peaks are measured, respectively. Additionally, the bike catchment areas (BCAs) and biking speeds of individual metro stations are measured using trajectory data; hence, a more realistic assessment of bike accessibility to metro systems can be obtained.

On the other hand, bike-metro integration has the flexibility to relieve the metro crowdedness due to its potential in increasing accessibility to metro systems (see Section 4.3). For instance, less crowdy metro stations beyond walking distance might become accessible within an acceptable time if biking is used as the access mode instead of walking. As a result, from the perspective of users, using biking to substitute walking might help them to avoid crowded metro stations without increasing the total access time (TAT). From the perspective of metro operators, the promotion of bike-metro integration might help to relieve the crowdedness of some metro stations. Thereby, we propose methods to determine the locations where users might use biking as the access mode to avoid crowded stations without increasing the TAT.

5.2 Metro Accessibility Level

1) Access time

The access time (AT) from a traveler location i to a metro station k depends on the corresponding distance and speed. In the case of a station with multiple entrances, the distance to the nearest entrance is taken and measured by using Dijkstra's shortest path

algorithm (denoted as Dis_{ik}). For different metro stations, the catchment areas might be different because the willingness of walking/biking depends on the context of a station (e.g., location and service quality). In order to derive the BCAs of individual metro stations, the 75th percentile distance of the access/egress trips of a metro station is regarded as its maximum acceptable biking distance (Lin et al., 2019; Wang et al., 2016). Similarly, the biking speeds heading to metro stations vary from station to station because the road condition around each metro station is different. Thereby, the average biking speed heading to station k (denoted as AvgS_k) is estimated as the average biking speed of its associated bike-and-ride trips.

$$\mathrm{AT}_{ik} = \mathrm{Dis}_{ik}/\mathrm{AvgS}_k \tag{5.1}$$

2) Scheduled waiting time

Based on the accessible metro stations of a traveler location, the corresponding accessible metro lines can be constructed. The scheduled waiting time (SWT) of a metro line is then decided by its service frequency and measured as half of the headway.

$$SWT_j = 0.5 * H_j = 0.5 * \frac{60}{F_j} \tag{5.2}$$

Where SWT_j is the scheduled waiting time for metro line j. F_j and H_j are the service frequency and headway of metro line j, respectively. For instance, for a metro line with a service frequency of 10 train/hour, the corresponding scheduled waiting time is 3 minutes. If the service frequencies of the two directions are different, the average value is calculated as the headway of the metro line.

3) Average waiting time caused by crowdedness

As mentioned in Section 5.1, the metro crowdedness can cause additional waiting time for passengers from two aspects: the train delay and the allowed boarding capacity. This study focuses on modeling the second aspect. Specifically, a passenger needs to wait for additional trains (e.g., waiting for the next train) when the train occupancy rate exceeds a certain threshold. Thereby, the average waiting time caused by crowdedness (AWTC) can be calculated as follows.

$$AWTC_{jk} = a_{jk} * H_j * RC_{jk} \tag{5.3}$$

$AWTC_{j_k}$ is the average waiting time caused by crowdedness for metro station k of metro line j. a_{jk} represents the average number of extra trains that a passenger needs to wait when he/she cannot get on board at station k of metro line j. H_j is the headway of metro line j. RC_{jk} is the ratio of crowdedness, which can be calculated as the ratio between the number of times that the train with an occupancy rate exceeding the threshold and the train frequency. Assuming the headway of a metro line is 6 minutes, 3 of the 10 trains in one hour are detected as fully loaded, and passengers need to wait for 1 additional

train to board, the corresponding $AWTC$ is then measured as $1 * 6 * \frac{3}{10} = 1.8$ minutes. Similar to the SWT, the AWTC is also measured as the average value across a time period. In contrast, the train crowdedness is measured for every metro station of a metro line because the crowdedness of two adjacent stations might be different depending on the number of boarding and alighting passengers. Additionally, different cities might use different thresholds of occupancy rate to define the condition that a passenger could not get on board. For instance, users of London Underground may not board the first train (i.e., waiting for the next train) when the occupancy rates exceed 70%, whereas the threshold is 85% for users of Santiago Metro (Raveau et al., 2014).

4) Total access time

Based on the above three components, the total access time (TAT) from location *i* to metro station *k* of metro line *j* is defined as

$$TAT_{i_{j_k}} = AT_{ik} + SWT_j + AWTC_{jk} \tag{5.4}$$

The total access time from location *i* to metro line *j* is then measured as

$$TAT_{i_j} = \min\left\{TAT_{i_{j_k}}\right\}, \qquad k \in K \tag{5.5}$$

where K represents all the stations of metro line *j* that can be accessed by location *i*. When two or more stations of metro line *j* (i.e., |K| > 1) are accessible, the TAT from location *i* to metro line *j* equals to the minimum TAT of its accessible stations.

5) Equivalent doorstep frequency

The total access time from location *i* to metro line *j* is transferred into equivalent doorstep frequency (EDF) as 30 minutes divided by the corresponding TAT.

$$EDF_{i_j} = \frac{30}{TAT_{i_j}} \tag{5.6}$$

6) Metro accessibility level

The metro accessibility level of a location *i* is calculated as a summation of the EDFs of its accessible metro lines.

$$MAL_i = EDF_{i_{jmax}} + \sum_{j \neq jmax} 0.5 * EDF_{i_j} \tag{5.7}$$

where $EDF_{i_{jmax}}$ represents the metro line with the largest EDF with respect to location *i*, and its weighting factor is set to be 1. A weighting factor of 0.5 is assigned to other routes (Transport for London, 2015).

5.3 Bike Accessibility to Shanghai Metro

In this section, the proposed indicator and method are applied to the test site Shanghai. A detailed analysis of bike accessibility to the Shanghai Metro is presented.

5.3.1 Data Preparation

We use population grids as the spatial unit for accessibility measurement. The population dataset originated from the 250 * 250 m Global Human Settlement (GHS) of 2015 provided by the Joint Research Centre of the European Commission (Schiavina et al., 2019). The road network, metro-related data (e.g., timetable), and bike trajectory are the same as those described in Section 3.2. The 75th percentile distances of individual metro stations obtained in Chapter 3 are used as the acceptable distances of individual stations. Additionally, the average biking speed around each individual metro station is measured and used to calculate the biking access time.

In terms of the metro crowdedness, Shanghai Metro provides a system, namely "Real-time info Display System of Shanghai Metro Passenger Flow[8]" to indicate the crowdedness of the metro system. The system is based on the data collected by automated fare collection (AFC), automatic train supervision systems and dynamic train weighing systems. There are three different states of a metro station/an interval (in between two adjacent stations), namely "suspended", "crowded", and "clear", indicated by red, yellow, and green, respectively. Generally, green means the transportation capacity is sufficient and the station and metro train can provide normal service. Yellow represents operational congestion, indicating that the transportation service capacity is insufficient, the train or station is in a crowded state. Red indicates the disruption of the operation, such as serious train delays and transit route closures (Shen et al., 2012). The crowdedness ratio of a metro station (see Section 5.2) is measured by counting the number of yellow states within a certain time period. A station is labeled as yellow (i.e., crowded) if it is under the state of limiting passenger crowd (e.g., parts of the entrance is closed) or the density of passengers on the platform exceeds 2 people/m^2. An interval is labeled as yellow if the number of passengers on the train exceeds 90% of the capacity of a train (including standee places) and the delay of the train is under 10 minutes (Shen et al., 2012). As a result, the crowdedness of a metro station has two forms, either the station alone is labeled as crowded (termed as form 1) or the station and an interval originated from the station both labeled as crowded (termed as form 2). Under the form 2, it is reasonable to assume that passengers need to wait for additional trains because of the high occupancy rate. On the other hand, form 1 means strategies are made to slow down the speeds of arriving

[8] http://service.shmetro.com/en/klssxx/index.htm

at the platform, prompting users' additional time to get on board than normal cases. In this study, users are assumed to wait for additional trains when either form 1 or form 2 crowdedness is observed. The crowdedness states of metro stations during one normal week (16.09.2019–20.09.2019) are collected with an interval of 2 minutes. For a specific hour, the crowdedness ratio of a metro station can then be calculated based on the number of times it is labeled as crowded among the corresponding 30 states. The α is set to be 1 for all the stations by assuming passengers need to wait for one more train when a station is crowded.

5.3.2 MALs by Walking and Biking

Population grids with a distance less than the acceptable distances of metro stations are determined and their MALs are measured accordingly. Since frequencies of the train service and the crowdedness of metro stations are different during the morning and afternoon peaks. Two periods, i.e., 8:00–9:00 (morning peak) and 18:00–19:00 (afternoon peak), are selected to analyze the MALs of grids inside the BCAs. As a comparison, the MALs by walking for both periods are measured by assuming a walking speed of 4.8 km/h and an acceptable walking distance of 800 m. According to (Adhvaryu et al., 2019; Saghapour et al., 2016), we herein use the quantiles of the MALs by walking during the morning peak to classify the MALs into 6 different levels: very poor, poor, moderate, good, very good, and excellent (Table 5.1). In comparison with the MAL by walking, two improvements made by the bike-and-metro integration are observed. First, the covered population and areas have been largely extended. The total population covered by the BCAs is two times as that covered by PCAs. Second, the proportion of the population with a MAL above poor has been increased sharply, i.e., from 39.7 % to 82.3 % for the morning peak, and from 40.4 % to 83.2 % for the afternoon peak. A closer look at the spatial distribution of the MALs by walking and biking during the morning and afternoon peaks (Figure 5.1) also confirmed these two improvements. The MALs of population grids inside the central city (i.e., area inside the outer ring) show a noticeable improvement during both periods.

Table 5.1. MALs of population grids within the biking catchment areas.

MAL level	Morning peak (8:00–9:00)				Afternoon peak (18:00–19:00)			
	Walking		Biking		Walking		Biking	
	Grid	Population	Grid	Population	Grid	Population	Grid	Population
N/A	8,372 (65%)	6,857,375 (50%)	0 (0)	0 (0)	8,372 (65%)	6,857,375 (50%)	0 (0)	0 (0)
Very poor	369 (2.9%)	423, 477 (3.1%)	2,599 (20.2%)	1,311,915 (9.5%)	407 (3.1%)	385,645 (2.8%)	2,591 (20.1%)	1,143,554 (8.3%)
Poor	812 (6.3%)	988,980 (7.2%)	1,718 (13.3%)	1,129,977 (8.2%)	795 (6.2%)	939,554 (6.8%)	1,820 (14.1%)	1,167,915 (8.5 %)
Moderate	1,075 (8.3%)	1,479,134 (10.7%)	2,662 (20.7%)	2,354,403 (17.1%)	1,066 (8.3%)	1,481,455 (10.8%)	2,687 (20.9%)	2,430,246 (17.7%)
Good	701 (5.4%)	1,081,554 (7.9%)	1,741 (13.5%)	2,012,530 (14.7%)	670 (5.2%)	1,081,979 (7.9%)	1,672 (13%)	1,939,309 (14.1%)
Very good	949 (7.4%)	1,742,552 (12.6%)	2,430 (18.8%)	3,524,040 (25.7%)	937 (7.3%)	1,750,218 (12.7%)	2,335 (18.1%)	3,490,463 (25.4%)
Excellent	609 (4.7%)	1,163,913 (8.5%)	1,737 (13.5%)	3,404,119 (24.8%)	640 (4.9%)	1,240,758 (9%)	1,782 (13.8%)	3,565,498 (26%)

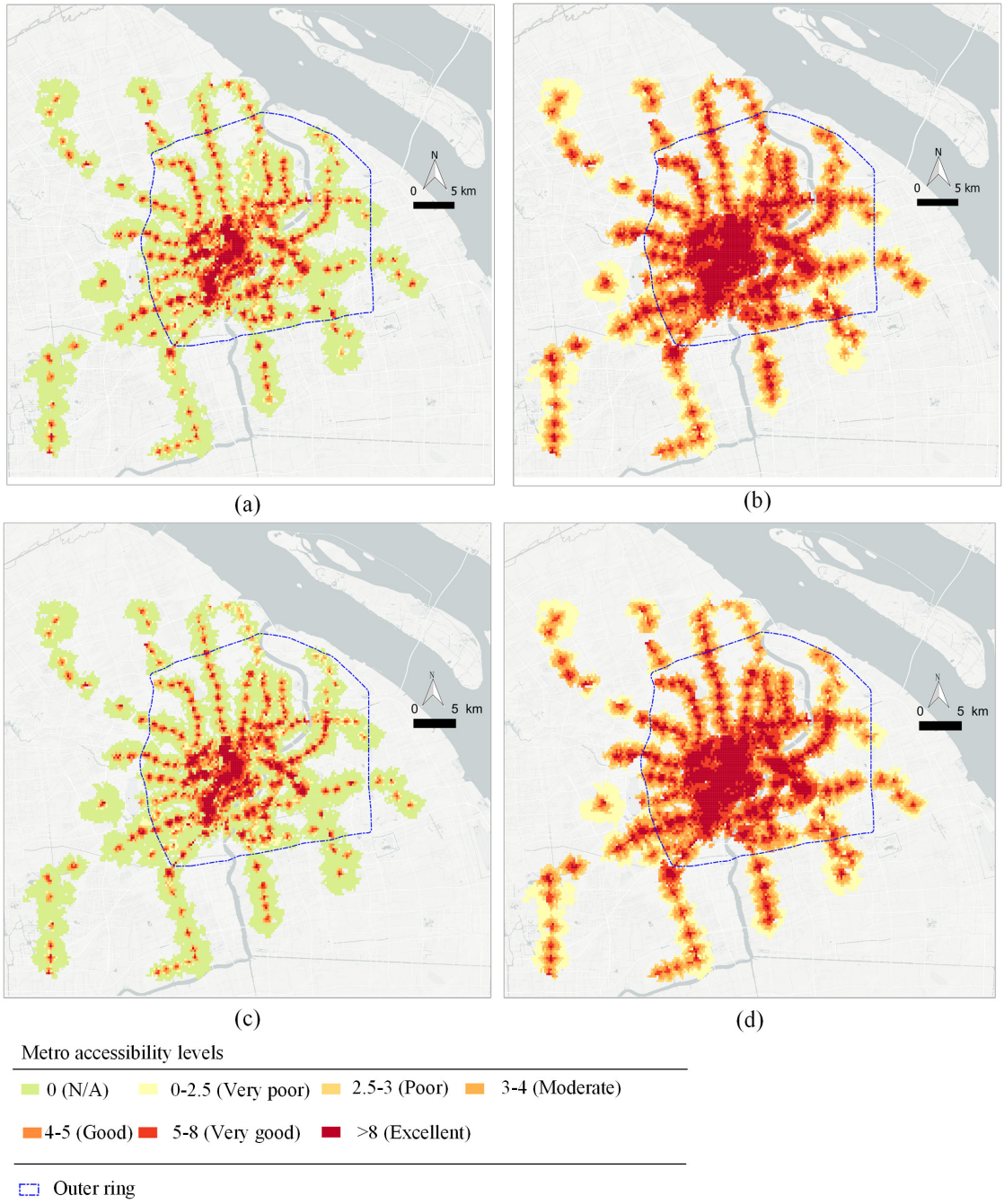

Figure 5.1. MALs of grids in the bike catchment areas during morning and afternoon peaks. (a) MALs by walking in the morning peak, (b) MALs by biking in the morning peak, (c) MALs by walking in the afternoon peak, and (d) MALs by biking in the afternoon peak.

5.3.3 MALs Constrained by Population Density

By combing with the population density distribution, the MAL map can provide fine-grained knowledge on how the metro accessibility is distributed with respect to different levels of population density. For the assessment and potential improvement of public accessibility, one type of situation needs special attention, i.e., areas with a high population density but poor metro accessibility. Figure 5.2 depicts the MAL distribution of the central city during the morning peak and its overlay with the population density. By overlaying distribution information, areas with a poor metro accessibility but a high population density are determined (labeled by the black dotted lines). Among the 7 labeled areas, areas 1, 2, 3, 4 and 6 are beyond the BCAs (i.e., MAL equals 0). Areas 5 and 7 have MALs below moderate but very high population density. The priorities of areas that need accessibility improvement can be assessed based on the levels of accessibility and population density. For example, area 1 would be the area with the top priority of metro accessibility improvement among the 5 areas beyond the BCAs. Because the 5 areas have the same level of MAL and area 1 has the highest population density among them. Similarly, the priority of area 7 should be higher than that of area 5 because area 7 has a larger population density and a lower MAL than area 5.

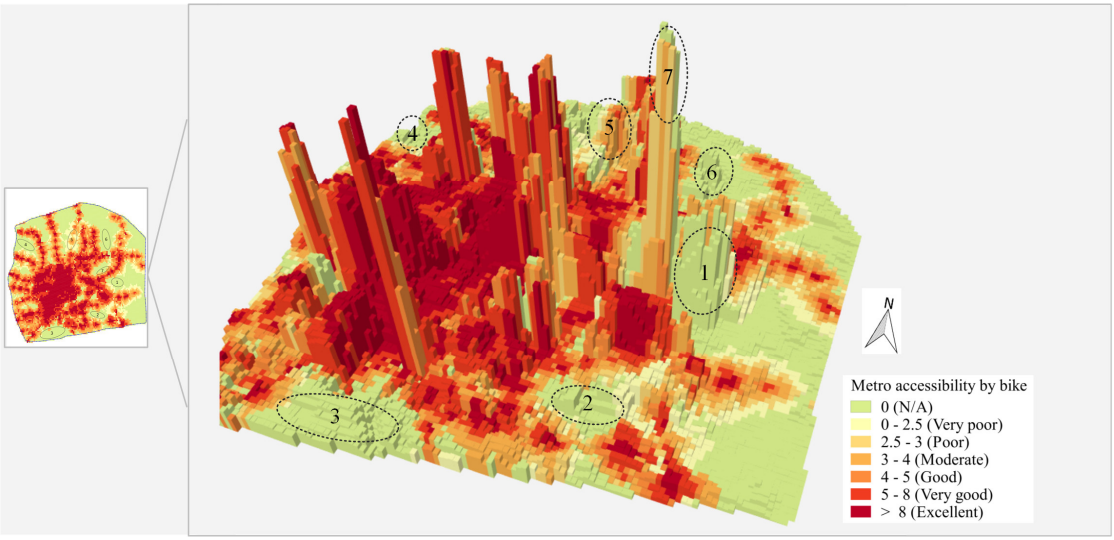

Figure 5.2. MALs constrained by population density during the morning peak in the central city.

5.3.4 MALs Decrease Caused by Crowdedness

As indicated by Table 5.1, the MALs for the morning and afternoon peaks are different. In general, the MALs by biking during the afternoon peak are slightly better than the

MALs during the morning peak, with 16.8% and 17.7% of the population under the moderate level, respectively. This is mainly due to the differences in metro service frequencies and crowdedness between the morning and afternoon peaks. The result is also a little bit counterintuitive because the service frequencies during the morning peak are usually higher than that of the afternoon peak (the average headways for the morning and afternoon peaks are 3.7 minutes and 4.3 minutes in our case). The result can possibly be explained by the difference between the metro crowdedness during the morning and afternoon peaks. The average AWTCs for the morning and afternoon peaks are 0.38 minute and 0.05 minute, respectively. We thus measure the crowdedness-caused accessibility differences by measuring the accessibility differences between MALs with and without crowdedness. Specifically, MALs without crowdedness are calculated by following a similar procedure described in Section 5.2 without the AWTC. The results are shown in Figure 5.3 and the corresponding statistics are listed in Table 5.2. The metro crowdedness shows a noticeably larger impact on the MALs of the morning peak than that of the afternoon peak, with 61.1% and 29.2% of the population's MALs being affected by the crowdedness during the morning and afternoon peaks, respectively. This is because much fewer metro stations are detected as crowded during the afternoon peak in comparison with the morning peak. Additionally, the spatial distributions of the affected areas during the morning and afternoon peaks are also different. The crowdedness-affected grids are mostly located near to two metro lines (i.e., line 2 and line 11) during the afternoon peak. Most of the affected areas during the afternoon peak are centered in the area inside the inner ring, i.e., the city center. In contrast, the affected areas during the morning peak are not only limited to the city center but also widely distributed in the suburban area. This can be partly explained by the unbalanced distributions of jobs and residences in Shanghai. The major commuting direction during the morning peak is from the suburban to the city center, and it reverses for the afternoon peak. Furthermore, people usually have more choices instead of going home directly during the afternoon peak, which might also help relieve the crowdedness.

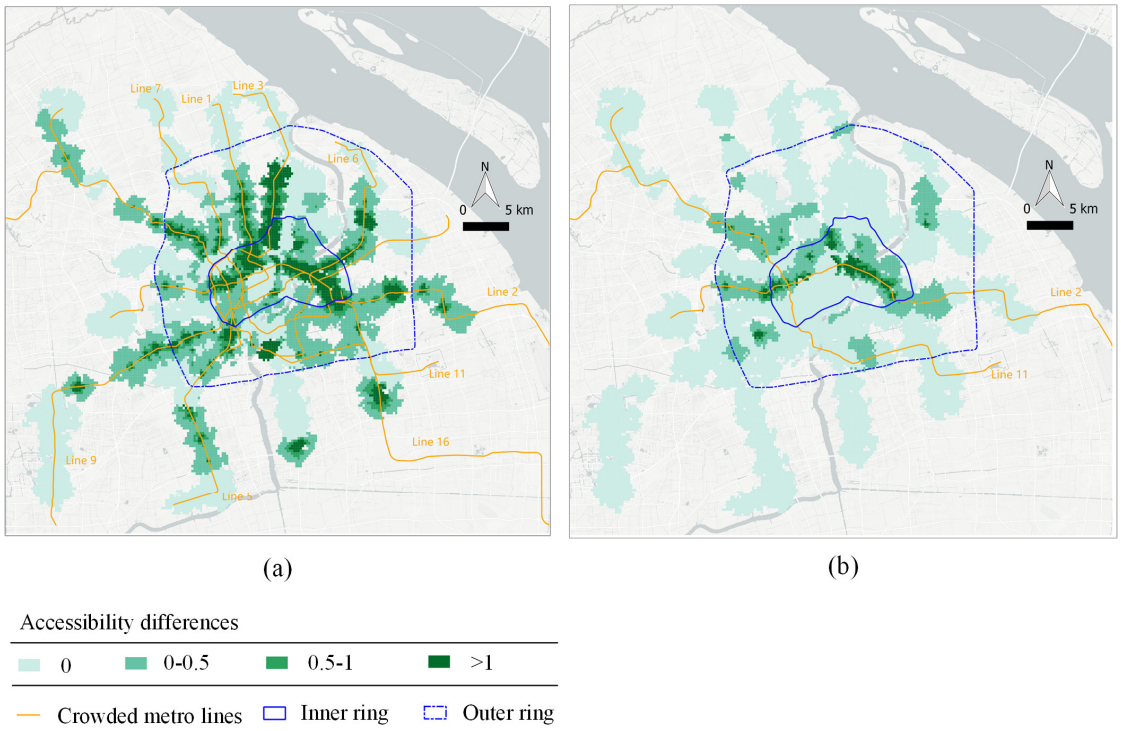

Figure 5.3. MAL differences caused by crowdedness during the morning and afternoon peak. (a) the morning peak, and (b) the afternoon peak.

Table 5.2. Proportions of grids and population in different ranges of MAL differences.

MAL differences	Morning peak		Afternoon peak	
	Grid	Population	Grid	Population
0	48.3%	38.9%	81.6%	70.7%
0–0.5	33.7%	33.9%	15.1%	21.6%
0.5–1.0	7.6%	10.5%	1.7%	4.1%
>1	10.4%	16.6%	1.5%	3.6%

5.4 Mapping Grids with the Possibility of Avoiding Crowdedness

It is possible to avoid crowdy stations without increasing the total access time by using biking to substitute walking as the access mode. The question here is to examine in which location(s) such possibilities exist and how they distribute spatially. The general

idea is to check if bike-metro integration could enable a traveler to get access to any less crowdy station beyond the walking distance without increasing the total access time (Figure 5.4). The crowdedness of a metro station is determined as the average crowdedness of its associated metro lines. Then, a metro station can be classified as a crowded or non-crowded station depending on the degree of crowdedness. To find all the potential shifts from crowded to non-crowded stations of a location i, the following steps are needed.

- **Step 1**: Find all crowded stations within the walking distance of location i, which are represented as $S_i(w)$.
- **Step 2**: Find all other stations beyond the walking distance but within the biking distance of location i, which are represented as $S_i(w2b)$.
- **Step 3**: For a crowded station $s_c \in S_i(w)$ and a non-crowded station $s_{nc} \in S_i(w2b)$. The corresponding walking TAT from location i to the crowded station s_c is $TAT_{is_c}(w)$, and the corresponding biking TAT from location i to the non-crowded station s_{nc} is $TAT_{is_{nc}}(b)$. If $TAT_{is_{nc}}(b) < TAT_{is_c}(w)$, then passengers in location i may avoid the crowded station s_c by using biking to access the non-crowded station s_{nc}.
- **Step 4**: Repeating step 3 to examine all possible shifts of (s_c, s_{nc}) for every individual traveler location.

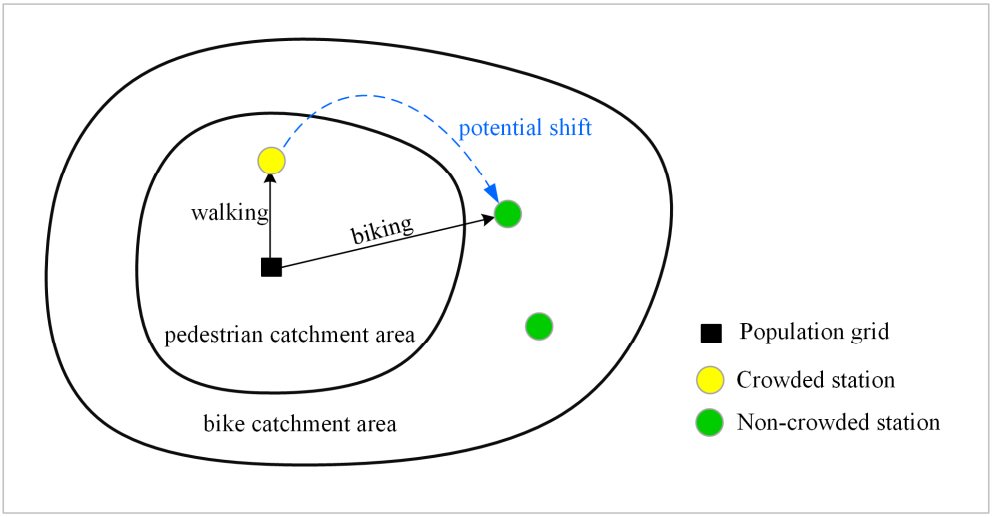

Figure 5.4. Illustration of the shift from crowded to non-crowded stations.

Based on the above 4 steps, we herein take a closer look at the morning peak because of its heavy crowdedness. The threshold for crowded and non-crowded stations is set

to be zero, i.e., stations with an average AWTC larger than zero are considered as crowded. As a result, among the population grids inside the 800 m PCAs, 64.4% of the population are inside the catchment areas of the crowded stations (termed as crowdedness-affected grids, see Figure 5.5 (a)). Only 19% of the population among the crowdedness-affected grids is determined to have the possibility to shift from crowded stations to non-crowded stations, which are depicted in Figure 5.5 (b). As noted by the red circles in Figure 5.5 (b), several areas (i.e., areas 1–5) around the crowded metro stations do not have a possibility to be shifted. For instance, area 1 is around several crowded metro stations of metro line 11, which are heavily affected by the metro crowdedness. This is because stations near to this area are also crowded stations and non-crowded stations are too far away (i.e., beyond the acceptable biking distances of grids in this area).

Among the grids with the possibility of avoiding the metro crowdedness, there are two types of shifts. The first type is the shift between stations from the same metro line. The second type is the shift between stations from two different lines. The proportion of type 1 and type 2 shifts are 21.6% and 78.4%, respectively. These two types of shifts are illustrated by using two cases as shown in Figure 5.6 (also see Figure 5.5 (b)). The first and second types of shifts are demonstrated by cases 1 and 2, respectively. The corresponding access times of different population grids are listed in Table 5.3. As noted in the table, bike-metro integration can not only help to avoid the crowdedness but also can save the total access time for some population grids (e.g., grid 3 in case 1). For case 1, a part of passengers within the pedestrian catchment areas of Chunshen Road station (i.e., the crowded station) can shift to Xinzhuang station to avoid the metro crowdedness. In this specific case, since most passengers board on Chunshen Road station need to transfer at Xinzhuang station, it is practical for passengers to bike directly to Xinzhuang station instead of walking to Chunshen station and then ride to Xinzhuang station. For case 2, the shift of departure station occurs between metro stations from two different lines, i.e., from line 3 to line 10. Under such conditions, passengers may need to take further criteria, such as the convenience of transfer and total travel time, into consideration. Nevertheless, the numeric evidence can provide a reference for users to select a better departure station. For instance, it might be attractive for passengers living in grid 6 of case 2 to shift from South Changjiang Road station to Xinjiangwancheng station and the total metro access time can be largely shortened from 18 minutes to 9.4 minutes.

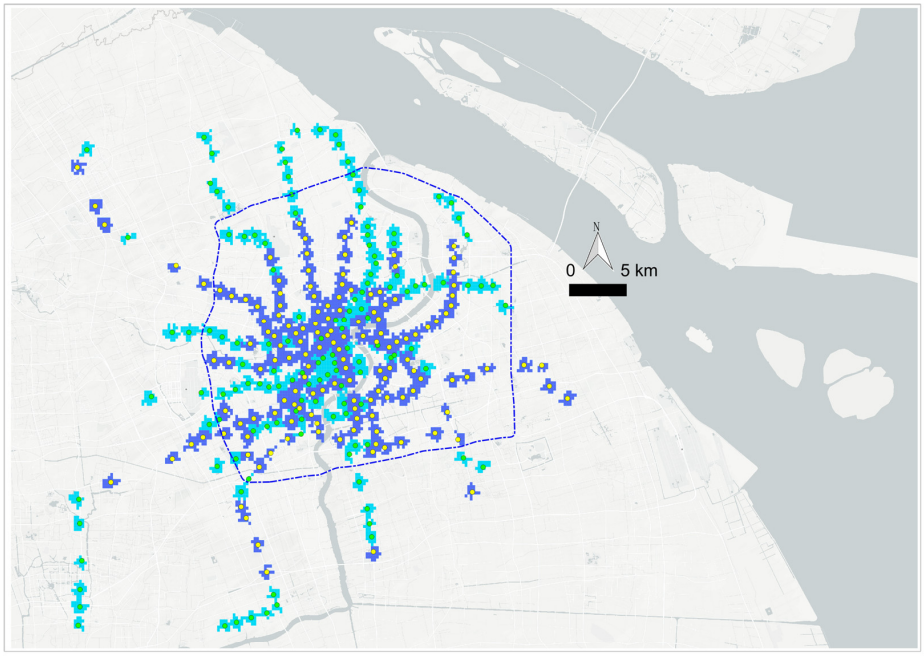

(a)

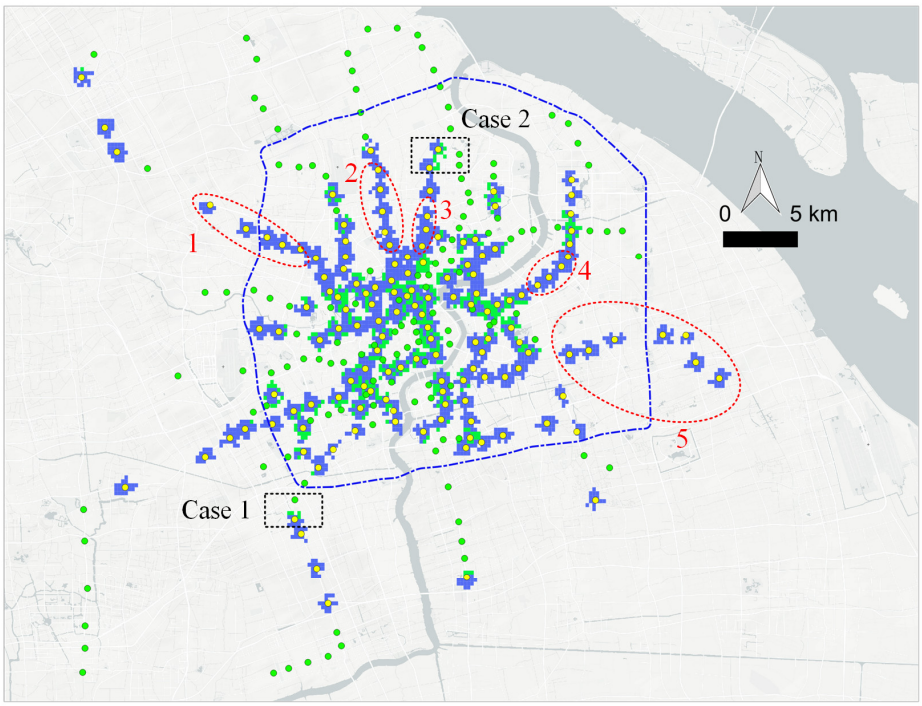

(b)

Non-crowded stations
Crowded stations
Grids within walking distance
Crowdedness-affected grids
Grids with possibility of avoiding crowdedness
Outer ring

Figure 5.5. Grids with the possibility to be shifted during the morning peak. (a) crowdedness-affected grids, and (b) grids with the possibility of avoiding crowdedness.

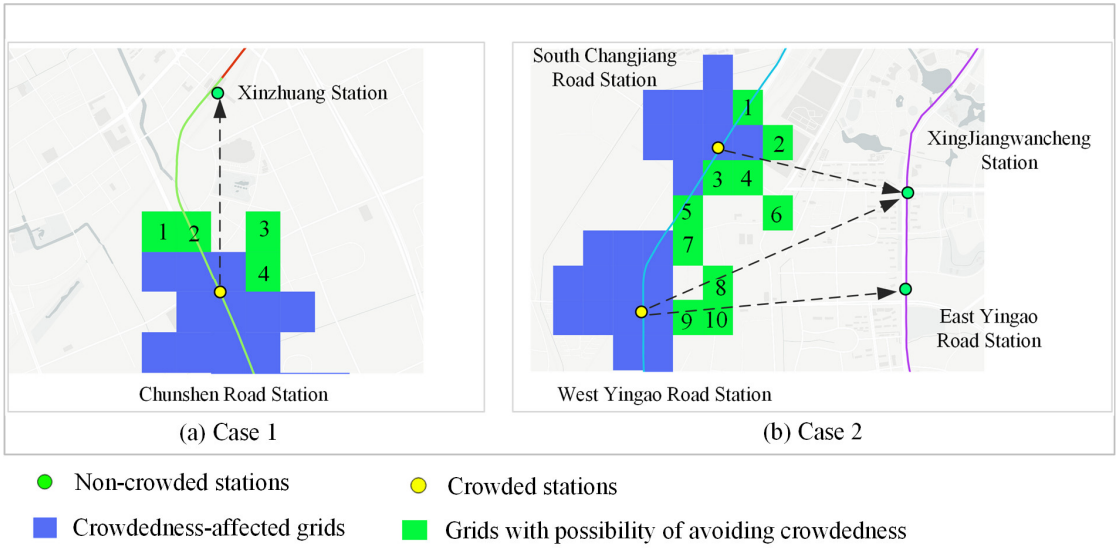

Figure 5.6. The shift of case 1 and case 2. (a) the shift between stations from the same line, and (b) the shift between stations from different lines.

Table 5.3. The access times of grids with the possibility of shift for cases 1 and 2.

Case	Grid	Crowed station	Non-Crowded station	TWAT[i]	TBAT[ii]
1	1	Chunshen Road station	Xinzhuang station	10.75	8.78
1	2	Chunshen Road station	Xinzhuang station	10.21	7.75
1	3	Chunshen Road station	Xinzhuang station	12.3	7.3
1	4	Chunshen Road station	Xinzhuang station	10.3	9.4
2	1	South Changjiang Road station	Songfa Road station	13.5	9.8
2	2	South Changjiang Road station	Xinjiangwancheng station	17.2	11
2	3	South Changjiang Road station	Xinjiangwancheng station	13.5	12.2
2	4	South Changjiang Road station	Xinjiangwancheng station	12.7	10.4
2	5	South Changjiang Road station	Xinjiangwancheng station	15.7	14.6
2	6	South Changjiang Road station	Xinjiangwancheng station	18	9.4
2	7	West Yingao Road station	Xinjiangwancheng station	16.2	14.5
2	8	West Yingao Road station	East Yingao Road station	17.8	12.5
2	9	West Yingao Road station	East Yingao Road station	13.1	12.3
2	10	West Yingao Road station	East Yingao Road station	16.9	11.5

i: TWAT, Total walking access time, unit minute

ii: TBAT, Total biking access time, unit minute

5.5 Discussions

5.5.1 The Advantages of MAL-based Measurements

The advantages of the MAL can be revealed in comparison to the coverage-based and the 2SFCA-based accessibility measurements.

1) Taking the coverage-based measures as a benchmark, additional factors, including access time, waiting time, and crowdedness are considered in the MAL. In this sense, the MAL can be understood as an enhanced indicator of the overlap degree of the catchment areas (see Section 4.3).
2) Taking the coverage-based measures as benchmark again, a finer spatial granularity of measurements toward accessibility and population density can be obtained. As a result, the MAL-based analysis bears more subtle knowledge for micro-level transport planning. For instance, specific areas that need metro accessibility improvement are determined by using the grid-level MAL map. In fact, Shanghai Metro already made some improvements toward area 1 and area 2 (see Figure 5.2) by opening new metro stations, which indicates the usefulness of the combined analysis of MALs and population density. Nevertheless, other areas (i.e., areas 3–7 in Figure 5.2) also deserve more attention from the public transport sectors. In addition to the costly metro station construction, measures, such as improving the frequencies of accessible trains (i.e., shorten the waiting time) and constructing attractive walking and biking environments, might help to improve the accessibility to metro systems in these areas.
3) Taking the 2SFCA-based accessibility measurements as a benchmark, transit crowdedness is explicitly modeled in the MAL indicator by transferring the crowdedness into additional waiting time. As revealed by the results in Figure 5.3, the metro crowdedness has a significant impact on the accessibility to transit, and should not be neglected.

5.5.2 Potential Extensions of the MAL Indicator

We regard this work as a starting point to trigger further ideas on fine-grained accessibility modeling. Several potential extensions of the MAL indicator are possible.

1) Enhanced crowdedness modeling

In this study, the crowdedness information is collected from the official website of the Shanghai Metro. In addition to such a data-driven approach, the crowdedness information can also be measured by using well-established modeling approaches. For instance, it is feasible to measure the crowdedness of adjacent metro stations (i.e., train interval) by using the capacity information of the trains, operation schedules, and the

estimation of passenger flow (Jiao et al., 2017). In addition to the impact on boarding, the metro crowdedness can also cause train delay and discomfort, which are not considered in the current study due to the data limitation. For the aspect of delay, automatic vehicle location data can be used as potential data to measure the vehicle delay time (Camus et al., 2005). The difficulty is to differentiate the delay caused by crowdedness and other factors (e.g., congestion). The aspect related to travel comfort can be more likely included in via-transit accessibility instead of to-transit accessibility (i.e., our focus). Furthermore, the comfort decrease caused by crowdedness is more subjective than objective.

2) Integration of additional factors

In addition to crowdedness, other perception-related factors, such as lighting and safety of transit stations, can be further incorporated into the accessibility measurement because of their impacts on user's affection and behavior toward transit stations. The emerging geotagged social media data contain rich clues to these factors. Moreover, service-specific factors may subtly influence the usefulness of the proposed indicator. For instance, the convenience of bike parking around transit stations can also affect users' perception toward the transit systems and thus might affect the bike accessibility to transit systems.

3) Higher temporal granularity

As revealed in Section 5.3.2, it is essential to make a distinctive measurement of accessibility to metro systems for different time periods because of the changing crowdedness and service frequency. The current MAL is measured on an hourly basis, and it can be improved by introducing higher temporal resolutions (e.g., every 10 minutes) because the metro crowdedness indeed changes more frequently than the hourly basis.

4) Extension to transit systems beyond metro

Finally, the indicator metro accessibility level, is applicable to measure the accessibility to other public transit systems such as buses, rail transit or general public transport (i.e., a combination of several public transport systems) as long as the corresponding crowdedness information can be obtained.

5.5.3 The Role of Shared Bikes

1) Shared bikes as a means of promoting transit accessibility

The coverage and MAL-based analysis both demonstrated that shared bikes could increase transit accessibility as compared with walking. The results revealed that the accessibility improvement varies across space and time. It is important to consider such spatiotemporal differences to make smarter decisions toward transport planning.

The accessibility improvement may also show disparities among different user groups depending on their socio-demographic characteristics. For instance, the ability to rent and ride shared bikes may vary from one group to another. Since public transport is regarded as a type of social welfare for transport disadvantaged groups, it would be worthwhile to explore how these users would benefit from the integration of shared bikes and public transit.

2) Shared bikes as a means of avoiding transit crowdedness

The proportion of the population with the possibility of avoiding metro crowdedness is relatively small (i.e., 19% of the crowdedness-affected population). If only the type 1 shift is considered to be effective, this possibility would be even smaller because only 21.6% of the shifts belong to the type 1. Furthermore, if the costs of shared bikes are considered, the possibility would further decrease. Such a result indicates bike-and-metro can only act as a supplementary means of relieving the metro crowdedness. Nevertheless, measures, such as increasing the availability of shared bikes and road quality around non-crowded stations, can be taken to increase this possibility. Additionally, users might consider factors (e.g., the total traveling time) beyond the total access time when selecting the departure metro stations. Thereby, it is worthwhile to integrating other factors into consideration thus providing more useful recommendations to users with different traveling destinations and purposes.

It is important to note that there are two different approaches of relieving the metro crowdedness by biking. The focus of this study is to use biking to substitute walking as the metro access mode instead of using biking to replace the short-distance metro trips (Sun and Zacharias, 2017). As a result, public transport sectors with the aim to relieve the metro crowdedness by biking could inspect both possibilities. For instance, it would also be interesting to know the possibility of relieving metro crowdedness by using biking to replace some short-distance metro trips in Shanghai.

5.6 Summary

This chapter proposes a MAL indicator constrained by the metro crowdedness to measure the accessibility to metro systems by biking. The impact of crowdedness is transferred to waiting time and thus incorporated into the accessibility measurement. The proposed indicator is applied to Shanghai as a case study. The results show that the population being covered and the population above a poor MAL level have both been doubled by using biking as the access mode. Areas that need accessibility improvement and their priorities are highlighted by overlaying the MALs with population density. Compared with the afternoon peak, a larger proportion of the

population's MALs are affected by the crowdedness during the morning peak. Ignoring the crowdedness leads to an overestimation of the MALs.

To explore how bike-and-metro integration could be used to relieve the crowdedness, we propose a method to determine grids with the possibility to avoid the metro crowdedness during the morning peak. The results show that bike-and-metro can act as a practical option for avoiding the crowded stations for some citizens living in the central city. However, such a possibility only limited to a small proportion of the crowdedness-affected population; thus, the bike-and-metro can only act as a supplementary means of relieving the metro crowdedness in Shanghai.

6 Conclusion and Outlook

6.1 Conclusion

The continuous urbanization calls for clean, efficient and sustainable transportation. While public transport represents a traditional and effective sustainable transportation mode, dockless shared mobility represents an emerging sustainable transportation mode. The thesis is devoted to the synergetic effects of these two transportation modes by means of data-driven approaches of accessibility assessment from multiple perspectives. From the methodological perspective, we proposed approaches of identifying bike-and-ride trips from massive bike trajectories and the approaches of trajectory processing. From the perspective of technical support, we developed an open-source tool for generating network-based transit catchment areas. With regard to the accessibility modeling, an enhanced indicator constrained by crowdedness is proposed to measure grid-level accessibility to transit. These data-driven approaches have demonstrated the radical progresses that allow a full usage of traditional knowledge and the potential of big data.

The major contributions of this thesis are summarized as follows.

- To measure the biking distances at individual transit stations, the methods of identifying the bike-and-ride trip and matching the raw trajectory to the road network are proposed. Specifically, a method to extract bike-ride-bike (BRB) trips is introduced; and the circular buffer to identifying bike-and-ride trips is decided based on how BRB users park and fetch their bikes around transit stations. To measure more realistic biking distances, an adapted version of map-matching algorithm is proposed to handle the FBF segments that frequently observed in the map matching of non-motorized trajectories. These methods can also be transferred to investigate the connection between rail transit and other dockless shared vehicles in other study areas. Furthermore, two regression models are employed to explore the influences associated with biking distances at individual metro stations.

- To support the coverage-based accessibility analysis, a methodological framework of generating transit catchment areas (TCAs) by non-motorized transport is proposed. The framework consists of three components: subgraph construction, extended shortest path tree construction, and contour generation. In addition to the basic case of the undirected road network and point facility, the framework can also be used to generate TCAs under the condition of directed road network and non-point facility. The accuracy and time efficiency evaluation showed that the framework achieves a better performance than alternative solutions. More importantly, the framework is provided as an open-source tool for the scientific community.
- To measure more realistic accessibility at a finer-grained level, the metro accessibility level (MAL) indicator is proposed. The indicator is an enhanced version of the public transport accessibility level (PTAL), which incorporates the impact of metro crowdedness. The necessity of explicitly modeling the crowdedness into transit accessibility is analyzed. The metro crowdedness is transferred to additional waiting time and incorporated into the accessibility modeling. Analytical results showed that ignoring the crowdedness leads to an overestimation of accessibility to transit, which demonstrates the usefulness of the proposed indicator.
- The thesis provides a systematic assessment of the bike accessibility to metro stations in Shanghai. From the perspective of data, multiple travel-related data sources, such as bike trajectories, smart card data, and metro crowdedness, are jointly used to derive a more realistic accessibility measurement. From the perspective of levels of detail, the coverage-based analysis and grid-based analysis are used to provide accessibility assessment at the regional and the local level. The analytical results provide a comprehensive understanding of how bike-and-ride could change the metro accessibility, and implications for policymaking are discussed in detail.

6.2 Outlook

On the basis of this work, a number of potential research topics need further in-depth investigations.

1) Integrating travel survey data

Individual information, such as socioeconomic attributes and trip purposes, are usually missing in trajectory-format travel data due to the privacy issue. In contrast, such information is normally included in survey-based travel data. How to make an appropriate combination of the “big” GPS trajectory and “small” travel survey data to measure accessibility would be a challenge and interesting research topic.

2) Extending the framework of TCA generation

The proposed framework of TCA generation can be improved in several aspects. First, in addition to spatial distance, factors, such as road slopes, turns, road qualities, and road levels, can be further modeled as travel impendence to determine a more realistic catchment area. Second, the framework is designed for generating TCAs by non-motorized transport, but can also be applied to generate TCAs by motorized transport where more efforts are needed to improve the computation efficiency. Third, from the aspect of implementation, designing a user-friendly interface such as interactive visual analysis could definitely promote the usability of the open-source tool. Furthermore, since catchment area is a concept widely used in multiple fields, such as human geography and hydrology, testing the suitability and extending the proposed framework to support research in these fields could be very meaningful.

3) Extending the accessibility modeling

Integrating the crowdedness into the accessibility measurement is an initial step toward a more realistic measurement of accessibility. Feedbacks from transport planners are needed to refine the crowdedness modeling, thus promote its applicability in transport planning. One the other hand, user-generated data (e.g., geotagged social media) can be integrated to model other soft factors, such as perceptive safety and lighting condition of transit stations, to enhance accessibility modeling.

4) Comparative case study

To obtain a more comprehensive understanding of the integration of dockless shared vehicles and public transit. The current accessibility analysis can be extended from to-transit assessment to via-transit assessment. Furthermore, it is interesting to apply the proposed methods to investigate the effect of dockless shared vehicles and public transit in other cities. A comparison between the bike-and-ride in different cities could provide more insights for policymaking.

Bibliography

Adhvaryu B, Chopde A and Dashora L (2019) Mapping public transport accessibility levels (PTAL) in India and its applications: a case study of Surat. *Case Studies on Transport Policy*. DOI: 10.1016/j.cstp.2019.03.004.

Ahmed M, Karagiorgou S, Pfoser D, et al. (2015) A Comparison and Evaluation of Map Construction Algorithms. *GeoInformatica* 19(3): 601–632. DOI: 10.1007/s10707-014-0222-6.

Alsger A, Assemi B, Mesbah M, et al. (2016) Validating and improving public transport origin-destination estimation algorithm using smart card fare data. *Transportation Research Part C: Emerging Technologies* 68: 490–506. DOI: 10.1016/j.trc.2016.05.004.

Antoniou C, Dimitriou L and Pereira F (eds) (2018) *Mobility Patterns, Big Data and Transport Analytics: Tools and Applications for Modeling*. *Mobility Patterns, Big Data and Transport Analytics*. Elsevier. DOI: 10.1016/c2016-0-03572-6.

Apparicio P, Cloutier MS and Shearmur R (2007) The case of Montréal's missing food deserts: Evaluation of accessibility to food supermarkets. *International Journal of Health Geographics* 6: 1–13. DOI: 10.1186/1476-072X-6-4.

Barry JJ, Newhouser R, Rahbee A, et al. (2002) Origin and destination estimation in New York City with automated fare system data. *Transportation Research Record* (1817): 183–187. DOI: 10.3141/1817-24.

Ben-Akiva M (1979) Disaggregate travel and mobility choice models and measures of accessibility. In: Hensher DA and Stopher PR (eds) *Behavioural Travel Modelling*. London: Croom Helm.

Benenson I, Martens K and Rofé Y (2010) Measuring the Gap Between Car and Transit Accessibility: Estimating Access Using a High-Resolution Transit Network Geographic Information System. *Transportation Research Record: Journal of the Transportation Research Board* 2144: 28–35. DOI: 10.3141/2144-04.

Bhat C, Stacey Bricka, Mondia J La, et al. (2006) *Metropolitan Area Transit Accessibility Analysis Tool*. DOI: 10.1017/CBO9781107415324.004.

Biagioni J and Eriksson J (2012) Map inference in the face of noise and disparity. *GIS: Proceedings of the ACM International Symposium on Advances in Geographic Information Systems*: 79–88. DOI: 10.1145/2424321.2424333.

Biba S, Curtin KM and Manca G (2010) A new method for determining the population with walking access to transit. *International Journal of Geographical Information Science* 24(3): 347–364. DOI: 10.1080/13658810802646679.

Boeing G (2017) OSMnx: New methods for acquiring, constructing, analyzing, and visualizing complex street networks. *Computers, Environment and Urban Systems* 65. Pergamon: 126–139. DOI: 10.1016/J.COMPENVURBSYS.2017.05.004.

Boissonnat J, Devillers O, Pion S, et al. (2007) Triangulations in CGAL. 21957(21957): 5–19. DOI: 10.1016/S0925-7721(01)00054-2.

Camus R, Longo G and Macorini C (2005) Estimation of transit reliability level-of-service based on automatic vehicle location data. *Transportation Research Record* (1927): 277–286. DOI: 10.3141/1927-31.

Cheng YH and Lin YC (2018) Expanding the effect of metro station service coverage by incorporating a public bicycle sharing system. *International Journal of Sustainable Transportation* 12(4): 241–252. DOI: 10.1080/15568318.2017.1347219.

China Internet Network Information Center (2018) *The 41st China statistical report on internet development*. Available at: http://www.cnnic.net.cn/hlwfzyj/hlwxzbg/hlwtjbg/201803/P020180305409870339136.pdf.

Currie G (2004) Gap analysis of public transport needs: Measuring spatial distribution of public transport needs and identifying gaps in the quality of public transport provision. *Transportation Research Record* 1895(1): 137–146. DOI: 10.3141/1895-18.

Currie G (2010) Quantifying spatial gaps in public transport supply based on social needs. *Journal of Transport Geography* 18: 31–41. DOI: 10.1016/j.jtrangeo.2008.12.002.

Daniels R and Mulley C (2013) Explaining walking distance to public transport: The dominance of public transport supply. *Journal of Transport and Land Use* 6(2): 5. DOI: 10.5198/jtlu.v6i2.308.

Delamater PL, Messina JP, Shortridge AM, et al. (2012) Measuring geographic access to health care. *International journal of health geographics* 11(1): 15. DOI: 10.1186/1476-072X-11-15.

Ding L, Krisp JM, Meng L, et al. (2016) Visual exploration of multivariate movement events in space-time cube. *The 19th AGILE International Conference on Geographic Information Science*.

Douglas DH and Peucker TK (1973) Algorithms for the reduction of the number of points required to represent a line or its caricature. *Cartographica: The International Journal for Geographic Information and Geovisualization* 10(2). University of Toronto Press Inc. (UTPress): 112–122. DOI: 10.3138/fm57-6770-u75u-7727.

El-Geneidy A, Grimsrud M, Wasfi R, et al. (2014) New evidence on walking distances to transit stops: Identifying redundancies and gaps using variable service areas. *Transportation* 41(1): 193–210. DOI: 10.1007/s11116-013-9508-z.

El-Geneidy AM, Tetreault P and Surprenant-Legault J (2010) Pedestrian Access to Transit: Identifying Redundancies and Gaps Using a Variable Service Area Analysis. In: *Transportation Research Board 89th Annual Meeting*, Washington DC, United States, 2010. Available at: https://trid.trb.org/view/909667 (accessed 13 June 2018).

Fayyaz SK, Cathy X and Porter RJ (2017) Dynamic transit accessibility and transit gap causality analysis. *Journal of Transport Geography* 59: 27–39. DOI: 10.1016/j.jtrangeo.2017.01.006.

Foda M and Osman A (2010) Using GIS for Measuring Transit Stop Accessibility Considering Actual Pedestrian Road Network. *Journal of Public Transportation* 13(Tcrp 1996): 23–40. DOI: http://doi.org/10.5038/2375-0901.13.4.2.

Forney GD (1973) The Viterbi Algorithm. *Proceedings of the IEEE* 61(3): 268–278. DOI: 10.1109/PROC.1973.9030.

Fransen K, Neutens T, Farber S, et al. (2015) Identifying public transport gaps using time-dependent accessibility levels. *Journal of Transport Geography* 48: 176–187. DOI: 10.1016/j.jtrangeo.2015.09.008.

Fu L and Xin Y (2007) A New Performance Index for Evaluating Transit Quality of Service. *Journal of Public Transportation* 10(3): 47–69. DOI: 10.5038/2375-0901.10.3.4.

García-Palomares JC, Gutiérrez J and Cardozo OD (2013) Walking accessibility to public transport: An analysis based on microdata and GIS. *Environment and Planning B: Planning and Design*. DOI: 10.1068/b39008.

Geurs KT and van Wee B (2004) Accessibility evaluation of land-use and transport strategies: Review and research directions. *Journal of Transport Geography* 12(2): 127–140. DOI: 10.1016/j.jtrangeo.2003.10.005.

Givoni M and Rietveld P (2007) The access journey to the railway station and its role in passengers ' satisfaction with rail travel. *Transport Policy* 14: 357–365. DOI: 10.1016/j.tranpol.2007.04.004.

Gordon JB, Koutsopoulos HN, Wilson NHM, et al. (2013) Automated inference of linked transit journeys in london using fare-transaction and vehicle location data. *Transportation Research Record* 2343: 17–24. DOI: 10.3141/2343-03.

Guerra E, Cervero R and Tischler D (2012) Half-Mile Circle. *Transportation Research Record: Journal of the Transportation Research Board* 2276(2276): 101–109. DOI: 10.3141/2276-12.

Gutiérrez J and García-Palomares JC (2008) Distance-measure impacts on the calculation of transport service areas using GIS. *Environment and Planning B: Planning and Design* 35(3): 480–503. DOI: 10.1068/b33043.

Guttman A, Antonin, Guttman, et al. (1984) R-trees: a dynamic index structure for spatial searching. In: *Proceedings of the 1984 ACM SIGMOD international conference on Management of data - SIGMOD '84*, New York, New York, USA, 1984, p. 47. ACM Press. DOI: 10.1145/602259.602266.

Haggett P, Cliff AD and Frey A (1977) *Locational analysis in human geography*. Second. London: Edward Arnold. Available at: https://www.popline.org/node/454260 (accessed 16 May 2019).

Handy SL and Niemeier DA (1997) Measuring accessibility: An exploration of issues and alternatives. *Environment and Planning A* 29(7): 1175–1194. DOI: 10.1068/a291175.

Hansen WG (1959) How Accessibility Shapes Land Use. *Journal of the American Planning Association* 25(2): 73–76. DOI: 10.1080/01944365908978307.

Hochmair HH (2015) Assessment of Bicycle Service Areas around Transit Stations. *International Journal of Sustainable Transportation* 9(1): 15–29. DOI: 10.1080/15568318.2012.719998.

Horner MW and Murray AT (2004) Spatial representation and scale impacts in transit service assessment. *Environment and Planning B: Planning and Design* 31: 785–797. DOI: 10.1068/b3046.

Huang J, Qiao S, Yu H, et al. (2013) Parallel map matching on massive vehicle GPS data using MapReduce. In: *Proceedings - 2013 IEEE International Conference on High Performance Computing and Communications, HPCC 2013 and 2013 IEEE International Conference on Embedded and Ubiquitous Computing, EUC 2013*, 2013. DOI: 10.1109/HPCC.and.EUC.2013.211.

Iacono M, Krizek K and El-Geneidy A (2008) *Access to Destinations: How Close is Close Enough? Estimating Accurate Distance Decay Functions for Multiple Modes and Different Purposes*. *University of Minnesota*. DOI: 10.1111/1467-6494.00086.

Ingram DR (1971) The Concept of Accessibility: A Search for an Operational Form. *Regional Studies* 5(2): 101–107. DOI: 10.1080/09595237100185131.

International Association of Public Transport (2018) *World Metro Figures 2018*. Brussels. Available at: https://www.uitp.org/sites/default/files/cck-focus-papers-files/Statistics Brief - World metro figures 2018V4_WEB.pdf.

Jang W (2010) Travel Time and Transfer Analysis Using Transit Smart Card Data. *Transportation Research Record: Journal of the Transportation Research Board* 2144: 142–149. DOI: 10.3141/2144-16.

Jenelius E and Koutsopoulos HN (2013) Travel Time Estimation for Urban Road Networks Using Low Frequency Probe Vehicle Data. *Transportation Research Part B* (53): 64–81. DOI: 10.1016/j.trb.2013.03.008.

Ji Y, Ma X, Yang M, et al. (2018) Exploring Spatially Varying Influences on Metro-Bikeshare Transfer: A Geographically Weighted Poisson Regression Approach. *sustainability* 10(1526). DOI: doi:10.3390/su10051526.

Jiao L, Shen L, Shuai C, et al. (2017) Measuring Crowdedness between Adjacent Stations in an Urban Metro System : a Chinese Case Study.: 1–14. DOI: 10.3390/su9122325.

Joseph AE and Bantock PR (1982) Measuring potential physical accessibility to general practitioners in rural areas: A method and case study. *Social Science and Medicine* 16(1): 85–90. DOI: 10.1016/0277-9536(82)90428-2.

Kerrigan M and Bull D (1992) Measuring Accessibility - a Public Transport Accessibility Index. In: *Proceedings of Seminar B held at the PTRC Transport, Highways and Planning Summer Annual Meeting*, Manchester, England, 1992, pp. 233–44. Available at: https://trid.trb.org/view/384147 (accessed 2 February 2020).

Kim KM, Hong SP, Ko SJ, et al. (2015) Does crowding affect the path choice of metro passengers? *Transportation Research Part A: Policy and Practice* 77: 292–304. DOI: 10.1016/j.tra.2015.04.023.

Kittelson and Associates (2003) *Transit Capacity and Quality of Service Manual*. Washington, D.C.: Transportation Research Board.

Kwan M-P (1998) Space-Time and Integral Measures of Individual Accessibility: A Comparative Analysis Using a Point-based Framework. *Geographical Analysis* 30(3): 191–216. DOI: 10.1111/j.1538-4632.1998.tb00396.x.

Kyung W, Young S and Heo J (2018) Utilizing mobile phone-based fl oating population data to measure the spatial accessibility to public transit. *Applied Geography* 92: 123–130. DOI: 10.1016/j.apgeog.2018.02.003.

La Paix Puello L and Geurs KT (2016) Train station access and train use : a joint stated and revealed preference choice modelling study. In: Geurs, K.T., Patuelli, R., Dentinho T (ed.) *Accessibility, Equity and Efficiency. Challenges for transport and public services*. Northampton,USA: Edward Elgar, pp. 144–166.

Langford M, Fry R and Higgs G (2012) Measuring transit system accessibility using a modified two-step floating catchment technique. *International Journal of Geographical Information Science* 26(2): 193–214. DOI: 10.1080/13658816.2011.574140.

Lee J, Choi K and Leem Y (2016) Bicycle-based transit-oriented development as an alternative to overcome the criticisms of the conventional transit-oriented development. *International Journal of Sustainable Transportation* 10(10): 975–984. DOI: 10.1080/15568318.2014.923547.

Lee W-C and Krumm J (2011) Trajectory Preprocessing. *Computing with Spatial Trajectories*: 3–33. DOI: 10.1007/978-1-4614-1629-6_1.

Lei TL and Church RL (2010) Mapping transit-based access: Integrating GIS, routes and schedules. *International Journal of Geographical Information Science* 24(2): 283–304. DOI: 10.1080/13658810902835404.

Li Q, Zheng Y, Xie X, et al. (2008) Mining user similarity based on location history. *GIS: Proceedings of the ACM International Symposium on Advances in Geographic Information Systems* (January): 298–307. DOI: 10.1145/1463434.1463477.

Li Y, Huang Q, Kerber M, et al. (2013) Large-scale joint map matching of GPS traces. In: *Proceedings of the 21st ACM SIGSPATIAL International Conference on Advances in Geographic Information Systems - SIGSPATIAL'13*, 2013. DOI: 10.1145/2525314.2525333.

Lieshout R (2012) Measuring the size of an airport's catchment area. *Journal of Transport Geography* 25: 27–34. DOI: 10.1016/j.jtrangeo.2012.07.004.

Lin D and Zhu R (2019) Understanding the integration of buses and metro systems using smart card data. *Proceedings of the ICA* 2: 1–6. DOI: 10.5194/ica-proc-2-74-2019.

Lin D, Zhang Y, Zhu R, et al. (2019) The analysis of catchment areas of metro stations using trajectory data generated by dockless shared bikes. *Sustainable Cities and Society*: 101598. DOI: 10.1016/j.scs.2019.101598.

Lin D, Zhu R, Yang J, et al. (2020) An Open-Source Framework of Generating Network-Based Transit Catchment Areas by Walking. *ISPRS International Journal of Geo-Information* 9(8): 467. DOI: 10.3390/ijgi9080467.

Lin T and Wilson NHM (1992) Dwell Time Relationships for Light Rail Systems. *Transportation Research Record* (1361): 287–295. Available at: http://trid.trb.org.globalproxy.cvt.dk/view.aspx?id=370918.

Lin T (Grace), Xia J (Cecilia), Robinson TP, et al. (2016) Enhanced Huff model for estimating Park and Ride (PnR) catchment areas in Perth, WA. *Journal of Transport Geography* 54: 336–348. DOI: 10.1016/j.jtrangeo.2016.06.011.

Lou Y, Zhang C, Zheng Y, et al. (2009) Map-matching for low-sampling-rate GPS trajectories. *GIS: Proceedings of the ACM International Symposium on Advances in Geographic Information Systems* (May 2014): 352–361. DOI: 10.1145/1653771.1653820.

Luo W and Qi Y (2009) An enhanced two-step floating catchment area (E2SFCA) method for measuring spatial accessibility to primary care physicians. *Health and Place* 15(4): 1100–1107. DOI: 10.1016/j.healthplace.2009.06.002.

Luo W and Wang F (2003) Measures of spatial accessibility to health care in a GIS environment: Synthesis and a case study in the Chicago region. *Environment and Planning B: Planning and Design* 30(6): 865–884. DOI: 10.1068/b29120.

Luo W and Whippo T (2012) Variable catchment sizes for the two-step floating catchment area (2SFCA) method. *Health & Place* 18(4): 789–795. DOI: 10.1016/j.healthplace.2012.04.002.

Ma X, Wang Y, Chen F, et al. (2012) Transit smart card data mining for passenger origin information extraction. *Journal of Zhejiang University SCIENCE C* 13(10): 750–760. DOI: 10.1631/jzus.C12a0049.

Ma X, Wu YJ, Wang Y, et al. (2013) Mining smart card data for transit riders' travel patterns. *Transportation Research Part C: Emerging Technologies* 36: 1–12. DOI: 10.1016/j.trc.2013.07.010.

Martens K (2004) The bicycle as a feedering mode: Experiences from three European countries. *Transportation Research Part D: Transport and Environment* 9(4): 281–294. DOI: 10.1016/j.trd.2004.02.005.

Martínez FJ (1995) Access: The transport-land use economic link. *Transportation Research Part B* 29(6): 457–470. DOI: 10.1016/0191-2615(95)00014-5.

Mavoa S, Witten K, McCreanor T, et al. (2012) GIS based destination accessibility via public transit and walking in Auckland, New Zealand. *Journal of Transport Geography* 20(1): 15–22. DOI: 10.1016/j.jtrangeo.2011.10.001.

McGurrin MF and Greczner DJ (2011) Performance Metrics: Calculating Accessibility Using Open Source Software and Open Data. *Transportation Research Board Annual Meeting 2011* (June).

Meratnia N and Rolf A (2004) Spatiotemporal compression techniques for moving point objects. *Lecture Notes in Computer Science (including subseries Lecture Notes in Artificial Intelligence and Lecture Notes in Bioinformatics)* 2992: 765–782. DOI: 10.1007/978-3-540-24741-8_44.

Morris JM, Dumble PL and Wigan MR (1979) Accessibility indicators for transport planning. *Transportation Research Part A: General* 13(2): 91–109. DOI: 10.1016/0191-2607(79)90012-8.

Nassir N, Hickman M, Malekzadeh A, et al. (2016) A utility-based travel impedance measure for public transit network accessibility. *Transportation Research Part A: Policy and Practice* 88: 26–39. DOI: 10.1016/j.tra.2016.03.007.

National Association of City Transportation Officials (2018) *Shared Micromobility in the U.S.: 2018*. Available at: https://nacto.org/shared-micromobility-2018/ (accessed 13 January 2020).

Neuburger H (1971) User Benifit in the Evaluation of Transport and Land Use Plans.

Journal of Transport Economics and Policy 5(1): 52–57.

Newson P and Krumm J (2009) Hidden Markov map matching through noise and sparseness. In: *Proceedings of the 17th ACM SIGSPATIAL International Conference on Advances in Geographic Information Systems - GIS '09*, 2009. DOI: 10.1145/1653771.1653818.

O'Neill WA, Ramsey RD and Chou J (1992) Analysis of transit service areas using geographic information systems. *Transportation Research Record* 1364.

Okabe A and Sugihara K (2012) *Spatial analysis along networks : statistical and computational methods*. Wiley. Available at: https://www.wiley.com/en-au/Spatial+Analysis+Along+Networks%3A+Statistical+and+Computational+Methods-p-9780470770818 (accessed 23 April 2019).

Okabe A, Okunuki KI and Shiode S (2006) The SANET toolbox: New methods for network spatial analysis. *Transactions in GIS* 10(4): 535–550. DOI: 10.1111/j.1467-9671.2006.01011.x.

Páez A, Scott DM and Morency C (2012) Measuring accessibility: Positive and normative implementations of various accessibility indicators. *Journal of Transport Geography* 25: 141–153. DOI: 10.1016/j.jtrangeo.2012.03.016.

Pan H, Shen Q and Xue S (2010) Intermodal Transfer Between Bicycles and Rail Transit in Shanghai, China. *Transportation Research Record: Journal of the Transportation Research Board* 2144: 181–188. DOI: 10.3141/2144-20.

Pitot M, Yoigitcanlar T, Sipe N, et al. (2006) Land Use & Public Transport Accessibility Index (LUPTAI) Tool - The development and pilot application of LUPTAI for the Gold Coast. In: *29th Australasian Transport Research Forum*, 2006.

Polzin SE, Pendyala RM and Navari S (2002) Development of time-of-day-based transit accessibility analysis tool. *Transportation Research Record* (1799): 35–41. DOI: 10.3141/1799-05.

Potamias M, Patroumpas K and Sellis T (2006) Sampling trajectory streams with spatiotemporal criteria. *Proceedings of the International Conference on Scientific and Statistical Database Management, SSDBM*: 275–284. DOI: 10.1109/SSDBM.2006.45.

Raveau S, Guo Z, Muñoz JC, et al. (2014) A behavioural comparison of route choice on metro networks: Time, transfers, crowding, topology and socio-demographics. *Transportation Research Part A: Policy and Practice* 66(1): 185–195. DOI: 10.1016/j.tra.2014.05.010.

Rood T and Sprowls S (1998) *The local index of transit availability: An implementation manual*. Local Government Commission.

Roussopoulos N, Kelley S and Vincent F (1995) Nearest neighbor queries. In: *ACM SIGMOD Record*, 1995, pp. 71–79. DOI: 10.1145/568271.223794.

Saghapour T, Moridpour S and Thompson RG (2016) Public transport accessibility in metropolitan areas: A new approach incorporating population density. *Journal of Transport Geography* 54: 273–285. DOI: 10.1016/j.jtrangeo.2016.06.019.

Sanko N and Shoji K (2009) Analysis on the structural characteristics of the station catchment area in Japan. In: *11th Conference on Competition and Owership in Land Passenger Transport*, 2009, pp. 20–25.

Schiavina M, Freire S and MacManus K (2019) GHS population grid multitemporal (1975-1990-2000-2015), R2019A. *European Commission, Joint Research Centre (JRC)*. DOI: 10.2905/0C6B9751-A71F-4062-830B-43C9F432370F.

Seaborn C, Attanucci J and Wilson N (2009) Analyzing Multimodal Public Transport Journeys in London with Smart Card Fare Payment Data. *Transportation Research Record: Journal of the Transportation Research Board* (2121): 55–62. DOI: 10.3141/2121-06.

Sha Al Mamun M and Lownes NE (2011) A composite index of public transit accessibility. *Journal of Public Transportation* 14(2): 69–87. DOI: 10.5038/2375-0901.14.2.4.

Shanghai Municipal Bureau of Statistics (2019) *Statistical Communique of Shanghai on the 2018 National Economic and Social Development*. Available at: http://tjj.sh.gov.cn/html/sjfb/201903/1003219.html.

Shanghai Municipal Government (1998) *Shanghai Comprehensive Master Plan: 1999-2020*. Shanghai.

Sharkey JR, Horel S, Han D, et al. (2009) Association between neighborhood need and spatial access to food stores and fast food restaurants in neighborhoods of Colonias. *International Journal of Health Geographics* 8(1): 1–17. DOI: 10.1186/1476-072X-8-9.

Shen F, Lin Y and Pan Z (2012) Shanghai Metro Tri-Color Operating Status System. In: *The 7th Annual Conference of ITS China - Intelligent Transportation Application*, Beijing, China, 2012, pp. 529–534. ITS China.

Shen Q (1998) Location characteristics of inner-city neighborhoods and employment accessibility of low-wage workers. *Environment and Planning B: Planning and Design* 25(1): 345–365.

Shen Y, Zhang X and Zhao J (2018) Understanding the usage of dockless bike sharing in Singapore. *International Journal of Sustainable Transportation*. Taylor & Francis: 1–15. DOI: 10.1080/15568318.2018.1429696.

Small KA and Rosen HS (1981) Applied Welfare Economics with Discrete Choice Models. *Econometrica* 49(1): 105–130.

Sultan J, Ben-Haim G, Haunert JH, et al. (2017) Extracting spatial patterns in bicycle routes from crowdsourced data. *Transactions in GIS*. DOI: 10.1111/tgis.12280.

Sun G and Zacharias J (2017) Can bicycle relieve overcrowded metro? Managing short-distance travel in Beijing. *Sustainable Cities and Society* 35: 323–330. DOI: 10.1016/j.scs.2017.08.010.

Sun SN, Her J, Lee SY, et al. (2017) Meso-scale urban Form elements for bus transit-oriented development: Evidence from Seoul, Republic of Korea. *Sustainability (Switzerland)* 9(9). DOI: 10.3390/su9091516.

Sun Y, Shi J and Schonfeld PM (2016) Identifying passenger flow characteristics and evaluating travel time reliability by visualizing AFC data : a case study of Shanghai Metro. *Public Transport* 8(3). Springer Berlin Heidelberg: 341–363. DOI: 10.1007/s12469-016-0137-8.

Tirachini A, Hensher DA and Rose JM (2013) Crowding in public transport systems: Effects on users, operation and implications for the estimation of demand.

Transportation Research Part A: Policy and Practice 53: 36–52. DOI: 10.1016/j.tra.2013.06.005.

Transport for Greater Manchester (2016) *Greater Manchester Accessibility Levels (GMAL) Model*. Available at: http://odata.tfgm.com/opendata/downloads/GMAL/GMAL Calculation Guide.pdf.

Transport for London (2015) *Assessing Transport Connectivity in London*. London. Available at: https://data.london.gov.uk/download/public-transport-accessibility-levels/86bbffe1-%0A8af1-49ba-ac9b-b3eacaf68137/connectivity-assessment-guide.pdf.

Trépanier M, Tranchant N and Chapleau R (2007) Individual trip destination estimation in a transit smart card automated fare collection system. *Journal of Intelligent Transportation Systems: Technology, Planning, and Operations* 11(1): 1–14. DOI: 10.1080/15472450601122256.

Trépanier M, Morency C and Agard B (2009) Calculation of Transit Performance Measures Using Smartcard Data. *Journal of Public Transportation* 12(1): 79–96. DOI: 10.5038/2375-0901.12.1.5.

Tu W, Cao R, Yue Y, et al. (2018) Spatial variations in urban public ridership derived from GPS trajectories and smart card data. *Journal of Transport Geography* 69(3688): 45–57. DOI: 10.1016/j.jtrangeo.2018.04.013.

United Nations, Department of Economic and Social Affairs (2018) *World Urbanization Prospects: The 2018 Revision*. New York. Available at: https://www.un.org/development/desa/publications/2018-revision-of-world-urbanization-prospects.html.

Upchurch C, Kuby M, Zoldak M, et al. (2004) Using GIS to generate mutually exclusive service areas linking travel on and off a network. *Journal of Transport Geography* 12(1): 23–33. DOI: 10.1016/j.jtrangeo.2003.10.001.

van Soest D, Tight MR and Rogers CDF (2019) Exploring the distances people walk to access public transport. *Transport Reviews* 0(0). Taylor & Francis: 1–23. DOI: 10.1080/01441647.2019.1575491.

Wan N, Zou B and Sternberg T (2012) A three-step floating catchment area method for analyzing spatial access to health services. *International Journal of Geographical Information Science* 26(6): 1073–1089. DOI: 10.1080/13658816.2011.624987.

Wang R and Liu C (2013) Bicycle-Transit Integration in the United States, 2001-2009. *Journal of Public Transportation* 16(3): 95–119.

Wang Y, Zheng Y and Xue Y (2014) Travel time estimation of a path using sparse trajectories. *Proceedings of the 20th ACM SIGKDD international conference on Knowledge discovery and data mining - KDD '14* (5): 25–34. DOI: 10.1145/2623330.2623656.

Wang Z, Chen F and Xu T (2016) Interchange between Metro and Other Modes: Access Distance and Catchment Area. *Journal of Urban Planning and Development* 142(4): 04016012. DOI: 10.1061/(ASCE)UP.1943-5444.0000330.

Watson D (1992) *Contouring: a guide to the analysis and display of spatial data*. First. Oxford: Pergamon.

Weibull JW (1976) An axiomatic approach to the measurement of accessibility. *Regional Science and Urban Economics* 6(4): 357–379. DOI: 10.1016/0166-0462(76)90031-4.

Wulfhorst G, Büttner B and Ji C (2017) The TUM Accessibility Atlas as a tool for supporting policies of sustainable mobility in metropolitan regions. *Transportation Research Part A: Policy and Practice* 104: 121–136. DOI: 10.1016/j.tra.2017.04.012.

Xinmin Evening News (2017) 1.5 millions: Shanghai is facing a rapid increase of shared bikes. *Xinmin Evening News*. Available at: http://shanghai.xinmin.cn/xmsq/2017/08/19/31219645.html.

Xu WA, Ding Y, Zhou J, et al. (2015) Transit accessibility measures incorporating the temporal dimension. *Cities* 46: 55–66. DOI: 10.1016/j.cities.2015.05.002.

Yang C and Gidófalvi G (2018) Fast map matching, an algorithm integrating hidden Markov model with precomputation. *International Journal of Geographical Information Science* 32: 547–570. DOI: 10.1080/13658816.2017.1400548.

Young M (2016) Defining probability-based rail station catchments for demand modelling. In: *48th Annual UTSG Conference*, Bristol, GB, 2016, pp. 1–12.

Yuan J, Zheng Y, Zhang C, et al. (2010) An Interactive-Voting based Map Matching algorithm. In: *Proceedings - IEEE International Conference on Mobile Data Management*, 2010. DOI: 10.1109/MDM.2010.14.

Zhang Y, Lin D and Mi Z (2018) Electric fence planning for dockless bike-sharing services. *Journal of Cleaner Production* 206: 383–393. DOI: 10.1016/j.jclepro.2018.09.215.

Zhang Y, Lin D and Liu XC (2019) Biking islands in cities: An analysis combining bike trajectory and percolation theory. *Journal of Transport Geography* 80(February): 102497. DOI: 10.1016/j.jtrangeo.2019.102497.

Zhao F, Chow L-F, Li M-T, et al. (2003) Forecasting Transit Walk Accessibility : A Regression Model Alternative to the Buffer. *Transportation Research Record* 1835(1): 31–41.

Zhao J, Frumin M, Wilson N, et al. (2013) Unified estimator for excess journey time under heterogeneous passenger incidence behavior using smartcard data. *Transportation Research Part C: Emerging Technologies* 34: 70–88. DOI: 10.1016/j.trc.2013.05.009.

Zheng Y (2015) Trajectory data mining: An overview. *ACM Transactions on Intelligent Systems and Technology* 6(3): 1–41. DOI: 10.1145/2743025.

Zhou S, Ni Y and Zhang X (2018) Effects of Dockless Bike on Modal Shift in Metro Commuting: A Pilot Study in Shanghai. In: *Transportation Research Board 97th Annual Meeting*, 2018. Available at: https://trid.trb.org/View/1496506.

Zuo T, Wei H and Rohne A (2018) Determining transit service coverage by non-motorized accessibility to transit: Case study of applying GPS data in Cincinnati metropolitan area. *Journal of Transport Geography* 67: 1–11. DOI: 10.1016/j.jtrangeo.2018.01.002.

Acknowledgments

I would like to thank my dear supervisor Prof. Liqiu Meng for guiding me during the last four years. I like very much to discuss research with her because her insightful input always helps me to refresh my mind. She gives me enough freedom to explore interesting topics and support a lot for my academic activities. She helps me to get involved in teaching and encourages me to understand the education systems in Germany. I am deeply impressed by her board view toward international cooperation and cultural exchange between East and West. I appreciate the fascinating ideas and interesting stories she shared with us during our coffee break.

I am grateful to my co-supervisor Prof. Constantinos Antoniou for reviewing my thesis. His valuable comments from the transportation perspective largely improve my understanding of the transportation problems. His suggestions regarding the thesis structure deepen my knowledge in thesis writing.

My appreciation goes to Prof. Alexander Zipf for holding me as a guest researcher at Heidelberg University. I would like to thank colleagues of the GIScience team for their support before and during my exchange. I really enjoy my stay in Heidelberg.

I would like to thank Prof. Xiong You and Prof. Guomin Song, they made lots of efforts to support me to pursue a Ph.D. degree in Germany. I thank Dr. Yongping Zhang for his valuable advice for my Ph.D. research, I learned a lot during the cooperation with him.

Working together with interesting and talented colleagues is a great pleasure. Thanks for colleagues in the Chair of Cartography, Luise Fleißner, Stephanie Kruchen, Holger Kumke, Mathias Jahnke, Christian Murphy, Linfang Ding, Juliane Cron, Ekaterina Chuprikova, Hao Lyu, Edyta Paulina Bogucka, Ruoxin Zhu, Chenyu Zuo, Andreas Divanis, Bing Liu, Mohammad Abusohyon, and Rui Xin, for their support during my doctoral studies. In our bi-weekly research seminar, they shared a lot of interesting ideas and research works, and give me very timely and valuable suggestions regarding my research. I like our Christmas party, campus running, and hiking trip, these memorable moments make life more colorful.

Last but not least, I would like to thank my parents and my girlfriend Miss Yan Zhu for their love and support.